2010-03-16

Development of a Plasma Arc Manufacturing Process and Machine to Create Metal Oxide Particles in Water From Wire Feedstock

Jonathan Alan George
Brigham Young University - Provo

Development of a Plasma Arc Manufacturing Process and Machine

to Create Metal Oxide Particles in Water

From Wire Feedstock

Jonathan George

A thesis submitted to the faculty of
Brigham Young University
in partial fulfillment of the requirements for the degree of

Master of Science

Robert Todd, Chair
Tim W. McLain
Carl D. Sorensen

Department of Mechanical Engineering

Brigham Young University

April 2010

ABSTRACT

Development of a Plasma Arc Manufacturing Process and Machine

to Create Metal Oxide Particles in Water

From Wire Feedstock

Jonathan George

Department of Mechanical Engineering

Master of Science

A plasma arc erosion process can be used to create metal and metal oxide particles in the ultra-fine size range (<70 μm). An electric arc is struck between two metallic electrodes, submerged in water, melting the surface of the electrodes. When the arc collapses a high energy pressure wave strikes the molten surface of the electrode. When the pressure wave strikes the molten metal, small metallic particles are created from the molten metal and are immediately cooled in the water. Previous research developed a process that used a constant current power supply and electrode motion to create ultra-fine particles.

This research improves upon previous research by using a pulsed power supply similar to those used in Electrical Discharge Machining (EDM). The pulsed power supply eliminates the need for electrode motion and improves the rate of particle production, provides control over size of the particles created, and reduces the amount of energy needed to produce the particles. The new process improves the maximum particle production rate from 3.6 g/hr to 14 g/hr, provides a method to control the mean diameter of the particles produced, and reduces the amount of energy needed from 200 kWh/kg(previous constant current process) to 10.6 kWh/kg(using the pulsed power supply).

ACKNOWLEDGMENTS

TABLE OF CONTENTS

LIST OF TABLES

LIST OF FIGURES

NOMENCLATURE

t_{on}	Length of time that a current is flowing during a pulse
t_{off}	Length of time that current is not flowing during pulse
E_{ds}	Material property, the dielectric strength
V_{gap}	The voltage grop accros an electrode gap
i_{gap}	The current flowing through a discharge between two electrodes
$\bar{V}_{gap}$	The average voltage grop accros an electrode gap
$\bar{i}_{gap}$	The average current flowing through a discharge between two electrodes
$FPGA$	Field Programable Gate Array
$MOSFET$	Metal Oxide Field Effect Transistor
PID	Proportional Derivative Integral control method
EDM	Electrical Discharge Machining

CHAPTER 1.   INTRODUCTION

Ultra-fine metal oxide particles are useful in several areas. Ultra-fine particles can be used as abrasives, paint and adhesive additives, and as feedstock for plasma spray arc coatings. Aluminum oxide particles could be used as an abrasive material in place of garnet in water-jet cutting applications. The same aluminum oxide particles could be used as an additive in paints to make them more wear resistant. Because some metal oxides are electrically conductive they could be used in paints and adhesives to make them electrically conductive. Iron oxide particles could be applied to a surface with the plasma spray arc process to create magnetic films [1, 2]. Undoubtedly, more applications for these particles will be discovered as more ways are developed to create ultra-fine particles.

Many of the applications previously mentioned require very small particles. For example, if particles are used as an additive in a paint, the particles would need to be small enough to not produce any significant texture in the applied painted surface. These particles would need to be 70 μm or smaller. Particles with a size under 70 μm are considered ultra-fine particles. In many applications the performance of the particles are greater if the particles are smaller. For example, some particles are transparent to some light ranges because they are smaller than the wavelength of light [3].

In prior work a plasma arc process has been used to create these ultra-fine particles. The plasma arc process has been used because it produces, for the most part, only particles in the ultra-fine particle size range. Up to this point there have been two variations of the plasma arc process used to produce the metal or metal oxide particles here at BYU.

The first variation of the plasma arc process is a completely manual method where a human operator controls the process. This method has serious drawbacks in terms of product quality or consistency, production rates, and high labor costs. The manual process is very flexible in terms of size and shape of the electrodes used in the process because the human operator can easily

adjust to these changes. This manual method has many disadvantages because it is controlled by a human. The rate of production and the quality of the particles produced is limited by the slow response time of the operator. The variation introduced into the system by a human operator could be greatly reduced if the operator was replaced by a feedback control system.

The second variation of the plasma arc process, the rod process, was developed in previous research at BYU by Chris Lewis. [4] The rod process uses metallic rod electrodes that are fed toward each other as the rods are eroded. The rod process greatly improved the state-of-the-art by replacing the human operator with a digital control system to close the feedback loop. In this way the production rate and product quality were both increased. The production rate was improved by several times over the manual process.

These improvements to the process did not come without drawbacks. The rod process requires that the electrode used must be in the form of a one half inch diameter rod about 15 inches long. The dimensional tolerances and straightness of the rod required by the process are difficult to meet with the electrode materials used in the process. As a result, the cost of the electrode material in rod form is significantly more costly than when produced in other forms like wire.

Additionally, the rod process requires frequent operator adjustments to maintain consistent control of the process. These adjustments are required due to the way that the electrodes wear. The operator must frequently stop the process to remove and dress the ends of the electrodes. These maintenance issues are time consuming and labor intensive and also seriously limit the utilization of the process.

The objective of this research is to improve upon previous variations of the process and develop a new plasma arc process that increases production rate, improves the particle quality, and requires limited operator intervention and maintenance. The focus of this thesis is the development of a new process that uses a pulsed power supply with a feedback control system to meet the current research objectives. A secondary goal is to develop a process that uses wire feedstock rather than rods.

1.1 Plasma Arc Process

The plasma arc process used for the production of ultra-fine particles has many similarities to other plasma arc processes such as plasma arc welding. Two electrodes are placed in close proximity to each other in a dielectric fluid. In all the experiments discussed in this research deionized water was used as the dielectric. A voltage difference is placed between the two electrodes, as seen in Figure 1.1(a), causing the two faces of the electrodes and the dielectric between them to act as a capacitor. This gap between the electrodes will continue to act as a capacitor until the electric field is strong enough to overcome the strength or resistance of the dielectric fluid. Equation (1.1) shows the breakdown voltage of a capacitor where V_{bd} is the breakdown voltage, E_{ds} is the strength of the dielectric material and d_{gap} is the distance between the plates.

$$V_{bd} = E_{ds}\,d_{gap} \tag{1.1}$$

This relationship shows that the breakdown voltage is proportional to the distance between the capacitor plates. This means that as the electrodes get closer together the voltage required for the dielectric to breakdown is reduced. The dielectric strength of the material is an intrinsic property of a material. The dielectric strength of a material decreases with an increase in temperature and frequency. The dielectric strength of deionized water is on the order of 20kV/mm [5]. Given that the power supplies used in this research have an open circuit voltage of 80V, the electrode gap distance for dielectric breakdown is on the order of 4 microns or 0.00015 inches.

The plasma arc can be divided into five stages: pre-breakdown, breakdown, discharge, end of discharge and post-discharge. Chris Lewis' research focused on understanding the discharge stage of the process. During pre-breakdown, shown in Figure 1.1(a), a voltage difference is placed between the electrodes. The process will remain in the pre-breakdown stage until the strength of the electric field overcomes the dielectric strength of the gap. When the dielectric begins to breakdown it ionizes, as shown in Figure 1.1(b), the result is a conductive path between the electrodes. Current begins to flow, creating a plasma arc between the electrodes through the conductive ion column as shown in Figure 1.1(b). The creation of the arc begins the discharge stage of the process. While the arc is sustained, the heat of the arc causes material from both the cathode and the anode to melt and vaporize, then combines with the other material in the plasma channel.

(a) Pre-breakdown: voltage applied between the two electrodes

(b) Breakdown: dielectric breakdown, creation of the plasma channel

(c) Discharge: heating, melting and vaporizing of the electrodes

(d) End of the discharge: plasma implosion, removing of the molten metal pools

(e) Post-discharge: Solidifying and flushing of the eroded particles by the dielectric
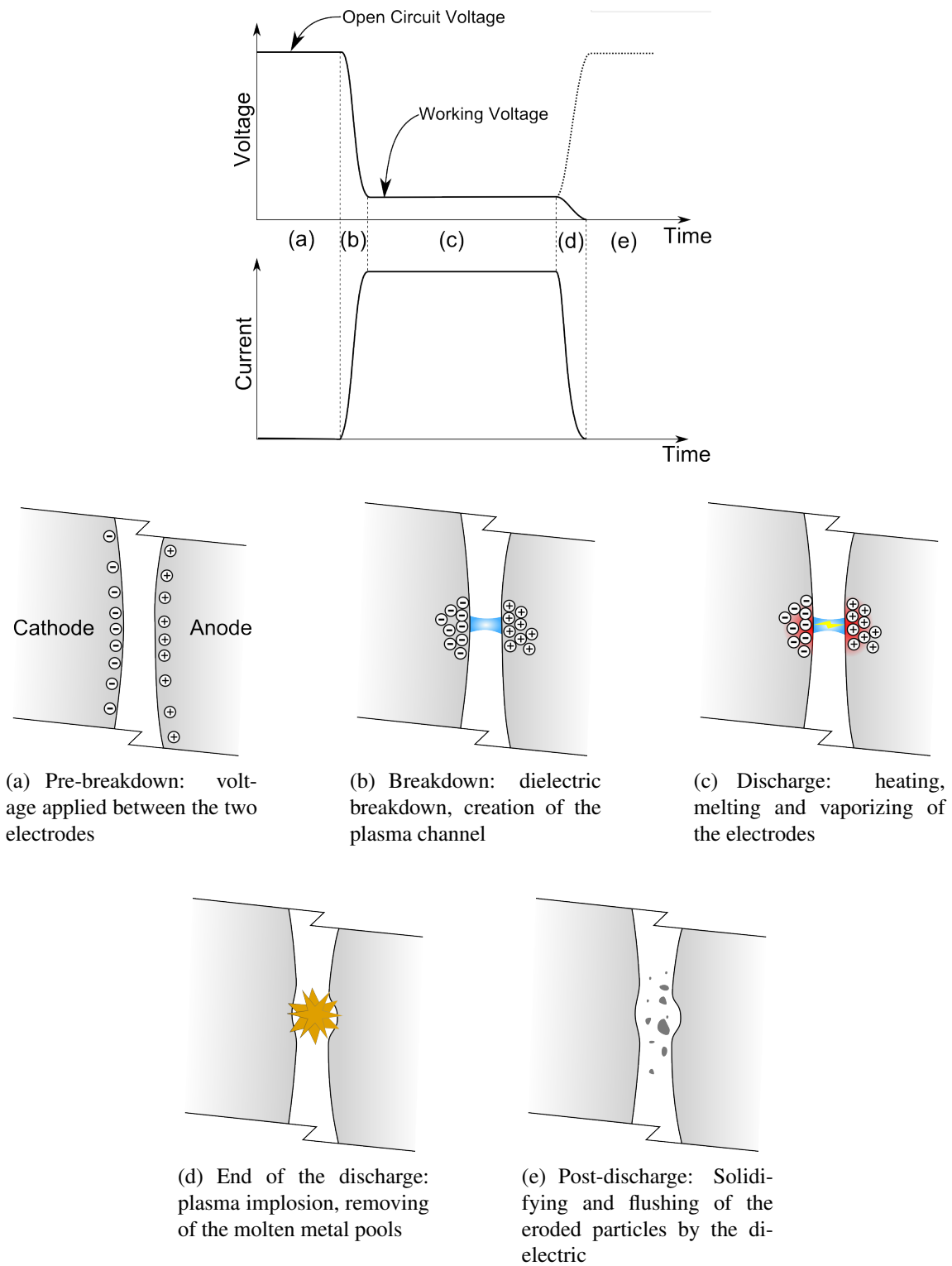
Figure 1.1: Plasma Arc Process Steps [6]

At some point, the conditions change and the arc cannot be sustained. The arc could become unstable because the electrode gap changed, the power supply was switched off, or the arc could switch to a different location on the electrode face. When the arc is broken, the end of discharge stage occurs. During the end of discharge stage the plasma channel implodes as shown in Figure 1.1(d). The particles suspended in the ion cloud upon implosion combine and form particles containing material from the dielectric and the electrodes. In the case of this process, many of the resulting particles will be metal oxide particles that formed from oxygen atoms in the water and metal atoms from the electrodes.

Particles made completely from the electrode material will also be formed. During the discharge stage, the heat from the arc creates a molten pool of metal on the electrodes. The shockwave from the implosion of the plasma column causes these pools of metal to be blown off the electrode into the dielectric fluid. During the final stage of the process, the particles are quickly cooled and removed from the electrode gap by the moving dielectric fluid. The particles formed from the molten pools of metal are more likely to be composed of the same composition as the electrode material because there is little time for the metal to oxidize prior to solidifying. This final Post-Discharge stage of the process is shown in Figure 1.1(e).

The main difference between the variations of the process is how the electrodes and power supplies are manipulated to control the length of the discharge stage. In the manual process, the length of the discharge stage is dependent on how the operator moves the electrodes. This dependence on the operator for particle consistency requires that the operator maintains the same conditions every time the process is run. The operator introduces a large amount of variation into the process because human operators do no react to the same situation the same way every time. In addition, a human operator has a slow response time in comparison to many digital control systems.

For the rod process, the length of the discharge stage is dependent on the motion control system and variations in flow of the dielectric fluid. Removing the human operator from the control loop greatly improves the product quality and production rate, however, there is still a large distribution of particle size. This is because there is no direct control on the length of the discharge time.

One of the main objectives of this research is to manipulate the power supply so that there is direct control of the length of the discharge stage. This research borrows technology from Electrical Discharge Machining, (EDM), to limit the length of the discharge stage. A control mechanism is implemented to turn the power supply off at a fixed time after the discharge stage starts. Limiting the time of the discharge stage limits the amount of energy in the discharge. It is hypothesized that the limited amount of energy in each discharge puts an upper limit on the volume of metal that can be melted, or vaporized. This limits the size of particles that can be produced and tightens the distribution of particle size that is produced.

In any variation of the process, feedback controls must be used to maintain a constant distance between the electrodes. In the case of manual control, the operator uses his sense of sight and sound to roughly determine if the electrodes are too close together or too far apart. In the case of the automated processes, either arc voltage, arc current or both are measured and used in a feedback loop to maintain a continuous process.

1.2 Process Design Challenges

In addition to the control problems noted above the use of rod electrodes in the previous processes had led to many problems in terms of process down time, production rates, raw material cost, and maintenance costs. Most of these issues are related to the fact that the previous processes have required bearings and seals where the rods enter the dielectric filled reaction chamber. If the need for these bearings and seals could be eliminated, then the process down time and maintenance cost would be dramatically reduced.

Seals were required in the rod process because the electrodes entered the reactor from the side below the water line. The seals were required to prevent the dielectric fluid from leaking out of the reactor. Bearings were required in the process to align the electrode with the seals. If the electrodes are not concentric with the seal, the seals will leak. Rods with fine surface finishes, high straightness and high tolerance diameters are required for the seals to function and to increase the life of the bearings. Rods with these properties are difficult to machine and therefore are expensive to purchase. If the need for the seals and bearings were eliminated then the cost of the electrodes, as well as maintenance of the process, would be greatly reduced. The downtime required for

replacement of the seals and bearings would also be eliminated increasing the productivity of the process.

The rod process also requires that the electrodes rotate to maintain a stable process. The rotation of the electrodes is what keeps the discharge from staying in one place on the electrode faces. If the process can be stabilized without using rotation, then many additional problems would be eliminated.

An additional problem in the rod process is the cathode growth rate. There is a large percentage of the metal that is eroded from the anode electrode that is deposited on the cathode electrode. Tests show that about 50% of the metal eroded from the anode electrode is deposited on the cathode electrode. This cathode growth both limits the particle production rate and causes the cathode electrode to increase in length. The random nature of the cathode growth also requires that the electrode be removed from the machine to remove the misshapen growth. Because the cathode electrode is constantly changing length and shape, the position of the cathode electrode must be controlled to stabilize the process.

Ideally, only one of the electrodes is consumable and the other electrode has zero growth or erosion. EDM machining processes show that it is possible, using a pulsed power supply, to nearly eliminated the rate of growth or erosion of one of the electrodes used in the process. It is hypothesized that the proposed new process would eliminate the need for bearings, seals, and maintenance problems that are present in the rod process in addition to eliminating the electrode growth problem.

The proposed new pulsed process would use wire as the consumable electrode. Most of the metal materials that might be used in the process are most readily available in wire form. A large volume of metal can be wound on a spool providing enough feedstock for days or weeks without need for maintenance. If the tip of the wire electrode has buildup or any other problems the tip can simply be cut off. No high cost or time consuming maintenance will be needed for a consumable wire electrode.

1.3   Contributions of This Work

The contribution of this research is to create a new pulsed power supply wire feed stock process (pulsed wire process) that improves the rate of production of ultra-fine particles while

improving the quality of particles produced. This new process will be able to have some control over the mean particle diameter produced, as well as reduced maintenance and operating costs.

These process improvements will be made possible by using a pulsed power supply, similar to those used in EDM processes, and wire feedstock as a consumable electrode. The pulsed EDM like power supply will make it possible to increase the rate of production, provide control over the average particle size, and eliminate the growth rate of the cathode electrode.

CHAPTER 2.   LITERATURE REVIEW

This chapter reviews the previous research performed related to the production of ultra-fine particles using the plasma arc process. The chapter is divided into five sections including an overview of the previous research on the rod process and other processes used to create metal and metal oxide particles.

An overview of the process and controls used in the rod process is presented in more detail in Section 2.1. A detailed description of the rod process is given to illustrate how it works and what parts still need improvement. Most of the changes to the process implemented in the wire process are a result of what was learned during the development of the rod process.

Section 2.3 provides information about Electrical Discharge Machining (EDM) processes. The final power supply used in the pulsed wire process is very similar to those used in EDM machining processes. The EDM process is basically the same process used to create ultra-fine particles except that the EDM process is designed to erode metal from a workpiece to create finished product. In the EDM process, ultra-fine particles are created, but they are a byproduct of the process.

Section 2.4 discusses the twin wire spray arc coating process. The twin wire arc spray process is used to coat surfaces with particles created by spraying molten metal particles onto the surface. The process is of interest in this research because it is a continuous process that uses an arc between two wires to create particles. The arc is significantly different from the arcs used to create ultra-fine particles in water or another dielectric medium, but the process is of interest because it uses two wires as feedstock material.

Section 2.5 discusses a process used by A. E. Berkowitz et al. to create ultra-fine particles using electrical discharges. The process designed by Berkowitz et at. uses vibration to create random electrode gaps between multiple electrodes in series. Because the electrodes are connected

in series, discharges are created at each electrode gap. This results in multiple simultaneous discharges that produce an erosion rate many times faster than that of a discharge across a single discharge gap. Because the electrode gaps are created randomly using vibration, the resulting ultra-fine particles have a large distribution of particle size.

Finally, Section 2.6 provides a brief description of a process used to create carbon particles using an arc in an inert gas. The power supply used in this process is of interest because it decouples the electrode gap distance from the open circuit voltage of the power supply. When these two parameters are decoupled, the electrode gap distance can be set at any reasonable distance and a discharge of arbitrary power can be created between the electrodes.

2.1 Rod Process in Detail

The rod process, as seen in Figure 2.1, developed at BYU is a crossover between a laboratory test machine and a process machine. The process was developed to accommodate a wide range of settings while maintaining the ability to be used as a production machine. The process used for this machine is similar to the original manual process. The major difference between the rod process and the manual process is that the rod process uses digital motion controls to replace the human hand and arms, and a digital feedback control loop to replace the operator's brain. By using digital systems to move and control the electrodes, faster and more consistent control is obtained.

The following subsections describe the theory of operation and control system used in the rod process. Following the description of the rod process the drawbacks of the process are discussed. The biggest drawback of the rod process is the need of rod shaped electrodes and the inability to control the maximum size of particles produced.

2.1.1 Theory Behind the Rod Process

The rod process uses four stepper motors to control the motion of the electrodes in the reactor. For each electrode there is a motor, seen in Figure 2.2, that controls the rotation of the electrode as well as another motor that controls the axial position of the electrode, as seen in Figure 2.3. The electrodes are constantly rotated to ensure that the entire electrode face is given

Figure 2.1: Rod Machine Front View

an opportunity to be eroded by the arc. The cathode electrode is rotated at a slow speed (.25 RPM) and the anode is rotated at a faster speed (50 RPM). The fast rotation of the anode keeps the erosion of the tip of the anode symmetric, and the high relative velocity between the anode surface and the cathode surface results in a more stable arc. The cathode electrode is also rotated to keep the erosion symmetric, but it is rotated at a slower rate to increase the life of the cathode electrode seal and bearings.

The gap between the electrodes is controlled by changing the axial position of the electrodes with respect to the reactor. The stepper motors controlling this axial motion are electronically geared together. The electronic gearing helps to keep the electrodes centered in the reactor. The ratio of the electronic gearing is set to keep the reaction centered in the reactor. The ratio is needed because the two electrodes erode at different rates. In fact, the anode electrode is eroded, and the cathode electrode grows. The controller works in such a way that it attempts to maintain a constant gap between the electrodes. If the electrodes were not being eroded, keeping a constant gap between the electrodes would be trivial. Because the electrodes are constantly being eroded,
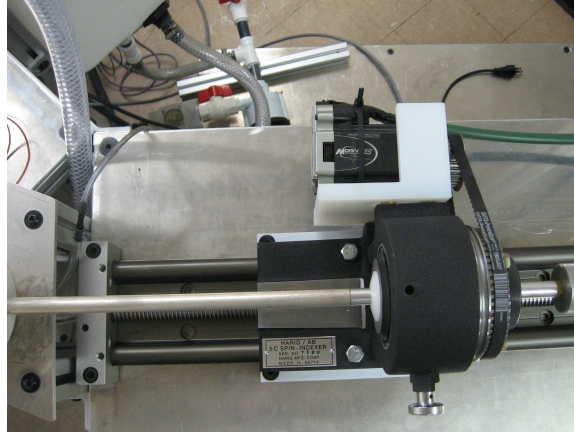
Figure 2.2: Rod Machine Electrode Assembly
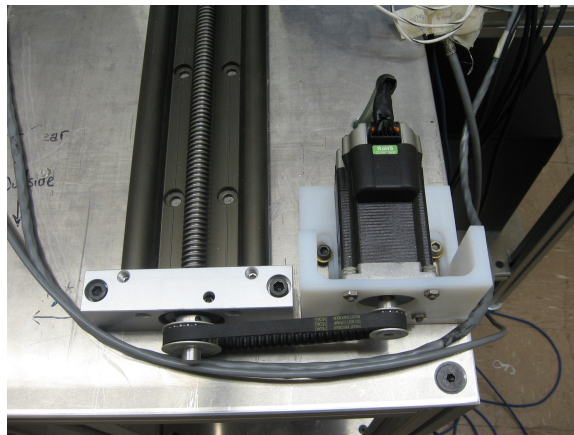
Figure 2.3: Electrode Axial Direction Motor

it is difficult to estimate the instantaneous electrode gap. The gap voltage, V_{gap} is used to estimate electrode gap, d_{gap}.

$$V_{gap} = I\,R_{gap} \tag{2.1}$$

$$R_{gap} = d_{gap}\,c_1 + c_2 \tag{2.2}$$

$$V_{gap} = d_{gap}\,I\,c_1 + I\,c_2 \tag{2.3}$$

Equation (2.1) shows Ohm's Law for the arc across the electrode gap. The power supply used in the rod process is a constant current supply so the current (I) in the equations is constant.

Equation (2.2) shows that the gap resistance, once the dielectric is ionized, is proportional to some constant c_1 and d_{gap} plus some constant c_2. As the gap distance decreases the resistance decreases. The constants c_1 and c_2 are dependent on the material properties of the dielectric, local geometry of the electrodes, and other environmental conditions. To show the general relationship between V_{gap} and d_{gap}, c_1 and c_2 are assumed to be roughly constant once the arc has started.

Equation (2.3) shows that the V_{gap} is proportional to d_{gap} by a value that is roughly constant plus the second constant c_2. In reality the power supply cannot keep the current exactly constant, and the variables c_1 and c_2 in Equation (2.2) do in fact change. However, the general principle that V_{gap} is proportional to d_{gap} can be used to estimate d_{gap} by measuring V_{gap}. The controller uses this principle to maintain V_{gap} at a constant voltage by changing the position of the electrodes. As V_{gap} increases above a predetermined set point, the electrodes are brought closer together. As V_{gap} decreases below the set point, the electrodes are moved farther apart. In this way d_{gap} is kept nearly constant, and as a result the arc is stabilized.

2.1.2 Rod Process Power Supply

The power supply used in the rod process is a constant current welding power supply. The particular power supply used in the process is a switched mode power supply. The power supply has an open circuit voltage of 80 VDC and is capable of supplying up to 350 amps in constant current mode. The rod process uses the power supply's lowest constant current setting of 30 amps. The welding power supply was a very convenient solution because it provided electrically isolated analog outputs for the voltage and current across the electrodes. Additionally, as a switched mode power supply, the welding power supply is very energy efficient.

2.1.3 Rod Process Control

The control system for the rod process was implemented with National Instruments hardware and software. Data acquisition hardware was used to convert the analog arc voltage and current signals from the welder to digital signals. A Labview Virtual Instrument was developed to filter the voltage signal to be used as the feedback input for a PID control loop. The output of the PID controller was used to set the velocity of the stepper motors that control the axial movement

of the electrodes. The PID setpoint is set at a constant voltage that depends on the material. The PID parameters were determined by trial and error.

The rotation of the electrodes was set at a constant speed. This rotation is key in keeping the reaction stable over a long period of time to keep the electrodes from wearing unevenly.

2.1.4   Rod Process Drawbacks

The development of the rod process and the experiments performed on it provided confirmation that the process could be stabilized through control, and that the desired particles could be generated. Unfortunately, there are some significant drawbacks in the rod process design. The end result of these drawbacks is non-optimal product quality and limited production rates.

Product quality, specifically particle uniformity, is non-optimal due to variation in the energy of each discharge. The objective of the rod process controller is to keep the electrodes constantly arcing. There is no mechanism to start or stop the discharge stage of the process. The length of the discharge stage acts in a chaotic way, with dramatic changes due to small changes in the inputs.

High speed video was used to study the behavior of the discharge stage in the rod process. Once the discharge stage started, the arc would wander on the electrode faces for some period of time. The wandering of the arc is a result of the variation of electrical fields, magnetic fields, thermal gradients, the thermal and mechanical effect of the dielectric fluid as well as the motion of the electrodes.

After some period of time, the arc becomes unstable at the current position and collapses. If conditions are right, a second arc will form between electrodes at a different location where the arc will be more stable at that moment in time. The high speed video along with oscilloscope current waveforms showed that during the time that the current waveform is nearly constant the discharge moves between many locations.

Because the length of the discharge stage and the wandering of the arc are dependent on the instantaneous electric, magnetic, thermal, and mechanical conditions, the particle size is chaotic. Some of discharges last for several microseconds and some last for many milliseconds. The vast difference in the time scales of these discharge times cause a large range in the size of particles produced.

14

The large distribution in particle size is only one problem limiting the production rate of the rod process. The electrodes require frequent maintenance and, as a result, the process is under utilized. Some of the maintenance that the electrodes require is also a result of the uncontrolled length of the discharge time. When discharges last for many milliseconds the size of the molten pool of metal on the electrodes can become large. When the discharge stops the metal in the pool is only partially removed from the face of the electrode. As a result some of the molten metal cools on the face of the electrode as large globs. A pit is formed where the molten pool of metal was. When these large globs and pits grow too large the process must be stopped and the electrode faces must be machined to remove irregularities in the surfaces. If the irregularities are not removed then the process becomes unstable, wastes material and reduces the production rate of the process. If the length of the discharge time was limited, then the large pools of metal would not form and these problems would be mitigated.

The seals and bearing that make the entry point for the electrodes into the reactor are another part of the rod process that require frequent maintenance. The combination of rotary and axial motion of the electrodes causes high wear to both the reactor seals and the bearings. When electrodes that are not straight and round are used, the bearing and seal wear rate is accelerated. The time and cost required to replace these components is significant and reduces the utilization of the process.

2.2 Rod Process Research

In previous research at BYU, Chris Lewis [4] researched the physics of the discharge stage of the process using numerical simulations. The research used a simulation code called Vector Fields to simulate the steady state characteristics of the discharge. The simulation used electrostatics principles to model discrete electrons and other charge particles in the electrode gap.

The simulation model was difficult to create due to the complex interaction of the system, the somewhat unknown model parameters, and the lossy dielectric nature of the water used in the system. However, it was shown that the method was useful for studying the nature of the actual discharge. Figure 2.4 shows a prediction of the expected primary electrode beam in a discharge.

One of the interesting results from the electrostatics model is the prediction that the current density in the cross section of the discharge is not constant. Figure 2.5 shows a current cross
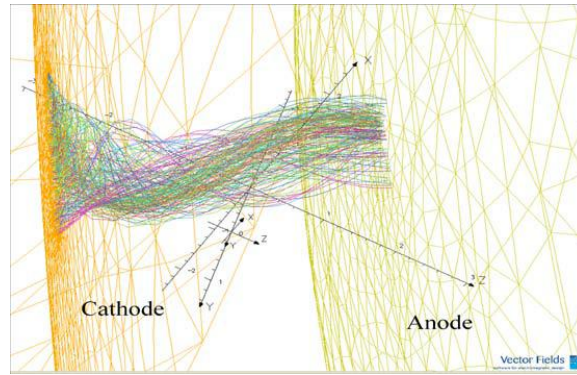
Figure 2.4: Model Simulation of the Primary Electrode Beam
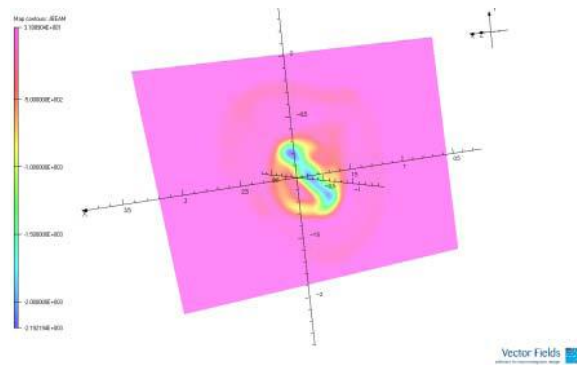
Figure 2.5: Discharge Cross Section Current Density Map

sectional density map of a discharge. These variations in the current density across the discharge will lead to different heating rates at different positions on the electrode shape. The random nature of the discharge current density could lead to variation in the size of particles created in the process.

2.3   EDM Process

EDM machining is a process that has greatly matured over the last 30 years. EDM machining processes use the plasma arc process to erode a cavity in a workpiece in the shape of an electrode. EDM processes are often used to machine cavities in tools for injection molding where the surface finish of the cavity must be very smooth. In general, the particles produced during EDM processes are considered waste and are filtered out of the dielectric fluid. However, some research has been done to determine how the size of the particles produced changes with EDM process parameter settings [7].

Figure 2.6: Sodick "Sinker" or "Plunge" EDM Machine
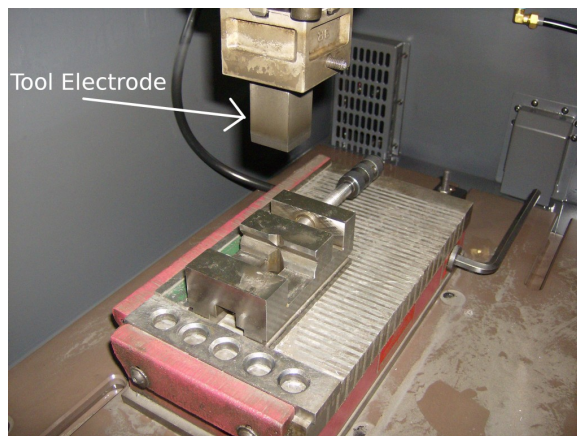
Figure 2.7: Sinker EDM Tool Electrode

Figure 2.8: Sodick Wire EDM

Figure 2.6 shows an example of a sinker EDM machine. This type of machine uses a tool electrode in the shape of the desired cavity to erode material from the workpiece. The term "sinker" comes from the fact that over time the tool appears to sink into the workpiece. The dielectric fluid used in sinker EDM processes is typically some kind of hydrocarbon oil, similar to kerosene. The tool and the workpiece are in a tank that is filled with the dielectric fluid while machining is taking place. Figure 2.7 shows a simple electrode tool used to create a square pocket. The shape of an electrode used in a sinker EDM is often very complicated so that it can be used to create an injection molding cavity, or some other tool. The EDM process has the disadvantage of low material removal rate in comparison to convention machining, but has the advantage of being able to create fine surface finishes, relatively tight tolerances, and the ability of eroding any conductive material regardless of its hardness.

Wire cut EDM is another common machining method used to machine tools with high hardness. A wire EDM machine can be thought of as an electrical discharge band saw. Figure 2.8 shows an automatic threading wire EDM machine. The machine uses small diameter brass wire with a diameter between 0.006 inches and 0.015 inches as the tool electrode. The wire is threaded between two wire guides that both guide the position of the wire and conduct electricity to it. While machining the wire is eroded, to prevent the wire from getting too thin or breaking the wire is constantly being replenished. The wire is pulled down through the bottom guide and new wire is unwound from a spool and fed through the top guide. The workpiece that is cut is clamped to
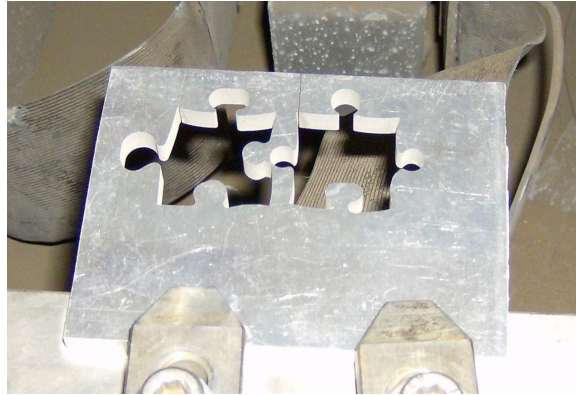
Figure 2.9: A Part Cut With a Wire EDM Machine

an electrically conductive table. The table is connected to the power supply making the workpiece one of the electrodes. Prior to the start of machining, the tank that the wire and the electrodes are in is filled with the dielectric fluid. Generally, the dielectric used for wire EDM is deionized water.

The wire is then fed through the workpiece eroding a slot slightly larger than the wire. The wire and the workpiece do not touch. The electrode gap between the wire and the workpiece is where the erosion happens using the plasma arc process. Figure 2.9 shows an example of a part created with the wire EDM process.

A third kind of EDM process commonly used is the drill EDM. Drill EDM machines are used to drill holes in hard materials are that difficult to machine with traditional drilling or cutting processes. The drill EDM process is also often used because it can create very small holes, down to a few thousandths of an inch, that are very deep.

The drill EDM process works much like a sinker EDM with a few exceptions. First, the dielectric fluid used in drill EDM process is generally deionized water. Second, the electrode is a metallic tube that is rotated while machining. Third, the tool and the workpiece in drill EDM applications are often not submerged in the dielectric fluid. The deionized water used in drill EDM process is pumped through the center of the tubular electrode constantly flushing the electrode gap. Drill EDM processes will be discussed further in Chapter 3.

2.3.1 EDM Process Overview

The EDM process is very similar to the rod process. The main difference is that in the EDM process there is a specific mechanism for preventing the discharge stage from lasting too long. The mechanism to prevent DC arcing is to switch off the current to the electrodes for a set period of time. If a discharge lasts too long, the discharge is referred to as a DC arc. When DC arcing happens between the tool and workpiece the surface finish of both are damaged. This damage happens because the DC arcing overheats a local area in the tool and workpiece causing large craters to form on both.

The time that the current is off is called t_{off}. The t_{off} time must be long enough for the dielectric fluid to recover, or in other words become non-conductive. Sometime the t_{off} must be increased to allow the removal of eroded particles from the electrode gap. After the t_{off} time has elapsed the current is turned back on for a time period of t_{on}. The cycle continues switching the current source on for the t_{on} and off for t_{off} seconds. The t_{on} time is typically longer than the t_{off} time. t_{on} must be short enough to prevent a large pit on the electrode or tool from forming. The t_{on} and t_{off} parameters are determined using designed experiments to optimize material removal rate and surface finish at a given current. Figure 2.10 shows the relationship between t_{on} and t_{off} and the waveforms of voltage and current.

At the start of the t_{on} period the current source is switched on. The voltage rises until breakdown occurs and current begins to flow. The time between the start of the t_{on} period and the start of current flow is called the ignition delay time or t_{delay}. During the ignition delay time the voltage will remain at the open circuit voltage. At the end of the t_{on} period the current source is switched off and both the current and the voltage drop. The t_{off} period starts once the t_{on} period has expired and the dielectric is then allowed to recover. If the t_{off} period is long enough, DC arcing will be prevented.

The t_{on} and t_{off} times are usually measured in microseconds. Typical values for t_{on} in sinker EDM applications are in the range of 1 to several thousand microseconds. Typical t_{off} values are in the range of 10 to 300 microseconds.

The EDM duty cycle is the ratio of t_{on}/t_{off}, and is a measure of the efficiency of the process. All of the work done to remove material from the workpiece is done during the t_{on} time.
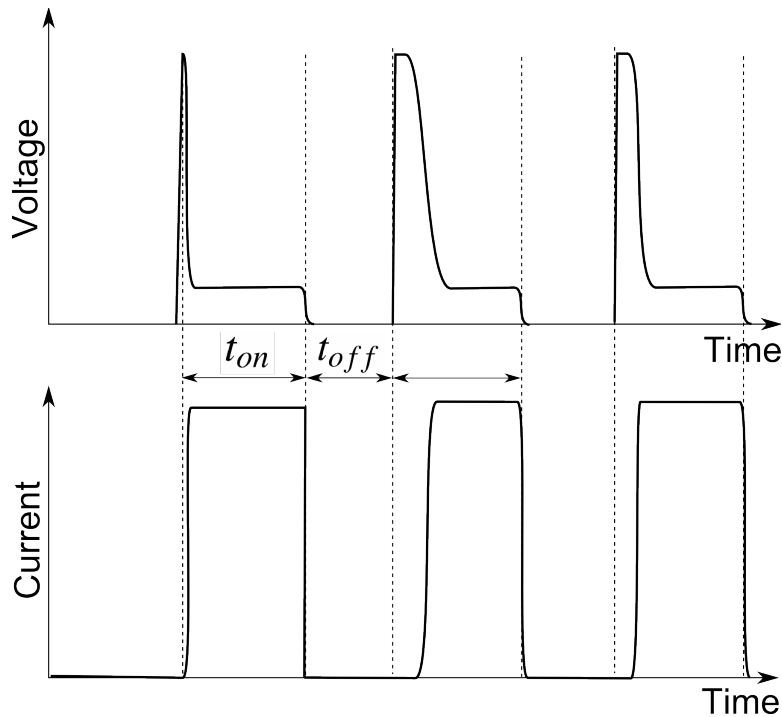
Figure 2.10: EDM t_{on} and t_{off} graph

The t_{off} time is necessary to prevent DC arcing, but does not contribute to material removal rate. So as the t_{off} time is reduced in comparison to the t_{on} time the efficiency of the process is increased.

Modern EDM controls have the ability to measure certain characteristics of the process and modify the t_{on} and t_{off} times to maximize efficiency while avoiding DC arcing. These controls detect when DC arcing starts, or is likely to start, and increase the t_{off} time until the DC arcing has stopped or is unlikely to start. Prior to the invention of these adaptive controls, experiments where usually performed to determine a minimum t_{off} time that prevents DC arcing. The minimum t_{off} time is used regardless of the t_{on} time. This method of using a constant t_{off} time is still common on low cost EDM equipment, especially hole drilling EDM equipment [8].

While the t_{off} time can be reduced to improve efficiency, it has no effect on the surface finish, as long as DC arcing does not occur. The depth and breadth of the craters, or surface finish, on the workpiece are a function of the energy delivered during each discharge. For a given current only t_{on} effects the size of the craters, or in other words the surface finish of the workpiece. Typically while roughing the workpiece the t_{on} time is much longer than while finishing. This is done to increase the machining efficient while roughing. If t_{off} is set at a constant to prevent DC

21
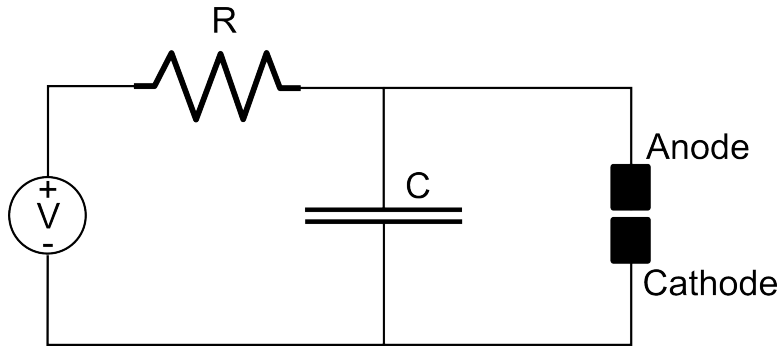
Figure 2.11: RC-type EDM Power Supply

arcing then the duty cycle, or the fraction of time spent removing material can be increased by increasing t_{on}. Increasing the current increases the material removal rate and decreases the quality of the surface finish.

2.3.2 EDM Power Supplies

Most EDM machines sold today use a power supply that has some kind of transistor switch that can be switched on and off with exact timing. The first EDM power supplies, or generators, used a RC circuit to create a naturally oscillating current source that strikes and breaks the arc due to the voltage in the capacitor. Figure 2.11 shows the basic circuit of the RC-type power supply.

The operation of the RC-type power supply is very simple. A constant voltage source applies a current limited by the resistor, R, charging the capacitor, C. The capacitor is connected in parallel with the electrode gap. Once the voltage across the capacitor is high enough to cause breakdown in the electrode gap a discharge is started. The discharge continues until the voltage across the capacitor is too low to sustain an arc. Figure 2.12 shows the voltage and current waveforms made by the RC-type power supply. The t_{on} and t_{off} times are not explicitly set with this type of power supply. The t_{off} time is set primarily by the RC time constant of the circuit. The t_{on} time is dependent on the electrode gap, but generally is not effected by the RC time constant.

There are many variations of the RC-type power supplies, but most do not have the ability to directly set the on and off time of the pulses created. RC-type power supplies also have the drawback that the energy of a pulse is limited due to the decay of the voltage across the capacitor
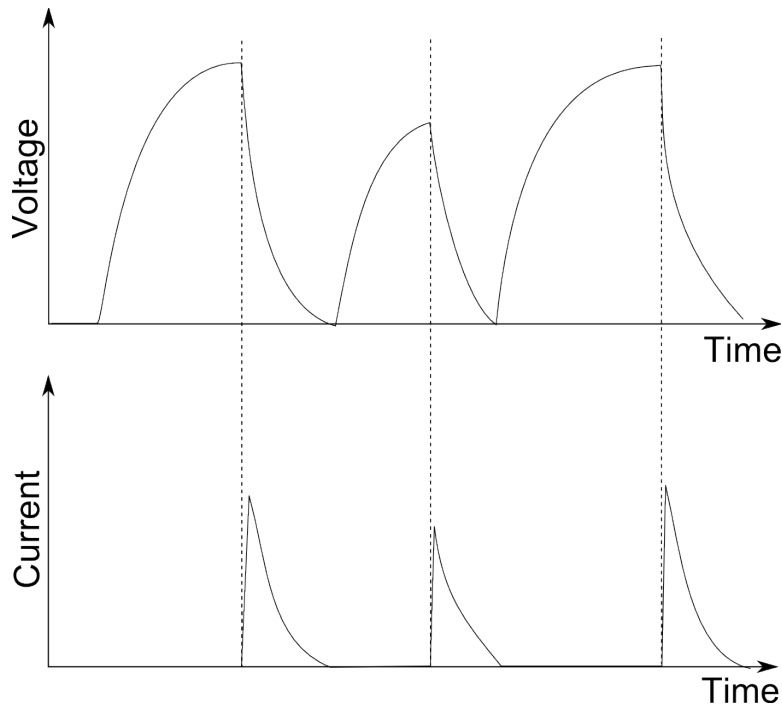
Figure 2.12: Voltage and Current Graphs for and RC-type Power Supply

during the discharge. RC-type power supplies are rarely used in modern EDM equipment because their limited power output and poor control over the pulse timing.

EDM power supplies using vacuum tubes were the first to use an electronic switching device to create current limited voltage pulses [6, 8, 9]. Figure 2.13 show the basic circuit of the current limited pulsed type EDM power supply. A resistive element is placed in series with an electronic switch to limit the current in the discharge. The value of the resistance is used to limit the current delivered in the discharge and the switching element is used to control the t_{on} and t_{off} values. This type of power supply decouples the pulse time parameters from current parameter allowing much higher energy output in comparison to the RC-type power supply.

Figure 2.14 compares the voltage and current waveforms of the RC-type power supply and the current limited pulsed type power supply. The energy output of a pulse is product of the area under the voltage curve and the area under the current curve. The RC-type waveform is shown in light gray with dashed lines. The current limited pulsed power supply waveforms are shown in darker gray with solid lines. Because the resistive current limited pulsed power supply can provide a near constant current during the entire pulse, the pulses it produces carry more energy

23
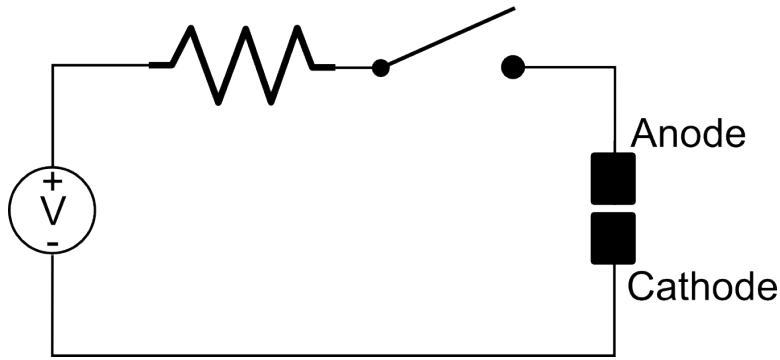
Figure 2.13: Switching Type Power Supply
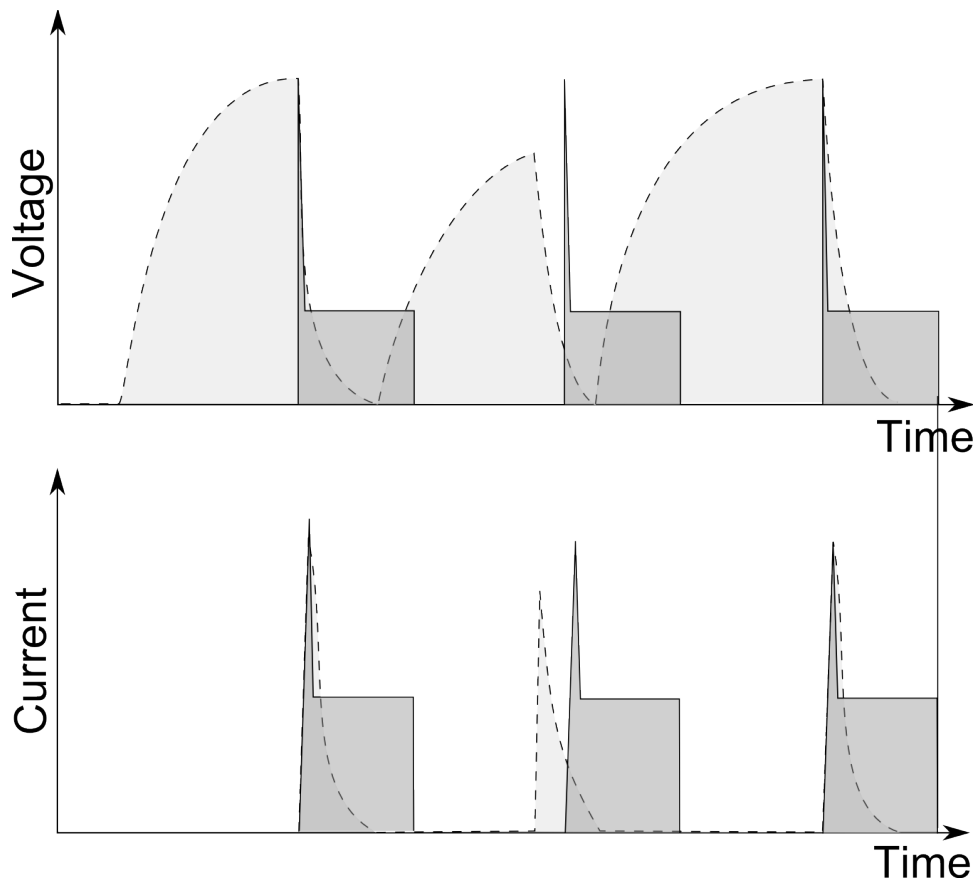
Figure 2.14: Voltage and Current Graphs Comparing RC and Switching Type Power Supplies

than a comparable RC-type power supply. Also note that the RC-type power supply does not have a constant pulse frequency or duration. Because the current and time parameters of the current limited pulsed type power supply are decoupled, exact t_{off} times can be guaranteed to allow the dielectric to recover before the next pulse.

The electronic switches used in pulsed EDM power supplies have changed as new switching devices were developed. The vacuum tubes used in the first of these EDM generators were expensive and unreliable. Soon after their development bipolar junction transistors, BJT's, replaced the vacuum tube switches increasing both the reliability and the power output of the power supplies. Later the BJT's were replaced with the more efficient MOSFET transistors, metal oxide field effect transistors, that are still in use today [6]. Some Wire EDM power supplies now use IGBT, integrated bipolar gate transistor, switches and are able to switch currents of several thousand amps in short durations.

These resistive switching type power supplies greatly increased the material removal rates of the EDM process. But even the power supplies that use MOSFET transistors are energy inefficient. A huge amount of power is converted to heat due to the resistive current limiting concept used in these power supplies.

In recent years several types of resonant switched mode EDM power supplies have been developed that greatly increase the electrical efficiency of the EDM process [10, 11]. The design of these power supplies is difficult due to the high frequency switching output that is required for EDM pulses. The specific design of these power supplies is generally kept proprietary by the companies that develop EDM machines. The use of this type of a power supply for the wire process is not appropriate for this research because its benefits over the resistive switching type power supply do not justify the additional complexity. The use of these resonate power supplies should, however, be considered for future development of the pulsed wire process.

During this research both the RC and current-limited pulse-type power supplies were used. The RC-type power supply is very simple to construct at low current levels. Because of this, the RC-type power supply was used to experiment the feasibility of the proposed process of using an EDM type power supply. Later, a drill EDM with a current limited pulsed type power supply was used to provide a proof of concept and to estimate the expected production rate. The final pulsed wire process also uses a current limited pulse type power supply due to the success of experiments on the drill EDM.
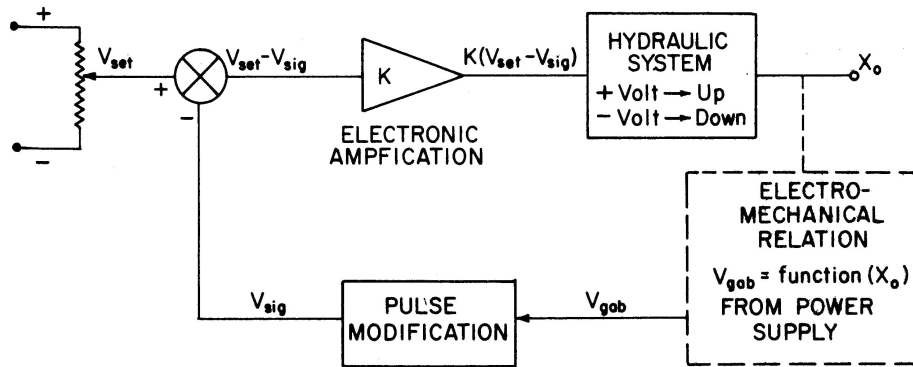
Figure 2.15: 1970's Proportional Hydraulic Controls [9]

2.3.3 EDM Controls

EDM controls are difficult to design because no adequate dynamic model of the EDM process exists, preventing the use of classical control design methods. The EDM process is also known for its highly non-linear nature. Many different types of controls have been developed for EDM process controllers from the simple proportional controllers to the complicated adaptive fuzzy logic controllers [12, 13]. All EDM controllers require the use of designed experiments to determine the correct controller and power supply settings to reduce tool wear and increase material removal rates to obtain a desired surface finish with a given combination of tool material and workpiece material.

The first wire EDM processes used hydraulic actuators to control the electrode gap distance. An electronics assembly would measure the voltage drop of the electrode gap and subtract the value from a constant setpoint voltage, producing an error signal. This error signal was sent to mechanical hydraulic valves. Typically, the valves were a simple three way valve or a proportional valve. The three way type valves could move the hydraulic ram at a constant velocity forward, backward, or not move at all [9]. The more advanced proportional valves would move the ram at a velocity proportional to the error signal. One example of this type of primitive EDM controller is shown in Figure 2.15. In this application a filter was developed to create a signal adequate for use in the controller. A RC-type power supply was used in this machine.

This first generation of on-off and proportional controls worked, but had limited material removal rates. The primary drawback with these types of control and actuation is the slow response of the hydraulic positioning system. Eventually electrical actuators replaced the hydraulic actuators. Electrical actuators could interface with the control electronics directly so the control loop response time was greatly reduced.

Most EDM machines in use today use servo motors, stepper motors, and linear motors. Linear motors are preferred in many applications because they have very high acceleration rates in comparison to their rotary counterparts. Unfortunately, fast response time is not the only characteristic that makes a good EDM controller.

EDM control is often difficult because the large changes in the nature of the electrode gap as the electrode progresses into a workpiece. These large changes in the process require robust controls systems. In die sinking EDM, as the electrode plunges into the workpiece, the surface area of the electrode engaged with the workpiece generally increases as time goes on. This change in surface area changes the way that the electrode gap acts. In addition, as the tool plunges deeper into the workpiece it is more difficult to flush the dielectric fluid into the electrode gap. These changing factors require a robust control system to maintain constant discharges.

The PID (Proportional-Integral-Derivative) type controllers are often considered a general purpose controller. P, PI, and PID type controllers have all been using in EDM applications [13,14].

2.4   Twin Wire Arc Spray Process

A search was made of arc processes that use two wire electrodes in a steady-state process to produce particles. The twin wire arc spray process is a coating process that does just that. In the spray arc process an arc is struck between two wires inside a spray gun. The spray gun is designed so that a high velocity jet of air shoots through the arc. The arc heats the metal wires. The molten metal is atomized by the jet of air. After being atomized the air jet propels the molten metal particles toward a target. Once the molten droplets collide with the target they flatten and quickly solidify. The objective of the process is to coat the target with the material that the wires are made of. These coatings vary from only a few thousandths of an inch, to one quarter of an inch thick. The process can be used to repair wear surfaces, or coat non-metallic objects. When the
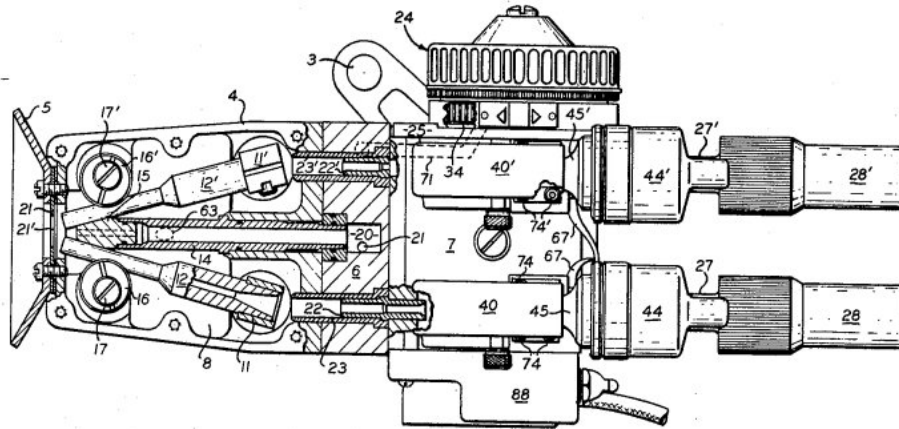
Figure 2.16: Twin Wire Spray Arc Gun [16]

process is used to repair a metal part the resulting coating is machinable but not as strong as the base metal mostly due to the porosity of the coating.

Figure 2.16 shows a drawing of a twin wire spray arc gun. Feed rollers similar, to those used in a wire feed welder, are used to feed the wires into the nozzle of a gun as the wires melt and become shorter. The wires are fed into the gun at the same rate, often by the same motor. Some of these processes simply feed the wire into the gun at a constant rate; however, more recent versions use the arc voltage as a feedback signal in a closed loop wire velocity controller [15]. These closed loop controls provide more reliable spray arc systems.

One of the main areas of research and invention with respect to the process is the method of aligning the wires in the nozzle [16, 17]. If the wires are not properly aligned they could not come into contact and the arc would never strike. Even if the wires do touch but are not well aligned, the process is unstable.

The twin wire spray arc process produces an arc in air. The dielectric strength of air is much lower than deionized water. This means that the arc gap is many times longer than a similar energy arc in deionized water. The longer arc does allow the process to be stable with small miss-alignments in the wires. In addition, in air the thermal conductivity is much less than water making it more likely that all the wire in the region of the arc will melt and be atomized. If wire alignment is a problem in the spray arc process, then it should be expected that wire alignment will be a significant problem in water where the conditions are less favorable.

28

Figure 2.17: Vibrating Reaction Chamber [1]

2.4.1   Arc Spray Power Supply

It is worth noting that the spray arc processes have used serval different kinds of power supplies. The power supplies used have been both DC and AC types of constant voltage and constant current types. Most of these power supplies have been welding power supplies, or very similar to welding power supplies. Most modern spray arc machines use a constant current power supply [15], especially those with voltage based wire velocity feedback controls.

2.5   Particle Generation With Pulsed Discharges

In 1987, A. E. Berkowitz et al. reported a method of using spark erosion to generate ultra-fine particles [1]. This method uses an RC-type power supply to generate random electrical discharges between large chunks of materials that are vibrated between two electrodes. Figures 2.17 and 2.18 show the configuration of the process. A bucket shaped reactor made of delrin is filled with chunks of the material that the particles are to be generated from. The large chunks are packed loosely between the two electrodes that are connected to the RC-type power supply. The reactor is filled with a dielectric fluid. The reactor is vibrated and the power supply is turned on.

The vibration causes randomly occurring gaps to form between the chunks of material. A high voltage power supply is used so that several discharges can occur in series. The vibration
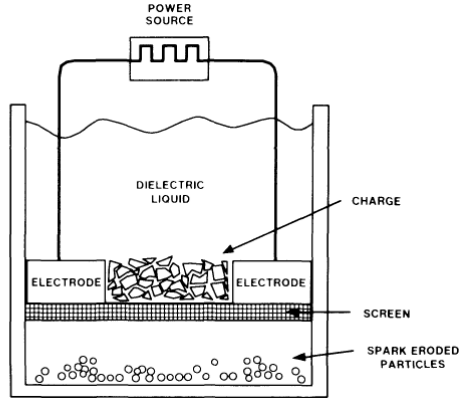
Figure 2.18: Schematic of the Vibrating Process Chamber [1]
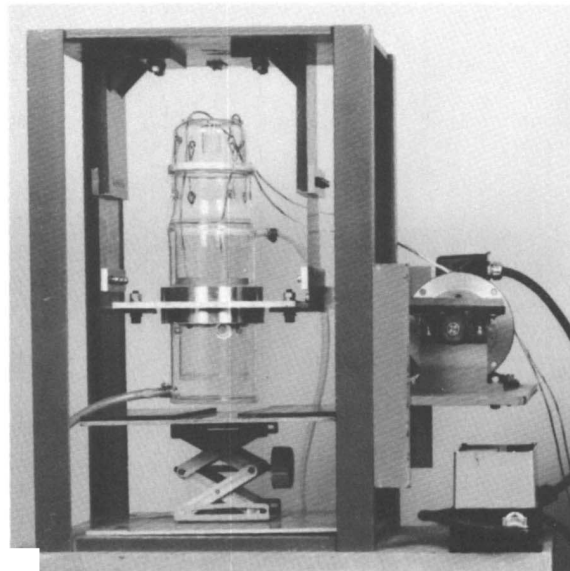
Figure 2.19: Vibrating RC-type Particle Generator [1]

results in random discharges between the electrodes through the large chucks and the gaps between them. Figure 2.19 shows the machine used to vibrate the reactor.

This is a practical method to produce multiple discharges in series. However, the method does produce a somewhat wide distribution of particle sizes. Figure 2.20 shows the relationship between the percentage of particles produced under 20 μm as a function of the power supply voltage for an iron based alloy eroded in water. Under optimal operating conditions only 50% of the particles produced are under 20 μm. Berkowitz et al. explain that the size of the particles
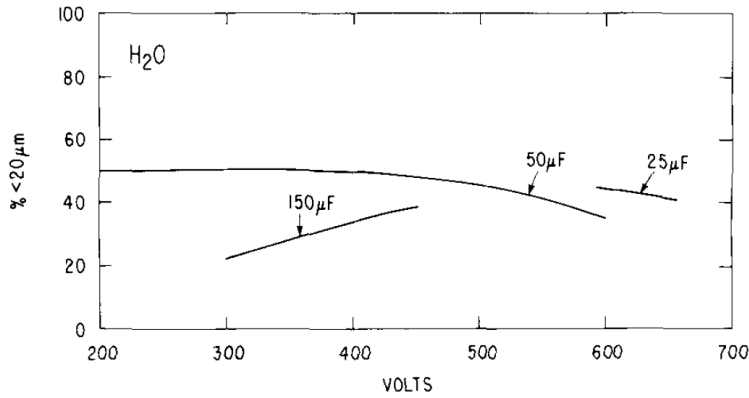
Figure 2.20: Relationship Between Voltage and % of Particles Under 20 μm. [1]
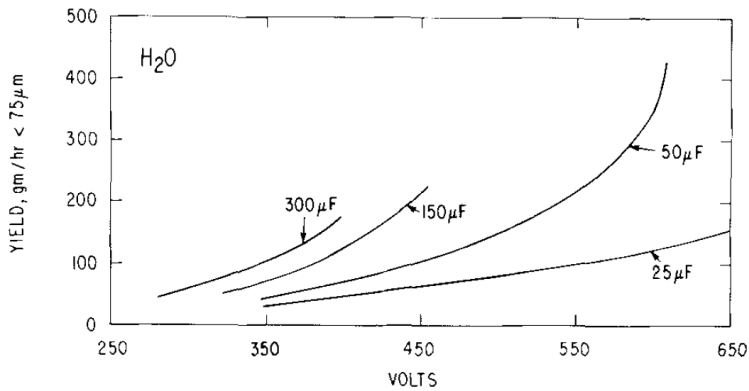
Figure 2.21: Relationship Between Voltage and Erosion Rate [1]

produced is mainly a function of the energy in the discharge. It is seen from the graph that as the voltage and capacitance are reduced, the particle size increases.

Figure 2.21 shows the relationship between voltage and the rate of erosion with the same iron based alloy as shown in Figure 2.20. From this graph it is seen that as the voltage, or energy stored in the capacitor, increases the rate of production increase. Also, as the capacitance increases at the same voltage the production rate also increases. In the case of this iron based alloy the erosion rate of 400 g/hour is possible with 40% of the particles being produced under $20\mu m$.

Berkowitz et al. also studied the amount of power required to create the iron based particles. It was determined that to produce 77 g/hour of particles less than 20 μm, 20 kW h/kg of energy is required.

31
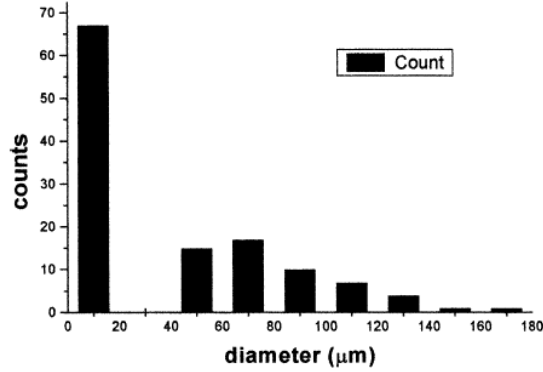
Figure 2.22: Size Distribution of U-Mo Particles [19]

It is suggested that the iron based particles produced in this process are useful in applications for creating magnetic films [1, 2]. Cabanillas et al. continued by applying the same principle to generate uranium-molybdenum particles [18, 19]. These experiments were performed in a plunge EDM machine using deionized water as a dielectric. The electrodes for these experiments were 6mm rods cast from an alloy of 90 wt% U and 10 wt% Mo.

The electrodes were eroded in a plunge EDM with 25 amps of current. The rate of erosion was 3.4 g/hour. The size distribution of the particles is a bimodal distribution as shown in Figure 2.22. The smaller particle distribution is centered at 10 μm and the larger particle distribution is centered at about 70 μm. The particle composition was analyzed using energy dispersive spectrometry. The resulting particles were found to be made of two materials. There is a thick outer shell of uranium oxide and a nucleus of the original U-Mo electrode materials.

2.6   Carbon Particle Generation with an Arc

Horvath and Gangl produced a new power supply for the production of carbon particles with a size between 10 and 100 nm [20]. The method is very similar to those previously discussed except the process is performed in an environment of nitrogen rather than water. Because the particles are produced in an inert gas, only carbon particles are created.

Figure 2.23 shows the typical RC-type power supply that can be used to generate the carbon particles. Horvath and Gangl designed a power supply that decouples initiation of the spark and
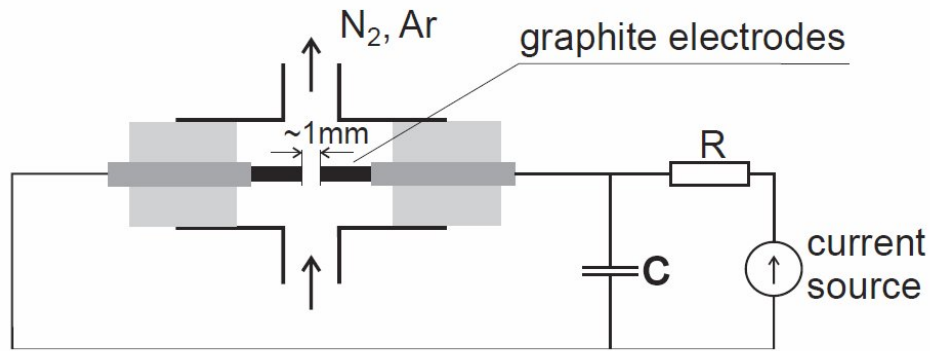
Figure 2.23: RC-type Carbon Particle Generator [20]

the discharge. As a result the electrode gap distance, the energy of the discharge, and the frequency of the sparks can be varied independently.

Figure 2.24 shows a new power supply design for this application. This new power supply has two parts. First, the low voltage RC portion of the power supply is the same as the original power supply. One of the main problems with the old supply is that a high voltage of several thousand volts was required to cause breakdown in the gap. Once breakdown occurred, only 100 to 200 volts are required for the discharge to continue. The new power supply uses a low energy pulse through a Tesla transformer to generate a high voltage, high frequency arc across the electrodes. This Tesla arc only lasts for just a moment, but is enough to cause breakdown to occur between the electrodes. Once breakdown occurs the main capacitor can discharge to create the carbon particles. Figure 2.25 shows these two stages of the process. Figure 2.25(a) shows the Tesla spark, and Figure 2.25(b) shows the discharge from the capacitor.
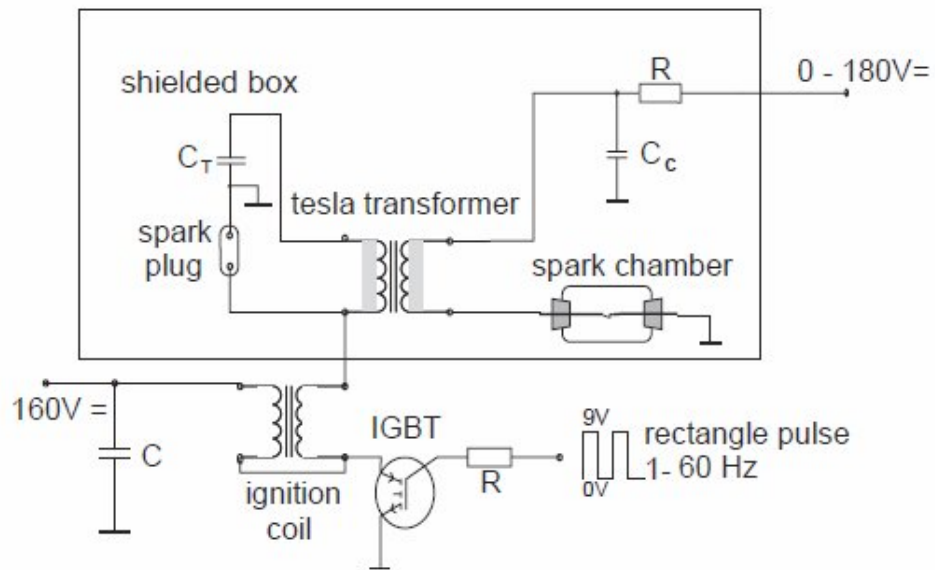
Figure 2.24: Tesla Type Power Supply [20]
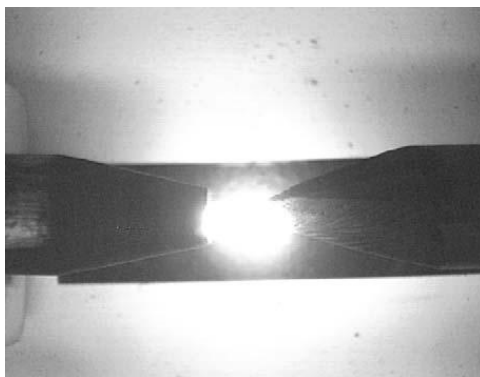
(a) Tesla Arc
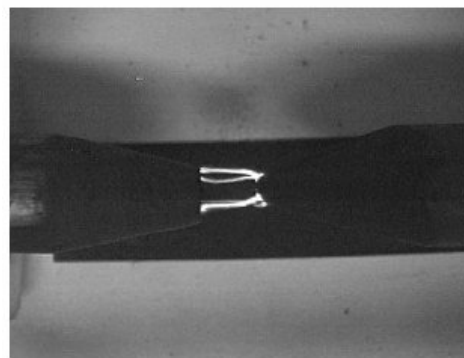
(b) Capacitor Discharge

Figure 2.25: Arc Produced with the Tesla Type Power Supply [20]

CHAPTER 3.   PRELIMINARY EXPERIMENTATION

Several preliminary experiments were performed to better understand how the pulsed wire process should be designed. Originally the goal of the research was simply to create a new variation of the rod process that used wire feedstock rather than rods. While attempting to create this new wire feed process, it was discovered that using a pulsing current across the electrode rather than a constant current had several advantages. This chapter briefly describes these preliminary experiments and the results from these experiments.

The first experiment involved an attempt to create a twin wire process prototype. A prototype was created to determine if a welding power supply could be used with two wire electrodes rather than rod electrodes. The prototype demonstrated that a welding power supply is not the optimal power supply for use with wire electrodes. The details are discussed in section 3.1. Also, the twin wire prototype showed that it is very difficult to align two wire electrodes and maintain a stable continuous process.

The second set of experiments used an RC EDM type power supply along with manual control to test the feasibility of pulsed EDM like power supplies. This experiment was created to determine if the EDM like pulsed power supply would create ultra-fine particles. The results of the experiment show that ultra-fine particles were produced, and that the process could be controlled to provide consistent results.

The third set of experiments was performed using a drill EDM machine. The experiments were performed to answer three questions. First, what is the average size and the statistical distribution of the size of particles created? Second, what is the erosion rate of the process using an EDM type pulsed power supply? Third, is the process able to be sustained over long periods of time? The results of the experiments show that all three of these questions were answered favorably. The process is controllable, the erosion rate is higher than the erosion rate of the rod process, and particles with a small average size were created with a small distribution of particle size.

In addition to answering the above three questions, the drill EDM experiments also showed that the settings on the power supply could be set so that the cathode electrode has a near zero erosion rate. This near zero wear rate can be used in solving the electrode alignment problem. Rather than using two wires, a single wire could be used as the anode and a larger electrode, like a flat plate, could be used as the cathode. Because the cathode is large in comparison with the wire anode, there is no need for close alignment of the electrodes. The advantages of this configuration will be discussed later.

The remaining sections of this chapter will discuss these three preliminary experiments as well as the results of the experiments. The results of these experiments provide a foundation for the development of the pulsed wire process.

3.1 Twin Wire Process Prototype

Inspired by the twin wire spray arc process discussed in Section 2.4 a set of experiments was performed to test the feasibility of using two wires as electrodes. A Constant current welding power supply was used in the twin wire prototype. Up to this point EDM type power supplies had not been used in the process. In fact, the twin wire prototype provided major motivation to move away from the use of a welding power supply toward pulsed DC power supplies like those used in EDM processes.

3.1.1 Twin Wire Experimental Setup

Figure 3.1 shows a CAD model of the prototype manufacturing process. Each of the wire feed assemblies shown feeds a wire through a copper tube. The copper tube guides and conducts electricity to the wire. The copper tubes are partially flexible and can be bent to align the wires at different angles with respect to each other. The wire feed assemblies are mounted above a glass tank filled with deionized water. The copper wire guide tubes were positioned so that the electrode gap is under water.
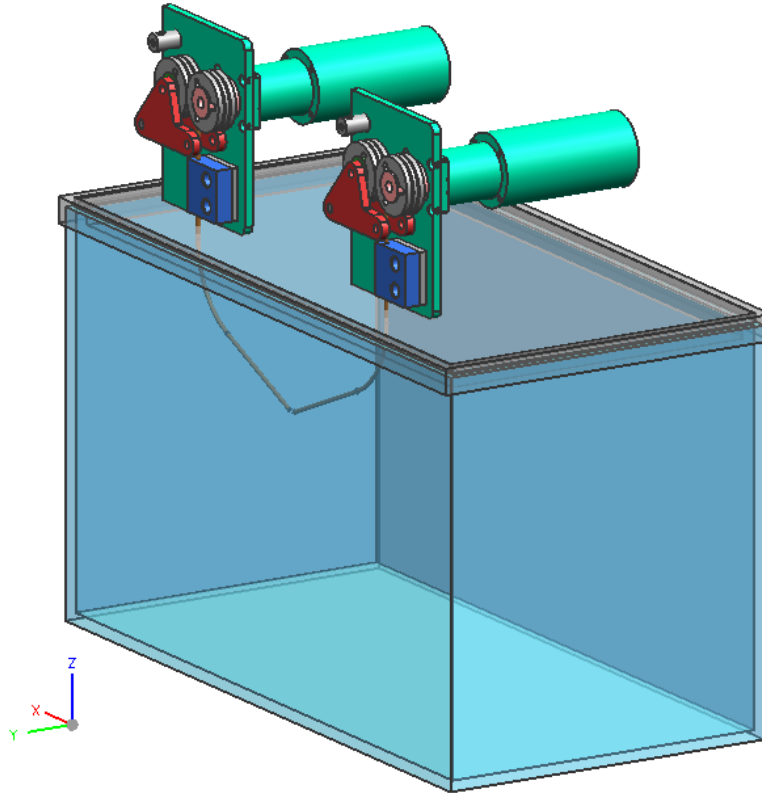
Figure 3.1: Twin Wire Prototype

3.1.2 Twin Wire Control System

The position of the wires was controlled by two DC servo motors. The servo motors drive the wires with drive rolls through a planetary gearbox with a 40:1 reduction ratio. The positioning resolution of the drive mechanism is just under one ten thousandth of an inch (.0001 inches). A micro controller was used to control the position of the servo motors with a PID feedback loop based on the electrode gap voltage.

3.1.3 Twin Wire Results

The twin wire prototype was used to experiment with several current settings from 5 to 60 amps. For each current setting and wire orientation the PID control parameters were tuned to attempt to create a stable arc between the wires. Unfortunately, a stable reaction was not realized for any power setting. The welding power supply could be used in two modes, a TIG mode for

currents from 5 to 30 amps, and a stick welding mode for current from 30 to 250 amps. At low currents in the TIG mode, an arc was only created when the wires separated after touching. When the wires separated, a very brief spark would be created, but an arc could not be sustained.

After there was no success using the power supply TIG mode, the stick welding mode was used. In this mode when the wires would touch, the power supply would provide a very large surge current causing about one quarter to one half inch of metal from each electrode to nearly instantly melt and fall to the bottom of the tank. When the controller was optimally tuned this behavior would be repeated several times a second. The wires would touch, a high current arc would melt the wires, and then the motors would advance the wires causing them to touch and the process to repeat.

The large surge current that causes the wires to melt is a result of the design of the welding power supply. It became apparent that it would be difficult to use this type of power supply in a process that uses wires as electrodes. It is believed that the welding type power supply works well with the rod process because the mass of the rods is much higher than the wires allowing them to adsorb the energy of the high current surge when an arc is struck.

3.2   Manual EDM Experiments

Because the results using a welding power supply with wire were poor it became apparent that if wire electrodes were to be used successfully, a different kind of power supply would be needed. EDM pulsed type power supplies are a natural replacement in this situation. EDM applications often use very small electrodes with good results. A prime example of this is the wire EDM process. The wire EDM process uses very small diameter wires in the range of 0.005 inches to 0.015 inches to machine conductive materials at relativity high current. Even though the wire is very small, it can endure the high energy pulses used to erode the workpiece. The key is that pulses are used rather than a constant current.

A simple low power, RC-type, power supply like those shown in Section 2.3.2 was prototyped to examine the feasibility of pulsed EDM power supplies as a power source in the process. The prototype power supply uses a set of DC power supplies in series to produce a constant voltage supply adjustable between 40 and 120 VDC. A power resistor with a resistance of 50 ohms and

several capacitors with capacitance values ranging from 2 to 50 μF were used in the prototype power supply.

The electrode gap distance was controlled manually. The cathode electrode was attached to a fixed base and the anode was mounted on the carriage of a linear slide. The electrode gap was controlled by moving the carriage of the linear slide toward or away from the cathode electrode. The electrodes were submerged in deionized water as usual. It is difficult to align two wire electrodes in this kind of manual test, so a wire electrode, the anode, and a plate electrode, the cathode, were used. Wire electrodes of various diameters ranging from 0.125 inches to 0.01 inches were tested with the RC type power supply. Creating a sustained set of pulses between the electrodes that would last several seconds before the electrode gap grew too large was easily achievable with all the wire diameters used in the test. The capacitor could be switched to a different value and the change in spark frequency could be heard. Also, as higher capacitance values were used, the erosion rate of the electrodes was increased. The higher capacitance value effectively increased the power in each pulse, increasing the rate of erosion.

In addition to stability of the arc, it was clear that small particles were being generated because a visible dark cloud of particles was seen being dispersed from the electrode gap while the sparking was stable. These particles were small enough to remain suspended in the water.

When the capacitor is removed from the circuit the power supply becomes a simple current limiting power supply similar to the welding power supply previously used. This simple current limiting power supply does not have any energy storage elements to create a high current surge like the welding power supply produced. In general, it was difficult to create sustained discharges without the capacitor in the circuit. There was one special case where a stable set of discharges could still be easily maintained. If a thin flexible foil electrode was used in combination with a wire as the other electrode, as shown in Figure 3.2, an interesting thing happened. The pressure wave created by the arc is enough to cause the foil electrode to deflect away from the wire electrode acting like a switch interrupting the flow of current.

Figure 3.2(b) shows the foil electrode starting to deflect, as the discharge continues the foil electrode continues to deflect. Figure 3.2(c) shows that the deflection of the foil electrode becomes large enough to interrupt the discharge. Once the discharge has been interrupted and the pressure wave is dissipated, the foil electrode returns to its original position and another discharge is started.

(a) Small Gap Just Prior to the Discharge

(b) Discharge Occurs, Pressure causes the foil Electrode to Deflect

(c) The Deflection of the Foil Becomes Large Enough to Interrupt the Discharge
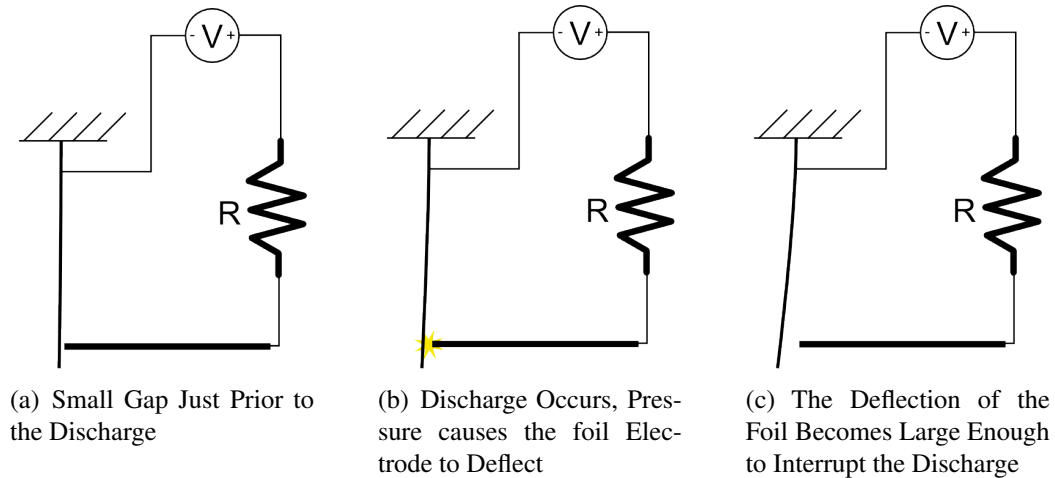
Figure 3.2: Pressure Wave Actuated Switching System

Thicker foils cause the frequency of this reaction to increase because the higher stiffness results in a higher spring back force. In the case of this configuration the power supply in combination with the electrodes are acting like a resistive switching power supply.

There are no energy storage elements in the circuit, unlike with the welding power supply, so there is no surge of current at the start of a discharge. The resistor simply limits the current preventing the thin electrodes from instantly being melted. The success of these experiments prompted further development with a power supply of the EDM type.

3.3   EDM Drill Experiment

Because the first experiments with the RC type EDM power supply were performed manually it was difficult to produce consistent particles for analysis. Analysis of the particles is important to determine particle size and distribution. In addition to particle analysis, the EDM Drill experiments were performed to estimate what power supply setting would produce an optimal erosion rate. A drill EDM machine was used to generate particles for analysis. A drill EDM was chosen rather than a sinker EDM because the drill EDM already has a system to align and guide small diameter round electrodes. In addition, the control system and power supply used in drill EDM processes are generally simpler.

Figure 3.3: Current EDM CT300F Drill EDM

The EDM drill used is a Current EDM CT300F seen in Figure 3.3. In this machine the tool electrode is the cathode and the work electrode is the anode. The machine uses tubular electrodes to erode holes in the workpiece. While eroding the hole deionized water is pumped through the tubular electrode to flush the eroded particles out of the electrode gap. This machine uses a servo motor to control the electrode gap between the electrode and the workpiece. The tool electrode is also rotated about its axis during the process. This rotation helps keep the process running smoothly and prevents uneven wear on the electrode.
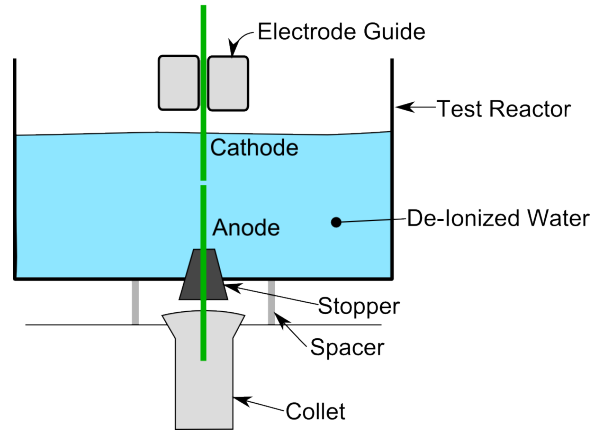
Figure 3.4: Drill EDM Experiment Electrode Configuration Diagram

3.3.1 Geometry of the Electrodes and Fixtures

In these experiments two wires are used as electrodes. The anode wire is clamped in a collet fixture and connected to the power supply. The cathode wire, from here on called the tool, is clamped into the tool chuck on the upper end of the machine. This tool chuck is connected to the negative side of the power supply. The tool is then lowered through the tool guide. The tool guide is used to keep the tool electrode centered in the hole during the process. This arrangement is shown in Figures 3.4 and 3.5.

To prevent contamination with other particles and to easily collect particles, a test reactor is used to hold a small amount of deionized water. The anode electrode enters this reactor through a rubber stopper on the bottom end. The tool electrode simply enters the reactor though the open top. The tool electrode is positioned directly above the anode electrode. Because the tool electrode is not tubular, deionized water cannot be pumped through it to flush the electrode gap. Non-optimal performance of the process can be expected due to the poor flushing conditions.

3.3.2 Power Supply and Control System

This particular EDM drill uses a fuzzy logic controller to maintain the electrode gap distance. The fuzzy controller is useful in this application because the electrode cuts a deep hole into the workpiece dramatically changing electrode gap conditions. The exposed area between the electrode and the workpiece increases changing the electrode gap resistance. As the hole gets
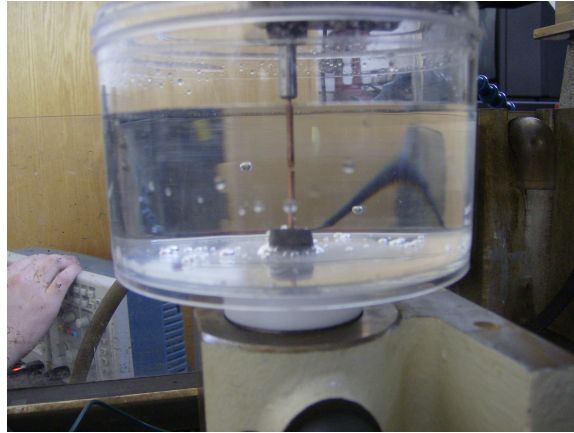
Figure 3.5: Drill EDM Experiment Reactor and Electrodes

deeper it also becomes much more difficult to flush out the eroded particles from the hole. These two changes in the process will require the controller to provide different motion dynamics to match the changing conditions. A fuzzy logic controller can sense changes in the process like poor flushing conditions and temporarily increase the electrode gap distance to flush the gap. Once the flushing conditions are better, the controller is returned to normal operation.

The company that manufactures the EDM drill was not willing to provide any details about the EDM power supply in the CT300F. However, by inspection the basic operation of the power supply is clear. Figure 3.6 shows a simplified schematic of the power supply in the EDM drill. The CT300F power supply uses a transistor to switch the electrode gap current on and off. A resistor bank in series with the electrode gap is used to limit the current across the electrode gap. The part of the power supply operation that is not clear is how the power supply and the controller interact to generate the pluses that turn the transistor on and off. The power supply does have settings for the pulse t_{on} and t_{off} times. It is unclear if the t_{on} time starts counting at the moment that the switch is turned on, or from the start of the discharge.

3.3.3 Experimental Process

A statistical screening experimental design was used to determine the what settings and parameters effect wire erosion rate using the EDM machine. The design used is a screening design for up to 8 variables. The design can be used to estimate what factors will have a significant effect on the rate of wire erosion. The design variables in the design are the Peak Current, Tool electrode
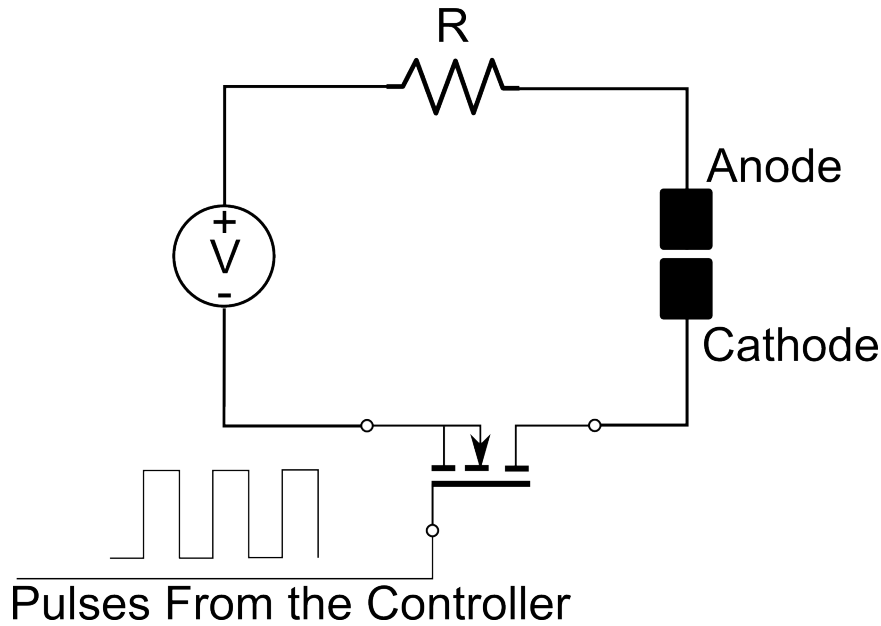
Figure 3.6: Drill EDM Power Supply Simplified Schematic

rotation rate, electrode diameter, t_{on}, and t_{off}. The order of the experiment was randomized to reduce the influence of uncontrolled variables. Prior to each run the wire electrodes were massed and the tips were ground flat. The reactor was drained, cleaned and filled with 500 mL of clean deionized water between each run. For each run the electrodes were mounted and aligned in the machine and the machine was run at the given settings for 4 minutes. Then the electrodes were removed from the machine and massed again to determine the erosion rate of each electrode.

3.3.4   EDM Drill Experiment Results

Table 3.3.4 shows the design and the response variable of the erosion rate for each run. The results of the experiment show that the peak current, electrode diameter and the electrode material are all significant factors that effect the rate of erosion. The rate of erosion increases as current and diameter increase. It is very likely that the t_{on} and t_{off} parameters have a significant effect on the rate of erosion, but the values were not changed enough to see a change in the rate of erosion.

One important note to make at this point is the rate of erosion of the cathode electrode. During the experiments with the EDM machine, the cathode has a near zero wear rate. In some high setting where the t_{off} time is short the cathode electrode actually grows over time. The twin

Table 3.1: EDM Drill Experimental Design and Results

Factor	Peak Current (Amps)	RPM	Diameter (inches)	Electrode Material	t_{on} (μs)	t_{off} (μs)	
High Setting	57	5	0.125	A	40	25	Erosion Rate
Low Setting	12	0	0.0625	B	35	20	(g/hour)
1	-1	-1	-1	-1	-1	-1	0.30
2	1	-1	-1	-1	1	-1	1.32
3	-1	1	-1	-1	1	1	0.24
4	1	1	-1	-1	-1	1	1.68
5	-1	-1	1	-1	1	1	0.78
6	1	-1	1	-1	-1	1	3.96
7	-1	1	1	-1	-1	-1	0.60
8	1	1	1	-1	1	-1	3.42
9	-1	-1	-1	1	-1	1	0.54
10	1	-1	-1	1	1	1	8.58
11	-1	1	-1	1	1	-1	0.30
12	1	1	-1	1	-1	-1	5.04
13	-1	-1	1	1	1	-1	0.90
14	1	-1	1	1	-1	-1	12.42
15	-1	1	1	1	-1	1	0.36
16	1	1	1	1	1	1	12.78

wire experiment showed that it would be difficult to align two wire electrodes and create a stable reaction. If the cathode electrode experiences near zero wear rates, then only one consumable electrode is needed. If the anode wire electrode is fed toward an electrode that is significantly larger than the diameter of the wire then fine wire alignment is no longer needed. The cathode electrode only needs to be large enough to prevent the wire electrode from missing it.

From the data it was concluded that a pulsed DC EDM type power supply is well suited for the particle generation process. Particles in an acceptable size range were generated at a reasonable rate.

The particles generated at the optimal erosion rate were analyzed using a scanning electron microscope, SEM, to determine particles size and distribution. Figure 3.7 shows a micrograph of the particles generated using 0.0625 inch diameter wire at 57 peak amps of current. The particles generated are smaller than those generated using the rod process with an average size of 200 nm with a range of plus or minus 70 nm. Also the distribution of particles size is very tight in comparison to that of the rod process.
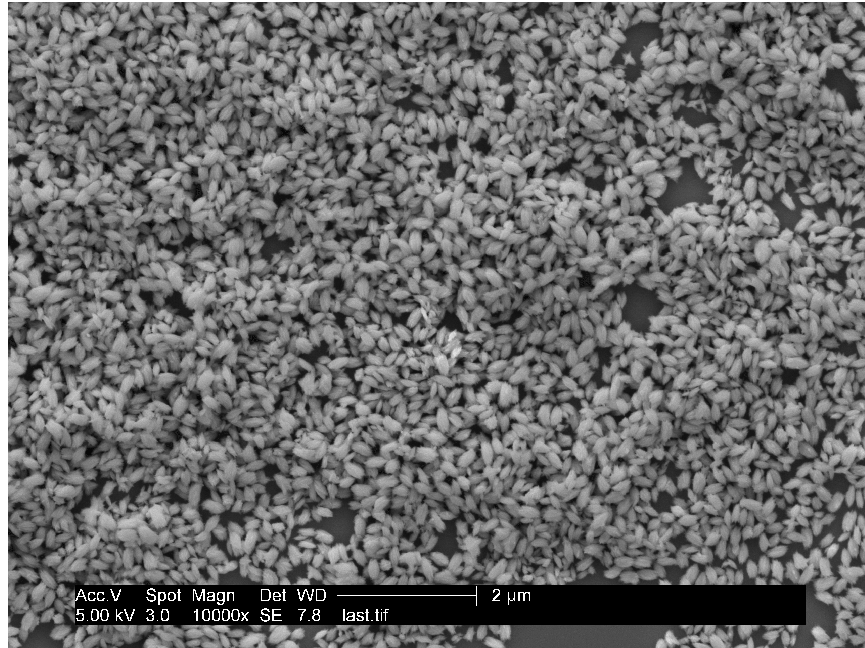
Figure 3.7: Micrograph of Particles Produced With the Drill EDM

These results show that using a pulsed DC power supply like those used in EDM processes will produce particles with a smaller average size and a much tighter distribution of particle size than those created with the rod process. Even though the EDM drill is successful in producing ultra-fine particles there are some reasons not to use an EDM machine for the production of particles.

EDM machines are optimized to maximize the rate or workpiece erosion and to produce fine surface finishes. Similarly, a machine designed to produce ultra-fine particles should be optimized to maximize the rate of erosion, or in other words the rate of particle production. In contrast, when generating particles there is no concern for the surface finish of the electrodes, only the quality of the particles being produced. EDM power supply settings that result in fine surface finishes usually have low material removal rates. When producing particles if there is no concern for the surface finish of the electrodes, it may be possible to produce small particles at a high rate using different power supply settings and control strategies than those of EDM. If an EDM machine were used to produce particles it would be difficult to modify the controller and power supply to determine if this is possible. By designing a machine specifically for the production of particles,

46

both the controller and the power supply can be designed to produce high quality particles at a high rate.

EDM machines also are quite costly due to the additional features that would not be used in particle production. EDM machines usually include dielectric filtration systems and dielectric chillers. A particle production machine may also require a chiller and a dielectric filtration system, but the chiller and filter system in the EDM machine could not be used because they include metallic components that are incompatible with the particles being produced. EDM machines also have CNC controllers, additional axes of motion controls, and other subsystems. These subsystems only add to the cost of the EDM machine without any added benefit with respect to particle production.

Because wire will be used as the electrodes in the pulsed wire process, a wire feed mechanism would also have to be integrated into an EDM machine to replace the linear actuator used to control the electrode gap distance. The base cost of the EDM machine, plus the replacement of all the metal components in the fluid system, modification to the controller and new wire feed system will result in a higher cost machine than a machine designed specifically to produce particles.

CHAPTER 4. DESIGN OF THE PULSED WIRE PROCESS

This chapter discusses the design of the pulsed wire process. The pulsed wire process is discussed in context of a specific embodiment of the process that is used to create ultra-fine copper and copper oxide particles.

4.1 Pulsed Wire Process Design

In light of the results of the three experiments discussed in Chapter 3, as well as experience from previous research, it was clear that a process with a pulsed power supply would be more likely to perform well with wire electrodes than with a constant current power supply. The manual and drill EDM experiments showed that current pulses rather than a constant current create a more stable process. Also the pulsed EDM like processes have the advantage of near zero cathode electrode growth or erosion. Near zero cathode growth provides the possibility of needing only one consumable electrode.

The twin wire experiments showed that if two identical diameter wire electrodes are used, the alignment of the wires must be very good to have a stable process. If the wire alignment is not good, then only a portion of the wire cross section is eroded wasting that portion of the electrode. The wire misalignment also creates a condition where the electrodes will touch while passing by each other creating a shorted condition.

To avoid alignment problems wire is only used for the anode electrode. The cathode electrode can have any topology that has a cross section significantly larger than the wire electrode. If the cathode electrode is large in comparison to the wire anode electrode, then the cathode electrode could then be considered to be a flat plate. Wire alignment issues are not a problem in this case because even with large variations in the diameter and alignment of the wire electrode the wire electrode will never miss the flat plate electrode. Figure 4.1 shows the case were the wire anode electrode is well aligned with the cathode electrode. Figure 4.2 shows the case were the alignment
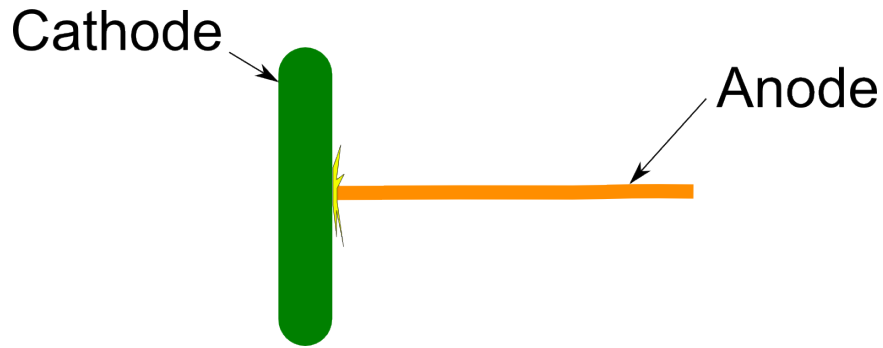
Figure 4.1: Pulsed Wire Process Electrodes (Well aligned)
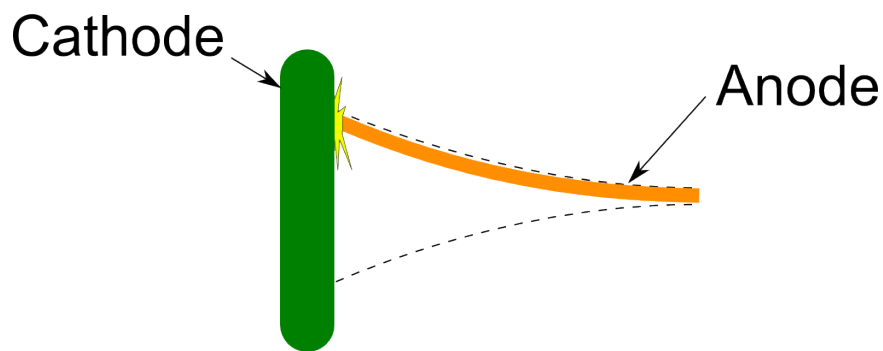
Figure 4.2: Pulsed Wire Process Electrodes (Poorly aligned)

of the wire anode electrode is aligned to the cathode electrode poorly. Because the cathode electrode is large in comparison to the anode electrode the cross section of the anode will still be totaly eroded.

The pulsed wire process uses a closed loop anode electrode motion control system. Stable, closed loop motion control is required to maximize the rate of erosion in the process. Both EDM process, and the rod processes show that the stability of the motion controller is key to maximizing the rate of erosion. Typically, the average electrode gap voltage drop is measured to estimate the electrode gap distance and close the motion control loop.

The pulsed wire process is defined as a process that uses a pulsed DC power supply creating current pulses between a flat plate electrode and a wire electrode whose position is controlled using a closed loop motion control system where the average arc gap voltage is used as the feedback signal.

A process machine was designed and constructed to prove the process and better understand how it compares to the rod process. The rest of this chapter discusses the machine built to use the pulsed wire process.

4.2 Mechanical Design of the Pulsed Wire Process

The mechanical design of the machine in terms of particle production can be split into two parts; the design of the reactor, and the design of the wire feed system. The design of these parts of the mechanical design has changed significantly as a result of the information gained during the development of the process.

Some of the key requirements the mechanical design must accomplish are the following:

- The new machine must use an anode in wire form

- The machine must be able to run continuously for long periods of time

- The machine should limit the need for frequent operator adjustment

- Seals in the reactor must be eliminated

The development of the mechanical portion of the process was completed at the same time that the idea of using a single wire electrode with a flat plate cathode electrode rather than two wires was developed. As a result, the reactor and the wire feed system can use two wires, or a wire anode electrode and a larger cathode electrode.

4.2.1 Reactor Design

One of the most time consuming maintenance requirements for the rod process is the replacement of the seals in the reactor. Because the rods are constantly rotating and translating, the seals and the bearings used in the reactor frequently need to be changed. Even when new seals were installed in the reactor the dielectric fluid still leaked out due to variations in the diameter of the rods and misalignment of the rods.

One of the major goals of the pulse wire machine was to eliminate the need for seals or bearings in the reactor. Wire is compliant and can be bent to turn a corner in the reactor unlike the

Figure 4.3: Reactor Tub Design

rod electrodes. An open top basin was used so that the wires could enter from the top without a need for seals. Figure 4.3 shows the layout of the pulsed wire reactor. The wire electrodes enter the top of the reactor guided by a Teflon tube. The Teflon tube is formed into a curve by a slot in the wire feed plate. As the wire is fed through the Teflon tube, it is bent into an a circular arc until the wire is horizontal and perpendicular to the flat plate electrode.

Because the electrodes enter from the top of the reactor and then are bent inside the reactor, no seals are required. The Teflon tubes will wear over time and will need to be replaced, but the replacement of the tubes is easy and will only be required one or twice a year rather than daily.

The design shown in Figure 4.3 was developed prior to the decision to use a flat plate cathode electrode. The reason for using a flat plate cathode electrode is to eliminate the need for close alignment between the electrodes. The wire used as the anode is copper wire with a diameter of .0625 inches. A second wire electrode with a diameter of .25 inches was used as the cathode electrode. The diameter of the cathode electrode is 4 times the diameter of the anode electrode; this makes the cathode electrode effectively a flat plate in comparison to the anode electrode. The cathode electrode is stationary, and the anode wire is fed using the wire feed system.

The dielectric fluid enters the reactor through a tube that flushes the dielectric gap and fills the reactor. The fluid exits the reactor through an overflow pipe as shown in Figure 4.3 (black pipe). The fluid that exits through the overflow pipe is drained into a 10 gallon storage tank. The fluid entering the reactor through the fill tube is pumped out of the same storage tank. The water in this closed loop system is recirculated till the concentration of particles in the fluid is high enough. After the concentration of the particles is high enough, a low flow rate peristaltic pump starts to remove fluid from the storage tank. A float valve in the storage tank keeps the fluid at the same level by adding clean deionized water. At steady-state conditions the concentration of the particles in the fluid is nearly constant and the fluid leaving the system leaves at the same concentration.

4.2.2 Wire Feed System

The ideal feed mechanism for wire feedstock in a continuous process is friction drive roller like those used in wire feed welders. The drive roller is ideal because it can feed an infinitely long wire without any pauses or interruptions. A set of U-Groove drive wheels from a Miller wire feed welder were used in the machine so that the rollers would be off-the-shelf components. The diameter of these drive rollers is about 1.6 inches.

Because the electrode gap in the process is very small, on the order of a few ten thousandths of an inch to a few thousandths of an inch, high resolution positioning of the electrodes is required. Also, the backlash of the positioning system must be low to prevent a large delay when the direction of motion is changed. To provide the fine resolution motion required a micro-stepping stepper motor along with a 10:1 gearbox was used to drive the roller. The stepper motor was driven with a 256 micro stepping controller that results in a theoretical 102,400 steps per revolution. With the 10:1 low backlash gear box there are approximately 200,000 steps per inch, or 0.000 005 inches per step.

The drive roller needs to be electrically isolated from the stepper motor because the electrical current is transmitted into the wire through the drive roller. To isolate the motor from the drive roller, a timing belt with Kevlar bands is used to transmit the torque from the gearbox to the drive roller. The timing belt electrically isolates the motor and the roller but introduces some torsional flexibility into the system.

Because the system has friction, stiction, torsional flexibility, and other effects the expected resolution of the wire positioning system is expected to be somewhat less accurate than 5 millionths of an inch per step of the motor. The resolution is expected, however, to be smaller than the electrode gap. It has been confirmed by experimentation that the resolution of the system is well under one ten-thousandth of an inch (.0001 inches).

4.3   Power Supply

The results of the experiments discussed in Sections 3.2 and 3.3 show that a pulsed DC power supply similar to those used in EDM machines is an appropriate match for the pulsed wire process. Pulsing the current across the electrode gap limits the length of the discharge time in the process. When the length of the discharge time is limited, the maximum particle size is also limited. Limiting the maximum particle size has a significant impact on the distribution of particle size.

The design chosen for the pulsed wire process power supply is a simple current limiting pulsed DC power supply. This design is very similar to the design used in the drill EDM described in section 3.3. Figure 4.4 shows the basic concept for this type of power supply. The power supply design uses a resistor to limit the current across the electrode gap. The resistor is a passive element so no active feedback loop is needed to provide a constant current. Ohm's Law is used to determine what resistance is needed for a given voltage and current.

There are three states that should be considered during the design of this type of power supply. The first state is the short circuited state where the electrodes are touching. Ideally the machine will never be in this state, but it is nearly impossible to completely prevent the electrodes from shorting out. Using Ohm's Law the current can easily be determined and is shown in Equation (4.1). This is the maximum current that can be expected in the system. Equation (4.2) shows the power dissipated by the resistor in this shorted state. The power dissipated by the resistor is very significant and is the largest loss in the power supply. This is because the resistor limits the current in the circuit by converting electrical power to heat. All the components in the current loop should be selected to handle the shorted current for an indefinite period. Failure to select components that will indefinitely handle the shorted current could result in failure of the power supply, or worse an electrical fire.
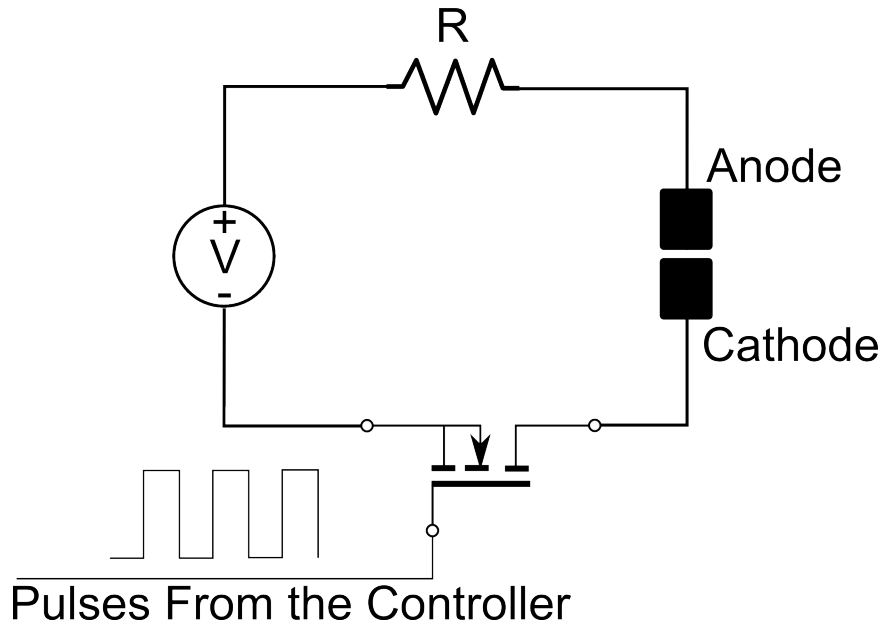
Figure 4.4: Pulsed Wire Process Power Supply Concept Schematic

$$I = V_{source}/R \tag{4.1}$$

$$P_{resistor} = IV_{source} \tag{4.2}$$

The second state that needs to be analyzed is the current during a discharge. Typically, once the discharge has started the voltage across the electrodes will be between 18 and 26 volts depending on the electrode gap distance. For the design of this power supply the electrode voltage drop, V_{gap}, will be assumed to have a value of 22 volts. Equations (4.3), (4.4), and (4.5) show the current, power dissipated by the resistor, and the power delivered to the electrode gap, respectively. The current and power dissipated by the resistor is less in this discharge state compared to the shorted state. The rate of wire erosion is roughly proportional to the average power delivered to the electrode gap. Because the current in the gap is constantly being switched on and off, the duty cycle of the process must be considered. The duty cycle is the ratio of t_{on}/t_{off}, or in other words the percent of the time that the current is flowing through the gap. The average power delivered to the electrode gap is shown in Equation (4.6).

55

$$I = (V_{source} - V_{gap})/R \tag{4.3}$$

$$P_{resistor} = I(V_{source} - V_{gap}) \tag{4.4}$$

$$P_{gap} = IV_{gap} \tag{4.5}$$

$$P_{gap-average} = IV_{gap}(t_{on}/t_{off}) \tag{4.6}$$

The final state that should be considered is the open circuit state. In this state the electrodes are far enough apart to prevent a discharge from forming. In this state only a small leakage current through the dielectric fluid is flowing through the circuit. The voltage between the electrodes at this time will be the voltage of the constant voltage power source. This open circuit voltage should be high enough to ionize the dielectric in the gap at a reasonable gap distance. If the voltage is too low, then the correct gap distance will be very short and difficult to maintain. The maximum gap distance at which the dielectric will deionize will increase as the open circuit voltage increases. However, as the open circuit voltage increases the power dissipated during the discharge stage increases making the power supply less efficient. Based on a survey of EDM machines in use, and experiments with the EDM process, the open circuit voltage of 80 volts DC was chosen.

Based on the experience gained with both the rod process and the EDM experiments a current range of 16 to 64 amps of peak current was chosen as reasonable current settings for the process. To provide this current range with an open circuit voltage of 80 VDC, a range of resistances between 3.5Ω and 0.875Ω are required. Table 4.3 shows a table of four peak current settings from 16 to 64 amps peak current along with the required resistance and required heat dissipation due to the resistance. These four peak current settings will use 3.5 Ω resistors in parallel to obtain the correct resistance. A setting of 16 amps requires a single 3.5 Ω resistor. Similarly, a current setting of 32 amps requires 1.75 Ω, or two 3.5 Ω resistors in parallel. The 48 amp current setting requires 3 resistors in parallel and the 64 amp current setting requires 4 resistors in parallel. A 3.5 Ω, 1000 watt power resistor was selected in order to provide enough heat dissipation for the application.

The power supply design requires an electronic switch to handle the high frequency switching of the load. A set of N-channel MOSFET transistors were selected for the supply. N-channel

Table 4.1: Required Resistance Values and Related Power Dissipation

Peak Current (Amps)	Resistance (Ω)	Power Dissipated (Watts)
16	3.5	896
32	1.75	1792
48	1.17	2688
64	0.875	3584
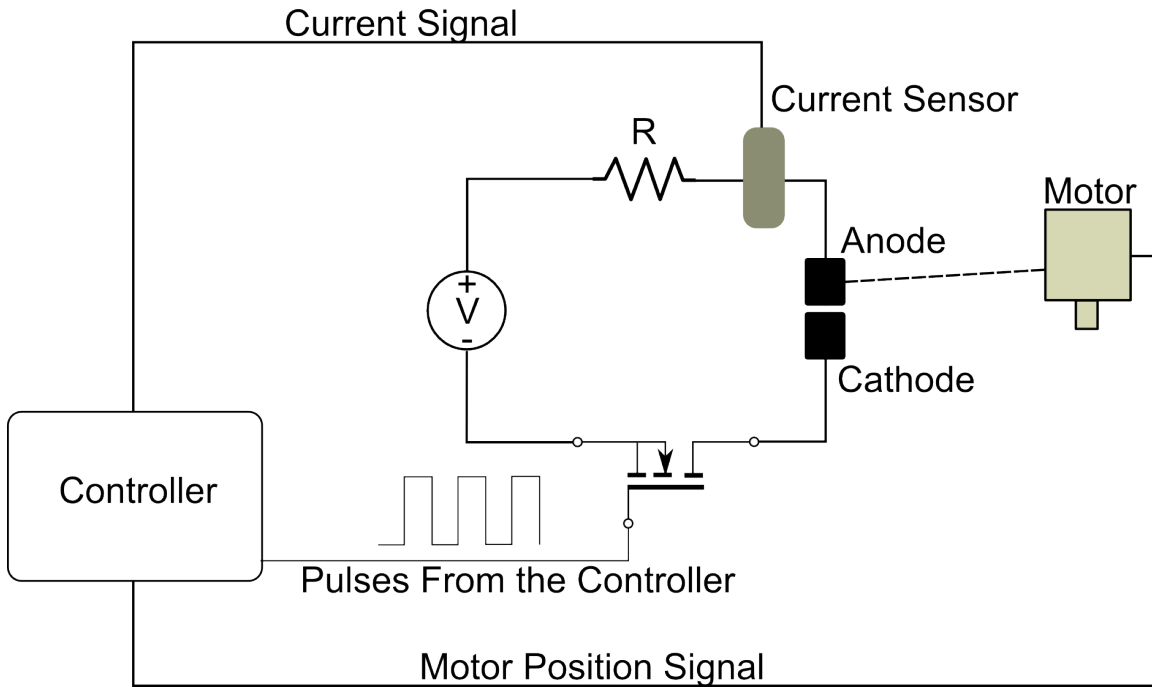
Figure 4.5: Pulsed Wire Process Electrical Schematic

MOSFET transistors were used in the power supply due to their low cost, high switching speed, and low on resistance. A MOSFET gate driver was also selected to improve the switching characteristics and reduced the switching losses of the transistors.

The power supply design requires a constant voltage source of 80 VDC. A custom made toroidal transformer was used to convert three phase 208 VAC power to three phase 55 VAC power. A three phase full bridge rectifier was then used to rectify the power into a DC voltage. An LC input filter was used to filter the rectified DC voltage to a nearly constant voltage of 80 VDC. The LC filter acts as a buffer between the erosion process and the three phase AC input. The entire power supply design is shown in Figure 4.5.

4.4 Design of the Control System

The control system for the pulsed wire process is very important. The control system uses measurements from the process to make corrective actions to the wire position, stabilizing the process. One important note is that overshoot (when the controller feeds the electrode too close together) should be avoided to prevent shorting the two electrodes. In addition, the rise time, or the time it takes to reach the setpoint, should be minimal to quickly react to disturbances in the system.

The electrode gap discharge is difficult to model accurately. The electrode is constantly changing in length, and the relationship between the electrode gap distance and the electrode gap voltage drop is quite non-linear. However, to roughly determine what kind of controller should be used, and what the optimal parameters are expected to be, a simplified model is sufficient.

A simplified model of the electrode gap can be described in terms of the electrode gap distance and the electrode gap voltage drop. As the electrode gap distance increases the electrode gap voltage increase. This relationship, although non-linear, can be approximated as a linear relationship. The input for this model is the electrode gap distance, and the output is the electrode gap voltage. The distance where the dielectric fluid just begins to breakdown is the distance where the electrode gap voltage will be equal to the open circuit voltage of the power supply. This data point is seen in Figure 4.6 as point A. The electrode gap distance and the voltage both decrease until the electrode gap is zero (electrodes shorted) and the discharge voltage is zero. The y-intercept of this model is zero and the slope of the line is $\frac{BreakDownDistance}{OpenCircuitVoltage}$. The open circuit voltage of the power supply used in the machine is 80 Volts. The breakdown distance is shown in Equation (4.7). Typical values for the dielectric constant are from about 500 to 8 kV/inch depending on the frequency and electrode shapes. This means that the line is in fact the dielectric constant of the fluid. The resulting linear model for the electrode gap is shown in Equation (4.8). If the electrode gap is to be modeled as a transfer function, where gap distance is the input and gap voltage is the output, then the transfer function is simply a constant, specifically the dielectric strength of the water.

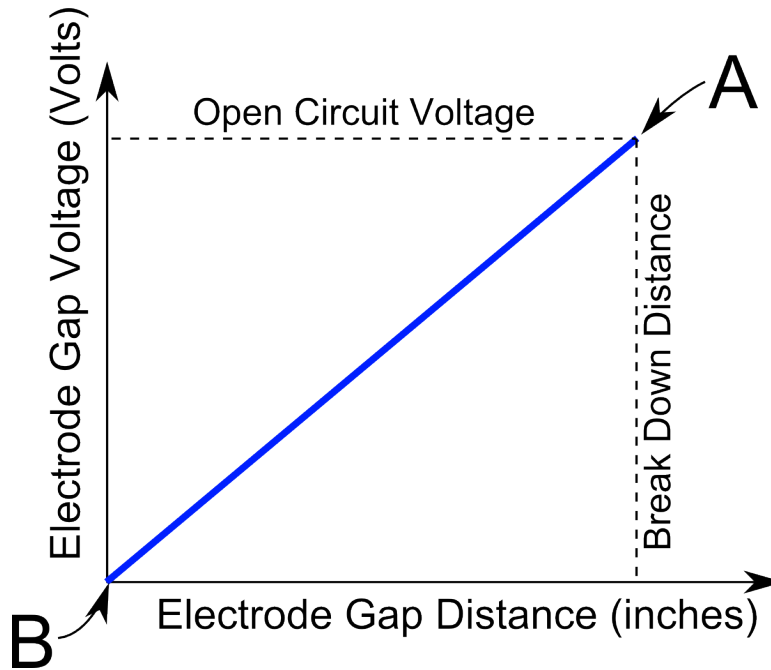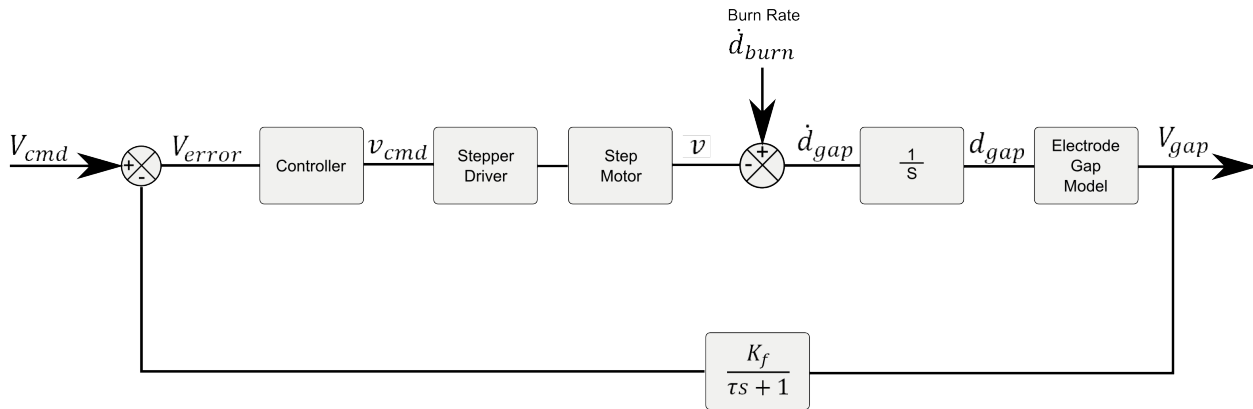Figure 4.6: Linearized Electrode Gap Model

Figure 4.7: Control System Block Diagram

$$D_{BreakDown} = \frac{V_{OpenCircuit}}{C_{dielectric}} \quad (4.7)$$

$$V_{gap} = E_{ds}D_{gap} \quad (4.8)$$

Figure 4.7 shows the block diagram of the pulsed wire process. Figure 4.8 is a diagram of the definition of x, d_{gap} and d_{burn}. The electrode gap distance is affected by both the wire feed
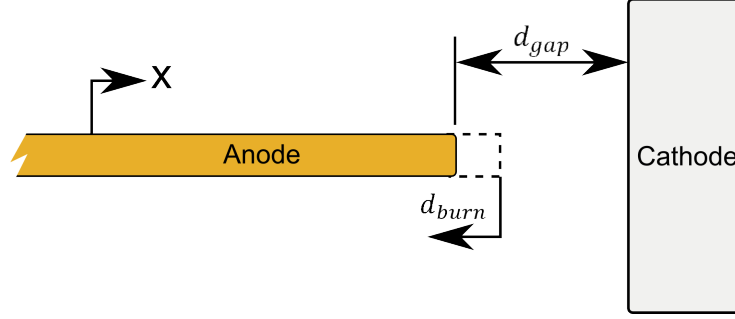
Figure 4.8: Variable Definitions

velocity, v, and the anode electrode burn rate, $\dot{d}_{burn}$. The stepper motor position is defined as x in Figure 4.8 and the stepper motor velocity is defined as v. The controller commands a velocity, and the stepper motor driver determines the step and direction pulses to make the motor move at the commanded velocity. The transfer function for the stepper motor and the motor driver is 1. In this model the anode electrode burn rate is modeled as a disturbance.

$$\dot{d}_{gap} = -v + \dot{d}_{burn} \tag{4.9}$$

$$d_{gap} = d_o - x + \int \dot{d}_{burn} \tag{4.10}$$

To determine what type of controller is needed several simple analysis were performed. First, an analysis was performed assuming that the controller is a simple proportional controller and ignoring the low pass filter on the feedback loop. If this is the case then the transfer function with commanded voltage as the input and the gap distance as the output is shown in Equation (4.11) where K_p is the proportional gain. Using the final value theorem to test for steady-state error shows that with no disturbances there is no steady-state error with a step input at V_{cmd}. Figure 4.9 shows the general shape of the expected response with a step change in V_{cmd}.

$$\frac{d_{gap}}{V_{cmd}} = -\frac{K_p E_{ds}}{s - K_p E_{ds}} \tag{4.11}$$

$$\frac{d_{gap}}{\dot{d}_{burn}} = \frac{E_{ds}}{s + K_p E_{ds}} \tag{4.12}$$
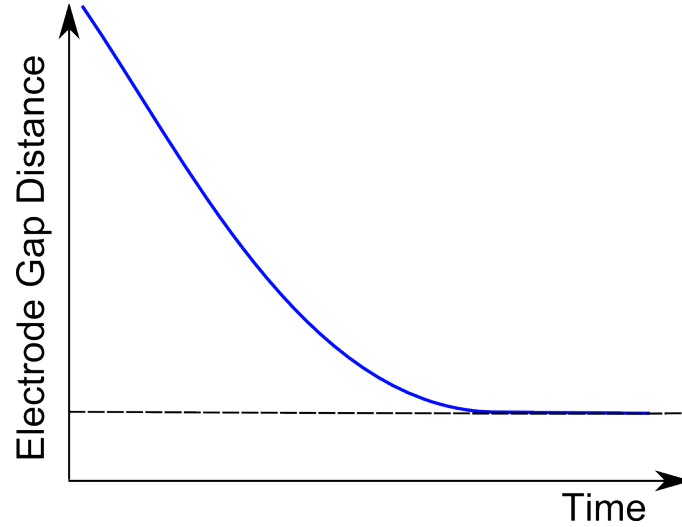
Figure 4.9: Ideal System With Proportional Controller

The effect of the electrode burn rate on the electrode gap distance is also very important. Equation (4.12) shows the transfer function for the electrode gap distance over the electrode erosion rate. Once again the final value theorem was used to determine if there is any steady-state error due to a step change in the input. The final value theorem showed that there is steady-state error due to a step change in the rate of erosion. The steady-state error due to a step change in the rate of erosion is $-1/Kp$. As the gain is increased the steady-state error is reduced but not eliminated. This shows that a simple proportional controller is not ideal for controlling the pulsed wire process.

$$\frac{d_{gap}(s)}{V_{cmd}(s)} = \frac{-E_{ds}K_p s - E_{ds}K_i}{s^2 + E_{ds}K_p s + E_{ds}K_i} \tag{4.13}$$

$$\frac{d_{gap}(s)}{\dot{d}_{burn}(s)} = \frac{E_{ds}}{s + K_p E_{ds}} \tag{4.14}$$

Next, the system was analyzed with a PI (proportional integral) controller. The low pass filter in the feedback loop has still been ignored. The addition of the integral term adds the ability to eliminate steady-state error from a step change in the burn rate. Equation (4.13) shows the transfer function for the electrode gap distance with the command voltage being the input. Equation (4.14) shows the transfer function for electrode gap distance with the rate of erosion disturbance as the input. The final value theorem was used to determine the steady-state error with a step change in the electrode rate of erosion. The result using the final value theorem is that the steady-state error
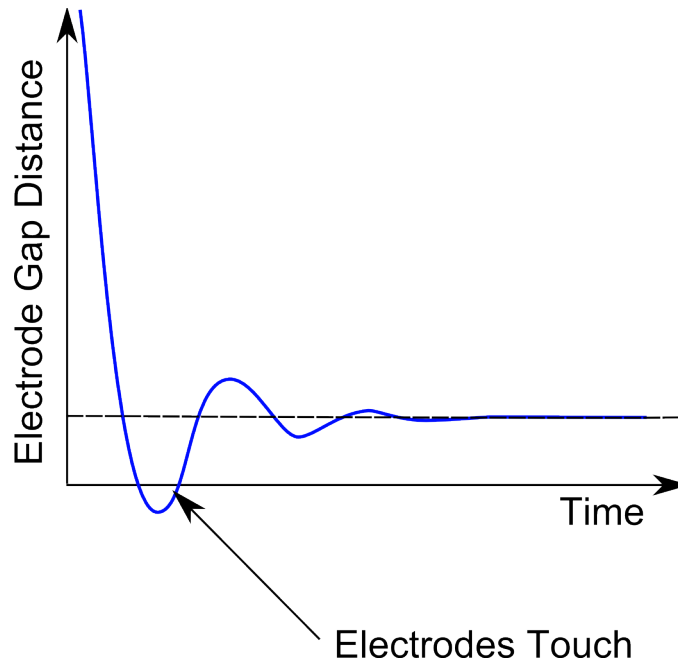
Figure 4.10: Response to a Step Change in $\dot{d}_{burn}$ with a PI controller

is zero. Figure 4.10 shows the general shape of the electrode gap response to a step change in the $\dot{d}_{burn}$ input; notice the oscillation and the overshoot.

Using a PI controller provides the ability to reject disturbances with the proportional term and eliminate steady-state error with the integral term. However, neither of these terms provides any damping to prevent the electrodes from shorting due to overshoot. Simply adding a derivative term to the controller and using a PID controller gives the ability to add damping to the system and reduce overshoot to prevent electrode shorting. Figure 4.11 shows the general shape of the response of the electrode gap distance using a well tuned PID controller. The steady-state error is eliminated by the integral term, the overshoot is reduced using the derivative term, and the disturbance rejection is high due to the large proportional term.

The arc discharge voltage wave form is similar to a square wave. The voltage should only be measured during a discharge. During the time between pulses the electrode gap voltage is zero. In the prototype machine a low pass filter was used to average the electrode gap voltage over many pulses. Because the electrode gap voltage is known and constant when the current is off, the changes in the voltage coming out of the low pass filter are only a function of the electrode gap voltage when current is flowing through the gap. The transfer function of a low pass filter is
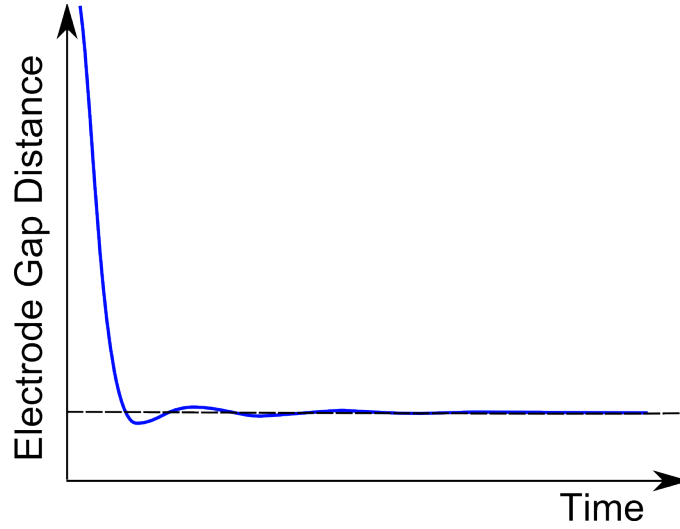
Figure 4.11: System Response to a Step Change in $\dot{d}_{burn}$ with a PID Controller

shown in Equation (4.15). Equation (4.16) shows the resulting closed loop transfer function. With the addition of the low pass filter, steady-state error is no longer zero. The steady-state error of the electrode gap distance due to a step change in V_{cmd} is zero if the low pass filter gain, K_f, is 1. The steady-state error due to a step change in burn rate is still zero. Ideally each pulse could be measured individually rather than using a low pass filter to estimate a moving average.

$$\frac{K_f}{1 + \tau s} \tag{4.15}$$

$$-\frac{\left(E_{ds}\,K_d\,s^3 + E_{ds}\,K_p\,s^2 + E_{ds}\,K_i\,s\right)\,\tau + E_{ds}\,K_d\,s^2 + E_{ds}\,K_p\,s + E_{ds}\,K_i}{s^3\,\tau + \left(1 - E_{ds}\,K_d\,K_f\right)\,s^2 - E_{ds}\,K_f\,K_p\,s - E_{ds}\,K_f\,K_i} \tag{4.16}$$

In addition to the motion controller a power supply controller was used to control the power supply transistors, switching the current across the electrode gap on and off. The motion controller controls the motion of the wire electrode. The power supply controller is implemented on an 8-bit micro controller connected to the power supply, and the motion controller is implemented on a PC running a real-time Linux operating system.

The power supply controller uses software timers to turn the power supply transistors on and off after the selected t_{on} and t_{off} times have expired. In addition, the power supply controller

detects when the discharge stage has started. The start of the discharge stage is detected by the fall of the electrode gap voltage below 40 volts. A comparator is used to compare the electrode gap voltage to a reference of 40 volts. When the electrode gap voltage falls bellow 40 volts the power supply controller senses the output from the comparator and the timer is reset and starts counting. Once the timer reaches the t_{on} time the transistors are turned off, and the current across the electrode gap is stopped. The counter is reset again and starts counting until the timer reaches the t_{off} time. At this point, the transistors are turned on again and the controller once again waits for the discharge to start.

It is important to wait for the discharge to start before starting to count the t_{on} time in order to produce pulses with equal energy. The discharge does not start immediately after the transistor is turned on. There is time required to ionize the dielectric and start the discharge stage of the reaction. If the timer were to start counting as soon as the transistor is turned on then the delay time would be counted as part of the t_{on} time reducing the length of the actual discharge. The power supply controller was implemented in software so that the configuration could easily be changed as the process changes in the course of its development.

The motion controller handles all the complex control of the process. The controller is built around an open source Linux based CNC software suite called the Enhanced Machine Controller, or EMC. This suite of software uses a robust real-time Linux operating system to close feedback loops in the operating system. The controller implemented in the pulsed wire process uses a few subsystems from the EMC suite.

Two PCI interface cards were used to connect the PC to the pulse wire machine. An FPGA (Field Programable Gate Array) based motion control card was used to provide digital I/O and to output the step direction signals to a stepper motor controller. The second interface card provides several analog to digital converters. The voltage and current signals are acquired using the analog to digital PCI card, processed by the controller on the PC. This controller calculates a new position for the motor. The EMC software produces a smooth motion path to the new position with limits on velocity and acceleration. The FPGA card then produces the step direction signals for the stepper motor controller to change the position of the stepper motor. The stepper motor changes the position of the electrodes to correct the electrode gap distance.

4.4.1 Voltage and Current Sensing

Great care was taken to electrically isolate the discharge power supply from all the control systems in the machine. This isolation is to provide safety to the operator and to reduce noise and offset in the voltage and current signals.

In the original design of the pulsed wire process, the electrode gap voltage was measured, converted to a digital signal, transmitted through optical isolation, converted back to an analog signal, and finally converted into a digital signal by the analog to digital PCI card in the PC. Unfortunately, several filtering and aliasing problems were produced with this configuration due to the signal being converted from analog to digital two times at two different rates. The signal was required to be converted from analog to digital twice because the analog to digital converter in the computer was not electrically isolated from the discharge power supply.

The way the current across the arc is sensed is fundamentally different from the way that the voltage was sensed. The current transducer used in the machine uses the hall effect principle to indirectly measure the current in a wire by measuring the magnetic field induced into a metallic ring in the current transducer. Because the transducer only measures the magnetic field produced by the current in the wire the signal it produces is already electrically isolated from the discharge power supply.

Because the power supply uses passive resistance to limit the current in the circuit if the current across the resistor is known, then the voltage across the resistor is also known. Also, if the voltage across the resistor is known, then the voltage across the electrode gap is also known. This means that only one of the two parameters of voltage and current really need to be measured.

Using Ohm's law for the resistor the voltage drop across the resistor at any given instant of time is given in Equation (4.17) as a function of the instantaneous current i. The only other element in the circuit is the electrode gap, so the remaining voltage must be across the electrode gap as shown in Equation (4.18), where the open circuit voltage of the power supply is V_d. The current transducer measures the average current, $\bar{i}$ over several discharges so the remaining terms must also be expressed as an average value. The average open circuit voltage $\bar{V}_d$ is shown in Equation (4.19), and the resulting average gap voltage, $\bar{V}_{gap}$, is shown in Equation (4.20).

$$V_r = iR \tag{4.17}$$

$$V_{gap} = V_d - V_r \tag{4.18}$$

$$\bar{V}_d = V_d \left(t_{on}/t_{off} \right) \tag{4.19}$$

$$\bar{V}_{gap} = \bar{V}_d - R\bar{i} \tag{4.20}$$

Using the relationship shown in Equation (4.20) the signal from the current transducer can be used to calculate the average electrode gap voltage. This reduced the number of signals to be measured and increases the reliability of the process. In practice this strategy has worked well.

4.4.2 PID Controller Adequacy

Spark erosion processes like the EDM process are known to be difficult to control. The process is difficult to control due to the changes in the electrode gap conditions. As a tool electrode burns into the workpiece, the dynamics of the electrode gap change. Adaptive controllers like fuzzy logic controls will detect changes in the process and react by changing the dynamics of the controller to improve the process control. In EDM processes, changes in the electrode gap are common due to several factors.

For example, in plunge EDM as the electrode erodes the workpiece the surface area between the tool and the workpiece in the electrode gap increases, changing the dynamics of the electrode gap. Also, as the electrode continues to burn deeper into the workpiece the dielectric flushing conditions are degraded. Changes in the flushing conditions can change the temperature of the electrodes, or resulting in frequent electrode shorting due to eroded particles being trapped between the electrodes. Adaptive fuzzy logic based controllers work well in EDM processes because they are able to detect changes in the system and react by changing the dynamics of the control law to compensate for these changes in the system.

In contrast, the electrode gap conditions in the pulsed wire process change very little over time due to the very near zero rate of erosion of the cathode and the constant cross sectional area of the anode wire. The geometry of the electrodes don't change significantly over time. Because the

electrode gap conditions are nearly constant there is no need for a sophisticated adaptive controller. When a more sophisticated controller is used when a simple controller is adequate it is often more difficult to implement and tune the complex controller. Because of this, a simple PID controller was developed to control the pulsed wire process.

Because an adequate dynamic model of the process is not available to select the proportional, integral, and derivative terms, heuristic tuning rules were used to select the P, I, and D terms. Rough settings for the controller were determined using the ZieglerNichols [21] method. then the parameters were hand tuned until the controller performance was acceptable.

4.5 Optimization of the Pulsed Wire Process Parameters

One of the main objectives of this research is to reduce the cost of manufacturing ultra-fine particles. The wire process with a pulsing power supply is expected to produce smaller, more consistent particles faster than the rod process. To meet this goal, the optimal settings of the power supply and controller should be determined. The plasma arc process is very difficult to model from first principles due to the complex interactions of electrical, magnetic, thermal, and chemical phenomenon. If a model of the process were created from first principles, experimental data would still be required to validate that model. Designed experiments were used to create a predictive model of the process. The predictive model is then used to select the optimal process settings to maximize the rate of production for a target particle size range.

4.5.1 Model Variables and Outputs

In this research there are three response variables of interest, the rate of electrode erosion (particle production rate), the average particle size, and the variance of the particle size. The possible factors that can effect these response variables are shown in Table 4.2. The frequency and duty cycle experimental variables are another way of stating the t_{on} and t_{off} times. The duty cycle term is simply t_{on}/t_{off}, and the frequency term is $1/(t_{on}+t_{off})$.

Due to the design of the power supply the open circuit voltage is fixed at 80 volts, so the open circuit voltage will not be considered in the experiments. It is known that a higher open circuit voltage would allow the electrode gap to be increased at the cost of more energy being lost

Table 4.2: Response Variables and Possible Experimental Variables of The Experiment

Response Variables	Possible Experimental Variables
Rate of Erosion	Peak Current
Average Particle Size	Frequency
Variance of Particle Size	Duty Cycle
	Dielectric Flow Rate
	Open Circuit Voltage
	Dielectric Conductivity
	Dielectric Temperature

to heat in the power supply. The experiments with the drill EDM machine show that the process will be stable with an open circuit voltage of 80 volts.

Several simple experiments showed that the process was more stable at low dielectric flow rates. This is likely due to the turbulence introduced into the electrode gap at higher flow rates. The turbulence in the electrode gap constantly change the electrode gap conditions resulting in a process that is difficult to control. Because of this effect on the process, very low to zero dielectric flow rates were used in the experimental procedure.

The concentrations of metal oxide particles in the deionized water were never increased to a level that would significantly change the conductivity of the dielectric water. In addition, when the processes is running at steady-state conditions the conductivity of the dielectric will be constant regardless of the other process settings. For these reasons the dielectric conductivity is also eliminated from the list of experimental variables

The rod process produced a large amount of energy from the arc that was converted directly into heat increasing the temperature of the dielectric fluid in the system. The change in dielectric fluid temperature was enough to require a chiller to be installed in the system to keep the fluid at a reasonable temperature. This same effect was expected with the wire process, but the pulsed discharges in the pulsing wire process do not add a significant amount of energy to the fluid, unlike the rod process. Most of the energy in the pulsing wire process is used to create particles, and very little is used to heat the dielectric fluid. Because the temperature of the water does not change significantly when the pulsing wire process is used, all the designed experiments were performed with the water at room temperature. This eliminated the dielectric temperature as a design variable.

4.5.2 Impact of Motion Control Parameters

The PID motion control parameters will clearly have an impact on the response variables. The PID parameters affect the stability of the process. If the PID parameters are poorly tuned then the rate of erosion will be reduced, and the size of the particles will vary more due to the variation in electrode gap distance. It is possible to tune the PID parameters for every experiment performed on the machine. However, if the PID parameters were tuned for each setting, then the effects from the design variables and the PID parameters would be confounded. It would be unclear if the change in the output at a given setting is a function of the PID parameters, the design variables or any combination of the two.

To prevent the confounding of the PID parameters and the design variables in the experiment, the PID parameters are held constant for all experiments performed on the machine. A set of PID parameters was found that allowed the process to be reasonably stable in the range of the design variables used in the experiment. After the designed experiment have been finished and the optimal settings for peak current, pulse frequency, and pulse duty cycle are determined, the PID parameters for that setting can be fine tuned to increase the performance at the optimal settings.

4.5.3 Expected Form of the Model

The three remaining design variables are peak current, frequency, and duty cycle. These are the design variables used in the experiments to create predictive models of the process. From a theoretical standpoint these three parameters are expected to have the largest effect on the process. The rate of erosion is largely a function of the amount of power delivered to the electrode gap [1]. As more current is delivered to the gap, the rate of erosion is increased. Peak current, pulse frequency, and pulse duty cycle all will have a large effect on the average power delivered to the electrode gap. The average power delivered to the gap, $\bar{P}_{gap}$, is shown in Equation (4.21) and is clearly linear with respect to the average gap current $\bar{i}_{gap}$. Equation (4.22) shows the average gap current as a function of the peak current, the function $q(\omega)$, and the Duty Cycle.

$$\bar{P}_{gap} = \bar{V}_{gap}\,\bar{i}_{gap} \tag{4.21}$$

$$\bar{i}_{gap} = i_{peak}\,q(\omega)\,DutyCycle \tag{4.22}$$

The duty cycle and the peak current of the pulses clearly have a linear effect on the average power delivered to the gap. So it would be expected that the peak current and duty cycle would have a nearly linear effect on the rate of erosion.

The function $q(\omega)$ in Equation (4.22) is a correction function for the pulse frequency ω. The model of the power supply shows that the resistors and conductors in series with the electrode gap are purely resistive elements. In reality the resistors and conductors used in the power supply have some parasitic inductance and capacitance. So the resistor bank used in the power supply really should be treated as a complex impedance, Z, having both resistance and reactance. As the pulse frequency increases the effective resistance of the resistor bank increases decreasing the current delivered to the gap. This means that as the pulse frequency increases the rate of erosion will likely decrease.

The average size of particle produced in the process is expected to correlate with the surface finish of the workpiece in EDM processes. Parameters in an EDM process that result in fine surface finishes would be expected to produce small particles. Surface finishes in EDM machining are generally smoother when the current is decreased and the frequency is increased. This effectively creates more frequent, lower energy sparks in comparison to a higher current lower frequency setting. The lower current and higher frequency pulses will erode less material for each discharge reducing the probability of creating larger particles.

Little is known about what might effect the variance in the size of particles produced in the process. It would be expected that a lower variance in particle size would be expected when the process is more stable. That is to say when the electrode gap is well regulated and all the discharges produced are the same. It is difficult to guess at how the design variables might effect the variance of particle size.

4.5.4   Selection of a Designed Experiment

The objective of performing the designed experiment is to determine the optimal setting for the process to operate at. Because of this a RSM, or response surface methodology, design should be used. One constraint in the design is that the power supply can only be set to four equally spaced current settings of 16, 32, 48 and 64 amps. This eliminates the possibility of using a full central composite design that requires 5 parameter setting. The remaining two factors of pulse frequency and duty cycle can be set to any setting in a reasonable range.

There are two RSM designs that would be possible to use with three factors and the constraints on the current settings. The first is a faced centered central composite design. This design uses three factor levels in each factor. This design has high variance on the edges of the design space, but has nearly flat variance in the middle of the design space where the optimal parameters are expected.

The second possible experimental design would be and I-optimal design. This design is a computer generated design that selects treatments from a subset of the full factorial design space. The treatments are selected on the basis of D-optimality, or the determinate of the information matrix composed from the treatments selected. An I-optimal design was created for the experiment and was compared to the face centered central composite design.

Both designs have the ability to create a quadratic predictive model from the data. The face centered central composite design was favored over the I-optimal design because the variance of the design is lower and more constant though the center of the design space. The face centered central composite design is more commonly used so more tools are available to analyze it. Because of this the face centered central composite design was chosen over the I-optimal design.

4.5.5   Factor Levels

The factor levels in the face centered central composite design are linearly coded variables from -1 to 1. For each of the design variables, a maximum and minimum value must be selected to map to the coded factor levels. Table 4.5.5 shows the mapping between the coded factor levels and the values of the design variables. For the current design variable only four settings are possible and the higher settings are expected to be favorable so the higher three settings were selected.

71

Table 4.3: Mapping to the Coded Factor Levels

Coded Value	Current (Amps)	Pulse Frequency (kHz)	Pulse Duty Cycle (%)
-1	32	5	30
0	48	12.5	50
1	64	20	70

Table 4.4: Face Centered Central Composite Design

Treatment	Current (Amps)	Pulse Frequency (kHz)	Pulse Duty Cycle (%)
1	32	5	30
2	32	5	30
3	32	5	30
4	32	5	30
5	32	5	30
6	32	5	30
7	48	12.5	30
8	48	12.5	50
9	48	12.5	50
10	48	12.5	50
11	48	12.5	50
12	48	12.5	50
13	48	12.5	50
14	48	12.5	50
15	48	20	50
16	64	5	30
17	64	5	70
18	64	12.5	50
19	64	20	30
20	64	20	70

The maximum and minimum settings for the pulse frequency and duty cycle were selected to give extreme values that still result in a stable process. The process was run at each of the extreme setting to make sure that the process could operate stably at these settings. The resulting designed experiment is shown in Table 4.4. The design has 6 center points shown in the table as treatments 7-14. These six center point are used to estimate the variation in the system.

4.5.6 Experimental Procedure

Great care was made in the experiment to make sure than the operating conditions were the same for every run in the design. The order of the treatment was randomized to prevent background noise from being interpreted as a real parameter effects. Before each treatment was run the ends of the electrodes were flattened with a file and cleaned. The reactor was cleaned and filled with 4 liters of clean deionized water. Next, a marker was attached to the wire electrode next to a 5 cm scale. The maker was positioned so that the it points at the 5 cm mark on the scale. The reaction is started and the wire was eroded until the marker reaches the 0 cm mark on the scale. A stopwatch was used to measure the time required to erode the 5cm of wire. Care was taken to make sure that the particles in the fluid were well mixed and then one liter of fluid was collected in a vial for particle size analysis. The reactor was then cleaned and prepared for the next treatment. For each treatment in the experiment the rate of erosion was calculated based on the mass of a 5cm long wire and the time required to erode that length of wire.

The two remaining response variables, particle size and particle size variance, were measured using a Beckmann Coulter LS230 particle analyzer. Based on scanning electron microscopy the expected particle size range is from about 50 nm on the low end to about 50-100 μm on the high end. The LS230 instrument is a laser diffraction particle analyzer. Laser diffraction particle analyzers typically have a measurement range between 400 nm and 2000 μm. Laser diffraction methods will easily measure the larger particles but will be useless for measuring the smaller particles produced in the process. The LS230 has an addition PIDS (Polarization Intensity Differential Scattering) module for measuring particles from 40 nm to 800 nm.

The LS230 used was fitted with a small volume fluid module that requires only a 200 ml fluid sample. 200 ml of RODI(Reverse Osmosis Deionized) water was placed in the LS230 sample module and the machine was then calibrated and prepared to measure the sample. Then the container with the sample to be measured was shaken to disperse the large particles in the sample. A syringe was used to introduce fluid from the sample container into the LS230 sample module until the appropriate PIDS concentration was reached. A debubbling cycle was then run on the instrument to remove any air bubbles introduced in the sample chamber when the particles were introduced. The sample was then analyzed in three 90 second runs. The three runs were then averaged to produce single particle size histograms (see Appendix A).

Table 4.5: Second Composite Design (with Alpha points)

Treatment	Pulse Frequency (kHz)	Pulse Duty Cycle (%)
1	3.2	32.9
2	6.8	32.9
3	3.2	47.1
4	6.8	47.1
5	5.0	40.0
6	5.0	40.0
7	2.5	40.0
8	7.5	40.0
9	5.0	30.0
10	5.0	50.0
11	5.0	40.0
12	5.0	40.0
13	5.0	40.0

After the first designed experiment has been performed and the data analyzed, it became apparent that a second experiment would be required to properly characterize the rate of erosion in the process. This second experiment was required due to a lack of fit between the data and the predictive model created from the data. This lack of fit will be discussed further in Chapter 5. It was clear from the first experiment that the pulse current was a very significant factor. Additionally, it was clear that current has a positive effect on the rate of erosion.

Because current is now known to have a positive effect on the rate of erosion, and the objective is to find settings that will maximize the rate of erosion, the current was set at the maximum value for the second designed experiment. The two remaining parameters of frequency and duty cycle can be set at any reasonable value unlike the current setting that could only be set at 16, 32, 48, or 64 amps. With this greater flexibility a new design was selected for the second experiment.

A full central composite design with alpha points was selected for the second design. This design has 5 levels for each factor. In addition to changing the design for the second experiment the new design was centered around the expected maximum predicted from the first experiment. The design used for the second experiment is shown in Table 4.5.

The procedures for the second design were the same as the first. The results of both of the experiments are found in Chapter 5.

CHAPTER 5.   RESULTS

As was explained in Section 4.5.6, two designed experiments were performed to create a predictive model of the rate of erosion, mean particle diameter, and particle diameter variance for the proposed pulsed wire process. The raw data from the first experiment (current included as a factor) is found in Table 5.3. This data is shown in the randomized order that the runs were performed in. Table 5.3 shows the data for both the mean particle diameter and the particle diameter variance response variables.

For each of the three response variables (erosion rate, mean particle diameter, particle size variance) a predictive model was created using statistical tools commonly used in designed experiments. The factor effects were calculated using least squares regression and a t-test was used to determine the significance of each of the effects. The designed experiments used are capable of creating, at most, a quadratic predictive model.

Two designed experiments were performed for this research as shown in Chapter 4. The first designed experiment was created to create models for the erosion rate, mean particle diameter, and particle diameter variance. A second experiment was required to properly model the rate of erosion. These two experiments will be referred to as the first and second designed experiments, respectively.

Tables 5.1 and 5.2 show the maximum set of model terms that could be included to create predictive models for the two designed experiments. Only statistically significant terms should be included in a predictive model. Insignificant terms should be removed from these models. The models shown in these results were created using backward elimination of insignificant terms. Each model was created with an iterative process, where first a model was created that includes all the possible terms. Next, a t-test was performed for all the terms in the model. If any terms were not significant within a 95% confidence interval, then the least significant term was eliminated. Then a new model with the remaining terms was created, and a t-test performed on the remaining

Table 5.1: Possible Model Terms for the Three Factor Experiment

Possible Model Terms
$Intercept$
$Current$
$Frequency$
$DutyCycle$
$Current^2$
$Frequency^2$
$DutyCycle^2$
$Current * Frequency$
$Current * DutyCycle$
$Frequency * DutyCycle$

Table 5.2: Possible Model Terms for the Two Factor Experiment

Possible Model Terms
$Intercept$
$Frequency$
$DutyCycle$
$Frequency^2$
$DutyCycle^2$
$Frequency * DutyCycle$

terms and the least significant term was again removed from the model. This process was followed until only significant factors remained. This method of eliminating insignificant terms is known as model trimming.

The frequency and duty cycle variables can be represented as the t_{on} and t_{off} pulse times. Some of the response variables may be better understood in terms of the pulse times rather than the frequency and duty cycle of the pulse. In these cases the equivalent pulse times can be calculated and used in place of the frequency and duty cycle variables in the design. A model can then be created using the method described above.

Because there is a non-linear relationship between pulse times and the frequency/Duty cycle variables, care should be taken when interpreting a model created using the transformed pulse time data. The transformed data will no longer have the original central composite design shape. The design will no longer be orthogonal or rotatable. This limits the accuracy of models produced

Table 5.3: Three Factor Designed Experiment Results

	Factor Levels			Pulse Times		Response Variables		
Sample	Current (amps)	Frequency (kHz)	Duty Cycle (%)	Ton (µs)	Toff (µs)	Volume % Mean Diameter (µm)	Volume % Standard Deviation (µm)	Erosion Rate (g/hr)
1	32	5.0	70	140	60	11.630	13.000	4.50
2	32	5.0	30	60	140	7.510	8.468	4.80
3	64	12.5	50	40	40	7.111	7.345	7.69
4	48	20.0	50	25	25	1.284	1.013	5.65
5	64	5.0	30	60	140	7.241	7.786	7.60
6	32	12.5	50	40	40	1.250	0.977	4.44
7	64	20.0	30	15	35	0.988	0.706	3.26
8	48	5.0	50	100	100	4.275	5.726	7.09
9	48	12.5	50	40	40	6.844	9.161	6.37
10	48	12.5	30	24	56	5.168	7.855	4.86
11	48	12.5	50	40	40	7.167	9.205	6.22
12	48	12.5	50	40	40	6.235	7.562	6.34
13	48	12.5	70	56	24	6.876	7.610	6.43
14	32	20.0	70	35	15	1.968	1.800	4.30
15	64	5.0	70	140	60	10.500	12.560	3.52
16	48	12.5	50	40	40	4.300	6.215	6.23
17	32	20.0	30	15	35	10.640	10.990	1.77
18	48	12.5	50	40	40	4.641	6.320	6.07
19	64	20.0	70	35	15	5.821	7.206	5.33
20	48	12.5	50	40	40	3.891	4.717	6.31

using this method. However, this method was used with care to gain greater understanding of the pulsed wire process.

5.1 Rate Of Erosion Results

The rate of erosion is the most important response variable in this research. The rate of erosion determines the process production rate. Two designed experiments where performed in order to characterize the rate of erosion in terms of current, frequency, and duty cycle. Figure 5.4 shows the model and associated statistics that were created from the first designed experiment with the rate of erosion as the response variable. All insignificant effects have been trimmed from this model following the method described at the beginning of this chapter. A main point to note is

Table 5.4: First Experiment Model Statistics, Erosion Rate (g/hr)

Summary of Fit

RSquare	0.840303
RSquare Adj	0.766597
Root Mean Square Error	0.730038
Mean of Response	5.439
Observations (or Sum Wgts)	20

Analysis of Variance

Source	DF	Sum of Squares	Mean Square	F Ratio
Model	6	36.456550	6.07609	11.4007
Error	13	6.928430	0.53296	Prob > F
C. Total	19	43.384980		0.0002*

Lack Of Fit

Source	DF	Sum of Squares	Mean Square	F Ratio
Lack Of Fit	8	6.8688967	0.858612	72.1119
Pure Error	5	0.0595333	0.011907	Prob > F
Total Error	13	6.9284300		<.0001*
				Max RSq
				0.9986

Parameter Estimates

Term	Estimate	Std Error	t Ratio	Prob>|t|
Intercept	6.9935	0.731052	9.57	<.0001*
Current Amps(32,64)	0.759	0.230858	3.29	0.0059*
Frequency (kHz)	-0.096	0.030781	-3.12	0.0081*
Duty Cycle (%)	0.00895	0.011543	0.78	0.4520
Current Amps*(Duty Cycle (%)-50)	-0.0265	0.012905	-2.05	0.0607
(Frequency (kHz)-12.5)*(Duty Cycle (%)-50)	0.0074833	0.001721	4.35	0.0008*
(Duty Cycle (%)-50)*(Duty Cycle (%)-50)	-0.00401	0.000816	-4.91	0.0003*

that there is evidence that there is a lack of fit between the model and the data. The p-value for the lack of fit analysis is less than .05. This indicates that there is a lack of fit between the data and the model produced from the data. Essentially the lack of fit test says that there significantly more variation between the model and the data than there is in the data alone. This means that it is impossible using statistics alone to determine what effects are real, and what effects are simply artifacts of the model not fitting the data.

Another way to determine if there is lack of fit is by analyzing the residuals of the model created. If the residuals are random and without any patterns, then there is a good chance that there is no lack of fit. However, if there are clear patterns in the residual of the model, then there is a strong possibility that there is lack of fit between the model and the data. The residuals for this model are not random. There are patterns in the residuals that strengthen the conclusion that there is a lack of fit. The residuals are shown in Appendix A.

The lack of fit between the model and the data could be a result of the data not fitting a quadratic model, or the influence of uncontrolled variables. Another reason for the lack of fit could

Table 5.5: Second Central Composite Design (with Alpha points)

Treatment	Pulse Frequency (kHz)	Pulse Duty Cycle (%)	Rate of Erosion (g/hr)
1	3.2	32.9	12.54
2	6.8	32.9	12.90
3	3.2	47.1	10.38
4	6.8	47.1	12.69
5	5.0	40.0	13.11
6	5.0	40.0	13.55
7	2.5	40.0	9.95
8	7.5	40.0	12.84
9	5.0	30.0	13.50
10	5.0	50.0	11.75
11	5.0	40.0	13.61
12	5.0	40.0	13.55
13	5.0	40.0	13.33

be due to the reduced information obtained with a face centered central composite design vs. a full central composite design with alpha points. The face centered design only has three levels for each factor, but a full central composite with alpha points has 5 levels for each factor. These additional factor levels provide more information than the three factor levels can provide.

Because the face centered design resulted in data with a lack of fit a new designed experiment was created to gain a better understanding of what the real effects are that influence the rate of production of ultra-fine particles. This second designed experiment should be designed to gather more data using more factor levels.

It is clear from the data that current has a significant effect on the rate of erosion. It makes sense that as current increases, more energy is delivered to the electrode gap. This additional energy will melt more material per unit time, resulting in a higher rate of erosion. Current is the only factor in the original design that prevented the use of alpha points in the design. Because the current could only be set at three equally spaced levels using the current setting in a new design would limit the amount of information gathered. With the understanding that current has a positive effect on the rate of erosion (that can be estimated from the first experiment) a new design was created that does not include current as a factor.

This new designed experiment and the resulting rate of erosion data is shown in Table 5.5. The second designed experiment is a full central composite design with alpha points. The explanatory variables are frequency and duty cycle. The current setting was set at the maximum setting of 64 amps for this experiment.

It should be noted that prior to running this experiment, the motion control parameters (PID parameters) were tuned to create a more stable process in the design space of the second experiment. In the first experiment the performance of the motion control system was limited by the requirement that the process be stable over a large region of the design space. The second design covers less design space and is centered approximately around the settings that will maximize the rate of erosion.

Due to the changes to the PID parameters the maximum rate of erosion from the second experiment (13.61 g/hr) is clearly higher than the maximum rate of erosion for the first experiment (7.69 g/hr). This highlights the importance of selecting optimal PID control parameters to maximize the rate of production in the process.

Figure 5.6 shows the model and associated statistics created for the second design with the rate of erosion as the response variable. All of the terms in this model are significant so no model trimming was required. The correlation coefficient value for this model is .974, a high value indicating good correlation between the model and the data. The analysis of variance test clearly shows that the model explains the data much better than the mean alone. The lack of fit test indicates no evidence that there is a lack of fit between the data and the model.

Figure 5.1 shows a 3D plot of the predicted rate of erosion in terms of the frequency and duty cycle. It is clear that there is an optimal set of parameter settings that will maximum the rate of erosion. The model predicts that the optimal settings are a frequency of 5.5 kHz and a duty cycle of 35.6%.

The data can also be interpreted in terms of the pulse times (t_{on} and t_{off}). A model created for the rate of erosion in terms of the pulse times is shown in Figure 5.7. The correlation coefficient, analysis of variance test, and lack of fit statistics are all as good, or better than those for the frequency based model. Once again, all the model terms are significant so no model trimming was required. Just as the frequency and duty cycle model predicted, there is an optimal set of

Table 5.6: Second Experiment Model Statistics, Erosion Rate (g/hr)

Summary of Fit

RSquare	0.97372
RSquare Adj	0.954948
Root Mean Square Error	0.254559
Mean of Response	12.59231
Observations (or Sum Wgts)	13

Analysis of Variance

Source	DF	Sum of Squares	Mean Square	F Ratio
Model	5	16.806430	3.36129	51.8716
Error	7	0.453601	0.06480	Prob > F
C. Total	12	17.260031		<.0001*

Lack Of Fit

Source	DF	Sum of Squares	Mean Square	F Ratio
Lack Of Fit	3	0.28000078	0.093334	2.1505
Pure Error	4	0.17360000	0.043400	Prob > F
Total Error	7	0.45360078		0.2366
				Max RSq
				0.9899

Parameter Estimates

Term	Estimate	Std Error	t Ratio	Prob>|t|
Intercept	13.43	0.113842	117.97	<.0001*
Frequency(2.5,7.5)	1.1944938	0.127279	9.38	<.0001*
Duty Cycle(30,50)	-0.856461	0.127279	-6.73	0.0003*
Frequency*Frequency	-1.97625	0.193029	-10.24	<.0001*
Frequency*Duty Cycle	0.975	0.254559	3.83	0.0065*
Duty Cycle*Duty Cycle	-0.74625	0.193029	-3.87	0.0062*

Sorted Parameter Estimates

Term	Estimate	Std Error	t Ratio		Prob>|t|
Frequency*Frequency	-1.97625	0.193029	-10.24		<.0001*
Frequency(2.5,7.5)	1.1944938	0.127279	9.38		<.0001*
Duty Cycle(30,50)	-0.856461	0.127279	-6.73		0.0003*
Duty Cycle*Duty Cycle	-0.74625	0.193029	-3.87		0.0062*
Frequency*Duty Cycle	0.975	0.254559	3.83		0.0065*
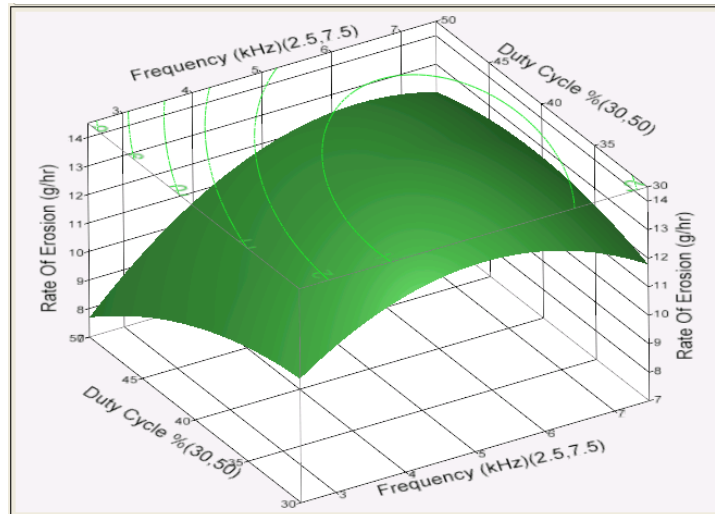
Figure 5.1: 3D Plot Of Erosion Rate as a Function of Frequency and Duty Cycle

81

Table 5.7: Second Experiment Erosion Model (Pulse times)

Summary of Fit

RSquare	0.982252
RSquare Adj	0.969574
Root Mean Square Error	0.209195
Mean of Response	12.59231
Observations (or Sum Wgts)	13

Analysis of Variance

Source	DF	Sum of Squares	Mean Square	F Ratio
Model	5	16.953692	3.39074	77.4801
Error	7	0.306339	0.04376	Prob > F
C. Total	12	17.260031		<.0001*

Lack Of Fit

Source	DF	Sum of Squares	Mean Square	F Ratio
Lack Of Fit	3	0.13273905	0.044246	1.0195
Pure Error	4	0.17360000	0.043400	Prob > F
Total Error	7	0.30633905		0.4723
				Max RSq
				0.9899

Parameter Estimates

Term	Estimate	Std Error	t Ratio	Prob>|t|
Intercept	12.095723	0.158488	76.32	<.0001*
Ton (ms)(0.015,0.16)	-4.283711	0.526135	-8.14	<.0001*
Toff (ms)(0.015,0.16)	3.4277845	0.539216	6.36	0.0004*
Ton (ms)*Toff (ms)	4.1282497	0.82791	4.99	0.0016*
Ton (ms)*Ton (ms)	-4.942756	0.720951	-6.86	0.0002*
Toff (ms)*Toff (ms)	-1.996118	0.357754	-5.58	0.0008*

parameters that will maximize the rate of erosion. The optimal setting for the pulse time based model are nearly identical to the frequency based model.

Once the model had been created, the prototype pulse wire machine was set at the optimal settings according to the frequency based model shown above. The machine was run at these settings. The PID parameters were tuned to produce optimal stability. The resulting erosion rate was measured to be 14 g/hr. This erosion rate it considered to be the optimal erosion rate for the machine. In general, these optimal settings should be similar in any machine that uses the pulsed wire process. However, the exact settings will probably be different for different wire sizes, different electrode material, different power supply designs and other parameters that might effect the process. It is also expected that an increase in the pulse current will increase the rate of erosion.

Table 5.8: Statistics for First Model, Mean Diameter (Freq.)

Summary of Fit

RSquare	0.233217
RSquare Adj	0.190618
Root Mean Square Error	2.76452
Mean of Response	5.767
Observations (or Sum Wgts)	20

Analysis of Variance

Source	DF	Sum of Squares	Mean Square	F Ratio
Model	1	41.84070	41.8407	5.4747
Error	18	137.56632	7.6426	Prob > F
C. Total	19	179.40702		0.0310*

Lack Of Fit

Source	DF	Sum of Squares	Mean Square	F Ratio
				0.4446
Lack Of Fit	1	3.50619	3.50619	Prob > F
Pure Error	17	134.06013	7.88589	0.5139
Total Error	18	137.56632		Max RSq
				0.2528

Parameter Estimates

Term	Estimate	Std Error	t Ratio	Prob>|t|
Intercept	9.1761667	1.58274	5.80	<.0001*
Frequency (kHz)	-0.272733	0.116562	-2.34	0.0310*

5.2   Mean Particle Diameter

A model with the mean particle diameter was created using the method explained at the beginning of this chapter. The resulting model and associated statistics are seen in Table 5.8. The correlation coefficient of the model is only 0.233, however, there is no evidence that there is a lack of fit between the data and the model. Also, the analysis of variance (ANOVA) test clearly shows that the model describes the data better than the mean alone. After the model was trimmed, the only significant effect remaining is frequency. The effect is negative, meaning that as the frequency increases the mean diameter of the particles decreases. The model for mean particle diameter in terms of frequency(kHz) is shown in Equation (5.1).

$$\bar{d} = 9.176 - 0.2727(Frequency(kHz)) \tag{5.1}$$

Table 5.9: Statistics for First Model, Mean Diameter (Time)

Summary of Fit

RSquare	0.305878
RSquare Adj	0.267316
Root Mean Square Error	2.630276
Mean of Response	5.767
Observations (or Sum Wgts)	20

Analysis of Variance

Source	DF	Sum of Squares	Mean Square	F Ratio
Model	1	54.87667	54.8767	7.9320
Error	18	124.53036	6.9184	Prob > F
C. Total	19	179.40702		0.0114*

Lack Of Fit

Source	DF	Sum of Squares	Mean Square	F Ratio
Lack Of Fit	7	40.12218	5.73174	0.7470
Pure Error	11	84.40818	7.67347	Prob > F
Total Error	18	124.53036		0.6400
				Max RSq
				0.5295

Parameter Estimates

Term	Estimate	Std Error	t Ratio	Prob>|t|
Intercept	7.0246853	0.738467	9.51	<.0001*
Ton (ms)(0.015,0.14)	2.9944888	1.063237	2.82	0.0114*

In this case it is useful to create a second model of the data using the pulse times instead of the frequency and duty cycle variables. This is done to determine if the main effect on mean particle diameter is indeed frequency, or one of the pulse times. Table 5.9 shows the results of a model and associated statistics created using the pulse times rather than frequency and duty cycle.

The correlation coefficient for the time based model is .305, slightly better than the frequency based model. Again, there is no evidence to show that there is a lack of fit and the ANOVA test shows that the model describes the data better than the mean alone. This model shows that the only significant effect on the mean particle diameter is the t_{on} time. This model shows that as the t_{on} time increases the mean diameter of the particles increases. It is interesting to note that in both of these models the pulse current had the least significant effect of any of the effects on the mean particle diameter. Current was expected to have a major effect on mean particle diameter. A possible explanation for independence of particle size and current will be given in Chapter 5. The model for mean particle diameter in terms of t_{on}(ms) is shown in Equation (5.2).

Table 5.10: Statistics for First Model, Diameter Variance (Freq.)

Summary of Fit

RSquare	0.274803
RSquare Adj	0.234514
Root Mean Square Error	3.126954
Mean of Response	6.8111
Observations (or Sum Wgts)	20

Analysis of Variance

Source	DF	Sum of Squares	Mean Square	F Ratio
Model	1	66.69306	66.6931	6.8208
Error	18	176.00109	9.7778	Prob > F
C. Total	19	242.69416		0.0177*

Lack Of Fit

Source	DF	Sum of Squares	Mean Square	F Ratio
Lack Of Fit	1	0.26175	0.2617	0.0253
Pure Error	17	175.73935	10.3376	Prob > F
Total Error	18	176.00109		0.8754
				Max RSq
				0.2759

Parameter Estimates

Term	Estimate	Std Error	t Ratio	Prob>|t|
Intercept	11.115267	1.79024	6.21	<.0001*
Frequency (kHz)	-0.344333	0.131844	-2.61	0.0177*

$$\bar{d} = 7.024 - 2.994\frac{t_{on}(ms) - 0.0775}{0.0625} \qquad (5.2)$$

5.3 Particle Size Variance

The variance is a value that describes how wide the distribution of particle size is. The variance is calculated from the particle size data. When only a specific size range of particles are to be desired, it is important to be able to control the particle size distribution. The model and associated statistics for particle size variance using current, frequency, and duty cycle is shown Table 5.10.

The correlation coefficient for this model is poor, however, there is no evidence to show that there is a lack of fit between the data and the model. The ANOVA test shows that the model fits the data better than the mean alone. The model shows that the particle size variance is a function only of the frequency of the pulse. As the frequency increases the particle size variance decreases. It is hard to say in this case if the frequency is really the cause of the change in the variance, or

Table 5.11: Statistics for First Model, Diameter Variance (Time)

Summary of Fit

RSquare	0.307461
RSquare Adj	0.268986
Root Mean Square Error	3.055735
Mean of Response	6.8111
Observations (or Sum Wgts)	20

Analysis of Variance

Source	DF	Sum of Squares	Mean Square	F Ratio
Model	1	74.61890	74.6189	7.9913
Error	18	168.07526	9.3375	Prob > F
C. Total	19	242.69416		0.0112*

Lack Of Fit

Source	DF	Sum of Squares	Mean Square	F Ratio
Lack Of Fit	7	50.24809	7.1783	0.6701
Pure Error	11	117.82717	10.7116	Prob > F
Total Error	18	168.07526		0.6942
				Max RSq
				0.5145

Parameter Estimates

Term	Estimate	Std Error	t Ratio	Prob>|t|
Intercept	8.2776691	0.857917	9.65	<.0001*
Ton (ms)(0.015,0.14)	3.4918312	1.23522	2.83	0.0112*

if the change in variance is really caused by the change in mean diameter (due to the change in frequency). Either way, as the frequency increases the variance decreases.

Table 5.11 shows the model created for variance based on the pulse times rather than the frequency and duty cycle. This model is nearly equivalent with the previous model except that it shows that the variance is a function of the t_{on} time. As t_{on} increases the variance increases. Once again it is difficult to determine if the t_{on} time is actually the cause of the change in the variance, or if the change in variance is actually tied to the mean particle diameter. These models simply show a correlation between the frequency/t_{on} variables and the variance, not causation.

5.4 Production Rates and Energy Consumption

The rate of erosion for the rod process, running at optimal settings, was measured for comparison to the pulsed wire process running at optimal settings. An experiment was run to determine what the erosion rate of the rod process is. To test the rate of erosion for the rod process

Table 5.12: Rod Process Erosion Rate Data (2 Hour Run Time)

Electrode	Starting Mass (g)	Ending Mass (g)	Change in Mass (g)
Anode	263.7	248.1	-15.6
Cathode	202.7	211.2	8.5

two electrodes, cathode and anode, were massed prior to a 2 hour run in the rod machine created for previous research at BYU. The process was run for two hours and then the electrodes were removed from the machine and massed again. Table 5.12 shows the results from the experiment. The optimal current setting used in the rod process is 30 amps. This setting results in an average current of 30 amps across the electrodes.

In two hours 15.6 grams were eroded from the anode electrode. About 8.5 grams of the metal eroded from the anode was deposited onto the cathode electrode. The effective rate of erosion for the rod process is then about 3.6 g/hr. The rate of erosion of the pulsed wire process, at optimal settings, is much faster than that of the constant current rod process. The measured rate of erosion using the pulsed wire process is 14 g/hr, nearly 4 times higher rate of erosion than the rod process. The actual measured average current in the pulsed wire machine when set at 64 amps is only 6 amps. The actual measured average current in the rod process is 30 amps. So even though the current setting is more than twice the current setting in the rod process the average current used in the process is much less.

This means that the power required to produce 1 gram of particles using the rod process is much greater than the power required to produce the same mass of particles using the pulsed wire process. A comparison of the two processes is shown in Tables 5.13 and 5.14. Table 5.13 compares the two processes only considering the energy delivered to the gap. This comparison ignores power supply losses. Table 5.14 compares the processes, including the losses in the power supplies of each system. Ignoring the power supply losses and only considering the actual power required for the process, the rod process requires 200 kWh/kg and the pulsed wire machine only requires 10.3 kWh/kg. Meaning that 19.4 times less energy is required for the pulsed wire process. Economically speaking, the pulsed wire process is much less expensive to operate.

Table 5.13: Energy Required Process Comparison (Neglecting power supply losses)

Process	Current Setting (Amps)	Measured Average Current (Amps)	Rate Of Erosion (g/hr)	Power Required (Watts)	Energy Required (kWh/kg)
Rod	30	30	3.6	720	200
Pulsed Wire	64	6	14	144	10.3

Table 5.14: Energy Required Process Comparison (Including power supply losses)

Process	Current Setting (Amps)	Measured Average Current (Amps)	Rate Of Erosion (g/hr)	Power Required (Watts)	Energy Required (kWh/kg)
Rod	30	30	3.6	847	235
Pulsed Wire	64	6	14	480	34.3

In addition to energy cost savings due to reduced energy required by the process there is a hidden savings. Nearly all the energy delivered to the electrode gap will be transformed into heat. In a macro sense, the electrode gap acts like a heating element submerged in the dielectric fluid. This means that the rod machine adds 200 kWh/kg of energy into the dielectric fluid. This amount of energy requires a chiller to keep the fluid in the system at a reasonable process temperature. Additional energy must be used to remove the added energy from the fluid. The pulsed wire machine only adds 10.3 kwh/kg into the dielectric fluid. Again this is nearly 20 times less than the rod process. In fact, with the reduced heat added to the fluid a chiller may not be required. Heat losses through tank walls and pipes may be enough to cool the fluid. Even is a chiller is required, the energy required to run a chiller will be much less than when using the rod process.

The power supply used the pulsed wire process prototype only has an electrical efficiency of 30 percent. However, more efficient power supplies could be created to reduce the amount of energy required to run the machine. Table 5.14 shows that even when considering the losses in the power supplies that the pulsed wire machine is still about 7 times more efficient than the rod machine.

5.5   Cathode Growth Rate

The growth rate of the cathode electrode is important to control. If the cathode electrode is increasing in size, it generally means that the cathode electrode will require periodic maintenance to remove the buildup from the cathode electrodes. The maintenance requirements due to the cathode growth rate are a major drawback for the rod process. The rod process had a high cathode growth rate. About 50% of the metal removed from the anode electrode was deposited on the cathode electrode. The pulsed wire process greatly reducing the cathode growth rate. The cathode growth rate of the pulsed wire process is always below 1%.

5.6   Independence of Particle Size and Current

One of the results that was not expected is that the mean particle diameter does not depend on the pulse current. It was expected that as the current increased, the amount of molten metal would increase resulting in a higher erosion rate and a higher mean particle diameter. The results do show that as current increases the rate of erosion increases. The data created in this research shows that the pulse current can be increased without increasing the mean diameter of the particles produced. This section of the thesis will attempt to provide a possible reason for this result.

When a pulse starts between the two electrodes, only a very small conductive path exists. The resistance of this conductive path is somewhat high. As current flows through the plasma channel, the plasma heats up decreasing the resistance of the channel causing more current to flow through the electrode gap. This additional current heats the plasma more, converting more fluid around the column into a larger diameter plasma channel. After some transient period (the transient period is very short in comparison to the pulse width) as the current capacity of the power source is reached, the plasma column will reach thermal equilibrium. For simplicity, the plasma column between the electrodes will be considered to be cylindrical with some diameter D.

Now, considering the cross section of the plasma column, there will be some average current density J. To further simplify the system, the current density will be assumed to be constant across the entire cross section.

Now consider the same electrode gap, only double the previous current across the gap. In order to conduct the additional current, the plasma column will have to increase in diameter

89
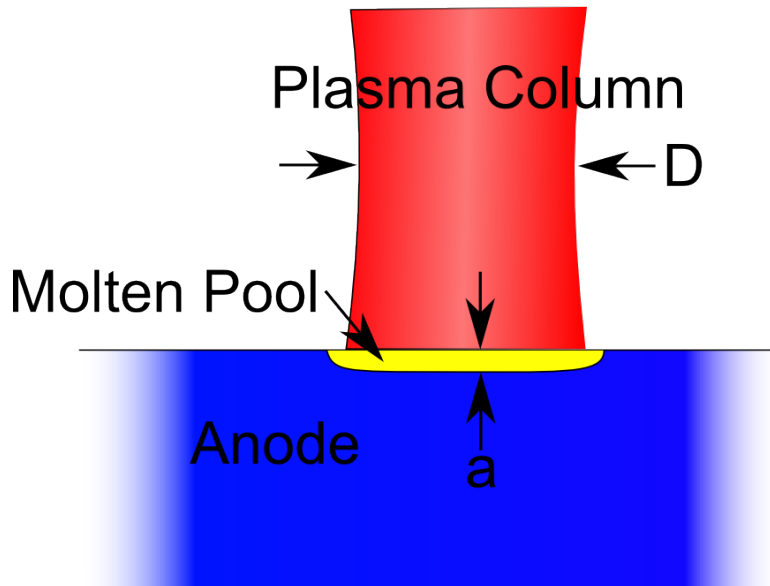
Figure 5.2: Molten Pool Thickness

to maintain thermal equilibrium. It is possible that the area of the plasma column cross section approximately doubles with a doubling of current. If this is the case, then the current density in the plasma column cross section is equal to the current density in the previous case.

If the current density in the plasma column cross section is nearly constant independent of current across the gap then the amount of heat per unit area on the electrode face will be nearly constant. Figure 5.2 shows a side view of the interface between the plasma column and the anode electrode. The diameter of the electrode, D, and the thickness of the molten metal pool, a, are shown in the figure. If the diameter of the plasma column is large in comparison to the thickness of the molten pool, then the thickness of the pool will be proportional to the amount of time that the pulse is on and independent of the current across the gap. An increase in current will increase the area on the electrode face that is melted, but only the pulse length will determine the thickness of the molten pool.

The particles are created when the plasma column collapses causing a large pressure wave to interact with the molten pool. It would be expected that the probability of creating larger particles would increase with an increase in the pool thickness. There will always be a probability of creating particles down to almost zero diameter due to the random nature of the plasma column implosion. The maximum expected particle volume would be the volume of the entire molten

pool. Both very small particle volume and particle volume approaching the pool volume are low. The average particle volume will be between these two extreme values. The existence of extreme values would suggest a particle size distribution from the extreme value family like the Gumbel, Frechet, or Weibull distributions [22].

CHAPTER 6.   CONCLUSIONS AND RECOMMENDATIONS FOR FUTURE WORK

6.1   Connection Between Particle Size and the Variance

If the particle size distribution extends from zero until some maximum, as suggested in the previous section, then it is very likely that the variance of the particle size distribution is connected to the mean particle diameter. That is to say that as the mean particle diameter increases the particle size variance would necessarily increase. This is due to the increase in distance between the minimum and maximum bounds of the size distribution function. Using a pulsed power supply limits the maximum possible particle size, thus reducing the particle size distribution in comparison to the rod process.

6.2   Comparison of the Pulsed Wire Process VS. Rod Process

The pulsed wire process has many advantages over the rod process. This section will summarize some of these advantages. The comparison is in terms of production rate, mean particle size, cathode growth rate, dielectric heating, and the need for rotation.

6.2.1   Increased Production Rate

The pulsed wire process clearly has a higher production rate in comparison to the rod process. The pulsed wire process produced particles at 14 g/hr. The rod process only produces particles at 3.6 g/hr. The pulsed wire process also requires nearly 20 times less energy to produce the same mass of particles as the rod process. Additionally, it is expected that the current can continue to be increased without changing the mean diameter of the particles produced.

6.2.2 Control Over Mean Particle Size

The data from the designed experiments shows that the mean particle diameter can be controlled using the pulsed wire process. This is a huge advantage over the rod process where there is no control over the mean particle diameter. The pulsed wire process controls the mean particle diameter limiting the time over which the discharge stage of the process occurs. For the pulsed process that value is the t_{on} time. Because the t_{on} time is controlled the maximum particle size is limited; there is virtually no chance of producing particles greater than 100 μm. This is a great advantage over the rod process where large particles had to be filtered out of the system to prevent damage to pumps and other parts of the fluid system.

6.2.3 Near Zero Cathode Growth/Erosion

The Rod process is greatly hampered by the amount of growth that occurs on the cathode electrode. The growth on the cathode electrode created a rough surface that results in process instability. When the cathode growth becomes too large the electrode must be removed from the system and the build up removed to restore system stability. The cathode growth rate generally is about 50% of the erosion rate. This high cathode growth rate also decreases the effective rate of erosion.

The pulsed wire process has the advantage that the pulsing process greatly limits the amount of cathode electrode growth. The rate of cathode growth can be kept below 1% of the rate of erosion. This reduced rate of cathode growth greatly decreases or eliminates the requirement for dressing the electrodes. This greatly reduces the need for operator intervention in the process and increases process utilization.

6.2.4 Reduced Dielectric Fluid Heating

Another positive unexpected advantage of the pulsed wire process over the rod process is the greatly reduced amount of energy that is transferred to the dielectric fluid as heat. The rod process machine transfers about 200 kWh/kg into the process fluid. The pulsed wire process transfers 10.3 kWh/kg into the process fluid. The pulsed wire process transfers nearly 20 times

less heat into the process fluid. The reduction in the heating of the process fluid greatly reduces the expense of cooling the process fluid.

6.2.5   No need for Electrode Rotation

Unlike the rod process the pulsed wire process requires no rotation of the electrodes. The rod process required rotation of the electrodes for the process to be stable. This requires that there be two rotary actuators and two linear actuators to make the rod process work. The pulsed wire process requires a single linear actuator and no seals or bearings to leak or wear out. This reduction in system complexity and reduced part count make the pulsed wire process easier to maintain than the rod process.

6.3   Pulsed Rod Machine

Most of the advantages of the pulsed wire machine over the rod machine are made possible by the pulsing of the electrical current power supply. Because of this it should be possible to create a process that uses a pulsed power supply and rod feedstock. In some cases it may be easier to produce rod feedstock rather than wire feedstock. If an electrode material is not normally available in wire form, it may be easier to cast rod electrodes rather than buy the equipment for wire drawing. For these cases a pulsed rod process may have some advantages over the pulsed wire process.

A pulse rod process would be very similar to the pulsed wire process. The anode electrode would be a rod attached to a linear actuator. The cathode electrode would be a flat plate, or some other similar topology. The anode electrode would be fed into the cathode plate in very much the same way that the pulsed wire process works. The pulsed rod machine would have the advantages over a non pulsed rod machine of a higher production rate, control over mean particle size, low cathode growth rate and low process fluid heating. Nevertheless, in most cases, the advantages of using wire feedstock material would still outweigh using rod feedstock material even with a pulsed power supply.

6.4   Control Over Mean Particle Size

One of the main conclusions of this research is that the size of the particles produced in the pulsed wire process can indeed be controlled to some extent. The mean particle size is directly linked to the t_{on} time of the pulses. As the length of the t_{on} time increases the mean diameter of the particles increases.

Another interesting result is that the mean particle diameter in unaffected by changes in the current setting. Because the rate of particle production can be increased by increasing the current setting, the rate of particle production can be increased without changing the mean particle size.

6.5   Suggestions for Future Research

Suggested future research would include the following areas:

- Develop a pulsed rod process

- Determine the maximum reasonable current settings

- Experiment with more parameters to attempt to further control particle size variance

- Further research in reducing cathode electrode growth

- Experimentation with AC pulsed power supplies to eliminate electrode growth

6.5.1   Pulsed Rod Process

Additional research should be performed to determine what the effect of the wire diameter is on the process outputs. A large diameter wire is simply a rod. Research should be performed to see if some of the positive results found using the pulsed wire process are because of the small diameter electrode, or if the process is insensitive to changes in the electrode size

6.5.2   Maximum Current Settings

This research did not attempt to find the maximum reasonable current setting for the pulsed wire process or if there is a maximum. If the pulsed wire process is to be used in an industrial process then the rate of erosion, or the production rate for a process, is very important to know.

6.5.3 Additional Research on Particle Size

Additional research could be accomplished to determine if other process parameters change the mean particle diameter. For example, it may be possible that the temperature of the water has an effect on the mean particle size. Additionally, the diameter of the wire electrode used could have an effect on the mean particle size.

6.5.4 Cathode Growth Rate

The cathode growth rate was greatly reduced with the use of the pulsed power supply. Further reducing or eliminating this rate of growth could further simplify the process. Elimination of cathode growth would reduce or eliminate the need for maintenance on the cathode electrode.

6.5.5 AC Power Supplies

Neither this research nor the prior research at BYU has used any AC type power supplies. The use of an AC pulsed power supply could have additional unforseen advantages. One possibility is the reduction or elimination of electrolysis in the process. AC pulsed power supplies have been used in wire EDM processes [23] to improve the process, it might be expected that the use of an AC power supply for this process might be useful.

APPENDIX A.   RATE OF EROSION MODEL RESIDUALS

This section shows the main effect residuals for the first rate of erosion experiment and model. The first three plots show the residuals for the frequency based model, and the second three plots show the residuals for the time based model.
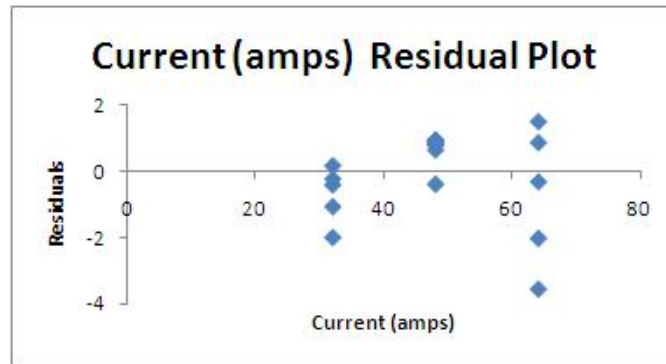
Figure A.1: Frequency based model Current Residuals

Figure A.2: Frequency based model Frequency Residuals
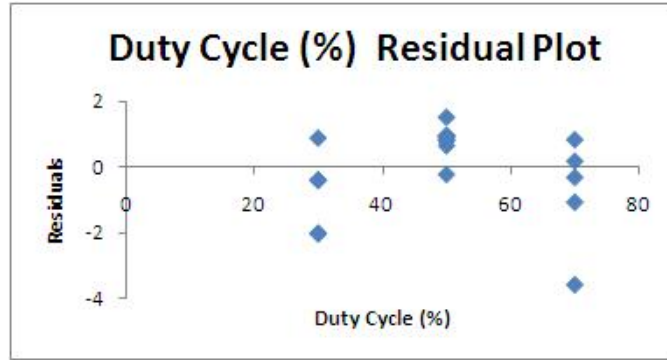
Figure A.3: Frequency based model Duty Cycle Residuals
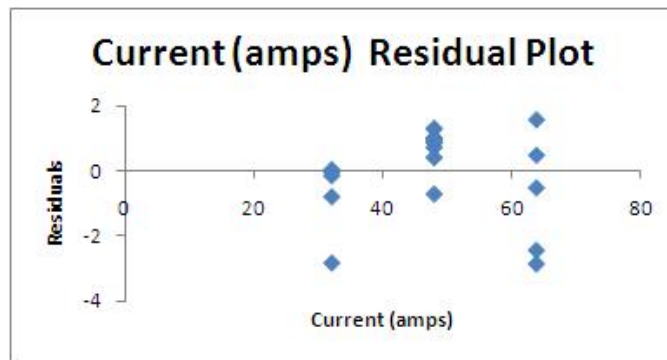
Figure A.4: Time based model Current Residuals
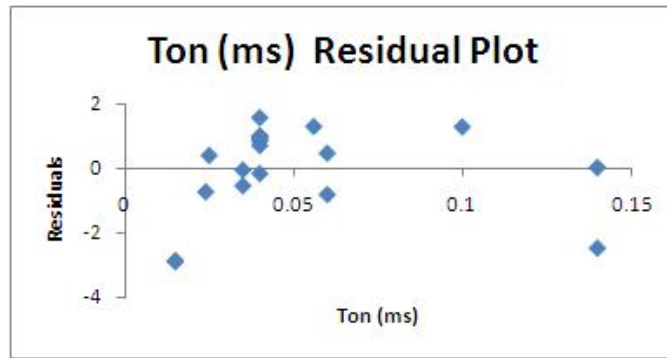
Figure A.5: Time based model t_{on} Residuals
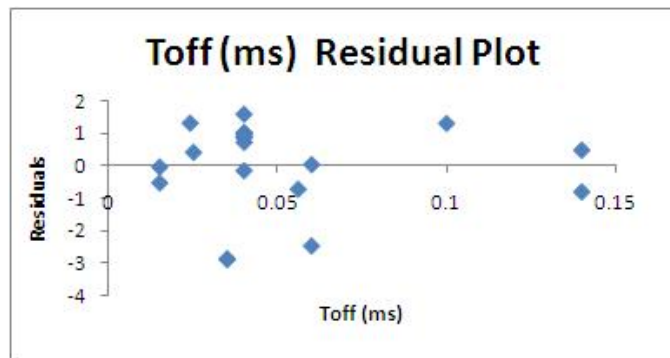
Figure A.6: Time based model t_{off} Residuals

101

APPENDIX B.   PARTICLE SIZE DATA

The following data shows the results of the data collected using the LS230 particle analyzer. The samples numbered (1-20) correspond to those found in Table 5.3.

File name: C:\LS32\Data\George\CuSample1_14-48_03.$av
File ID: CuSample1
Sample ID: CuOParticlesJonG
Optical model: Cu Particles.rfd   PIDS included
LS 230   Small Volume Module
                                  Run length: 91 seconds
Fluid: Water
 Average of 3 files:
  CuSample1_14-45_01.$ls
  CuSample1_14-46_02.$ls
  CuSample1_14-48_03.$ls
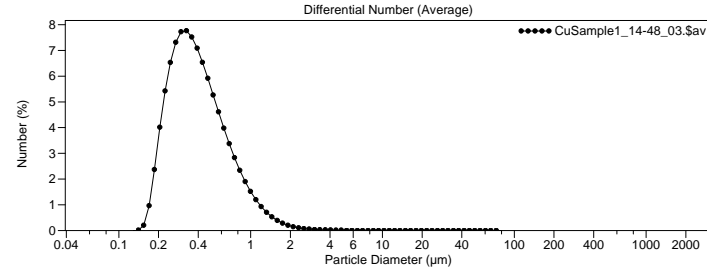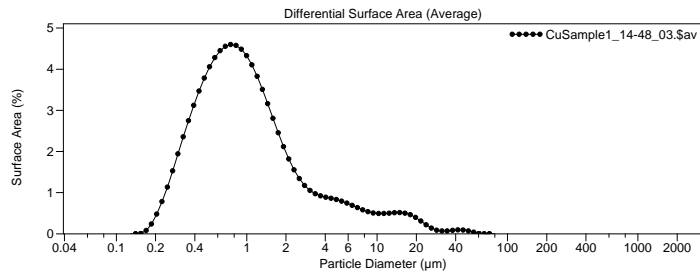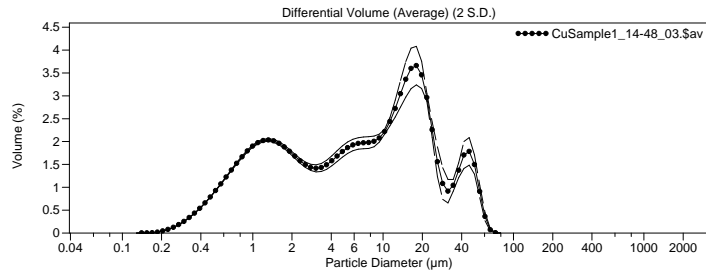
Differential Number (Average)

Volume Statistics (Arithmetic)   CuSample1_14-48_03.$av

Calculations from 0.0400 µm to 2000 µm

Volume:	100%		
Mean:	11.63 µm	S.D.:	13.00 µm
Median:	6.783 µm		
Mode:	18.00 µm		

<1 µm	<10 µm	<100 µm	<1000 µm
14.0%	58.4%	100%	100%

Surface Area Statistics (Arithmetic)   CuSample1_14-48_03.$av

Calculations from 0.0400 µm to 2000 µm

Surface Area:	100%		
Mean:	2.277 µm	S.D.:	4.615 µm
Median:	0.903 µm		
Mode:	0.755 µm		

<1 µm	<10 µm	<100 µm	<1000 µm
54.8%	95.0%	100%	100%

Number Statistics (Arithmetic)   CuSample1_14-48_03.$av

Calculations from 0.0400 µm to 2000 µm

Number:	100%		
Mean:	0.471 µm	S.D.:	0.360 µm
Median:	0.376 µm		
Mode:	0.326 µm		

<1 µm	<10 µm	<100 µm	<1000 µm
94.5%	99.99%	100%	100%

Figure B.1: Sample 1 Particle Size Data

File name: C:\LS32\Data\George\CuSample2_13-36_03.$av
File ID: CuSample2
Sample ID: CuOParticlesJonG
Optical model: Cu Particles.rfd   PIDS included
LS 230   Small Volume Module
Fluid: Water
 Average of 3 files:
 CuSample2_13-33_01.$ls
 CuSample2_13-35_02.$ls
 CuSample2_13-36_03.$ls
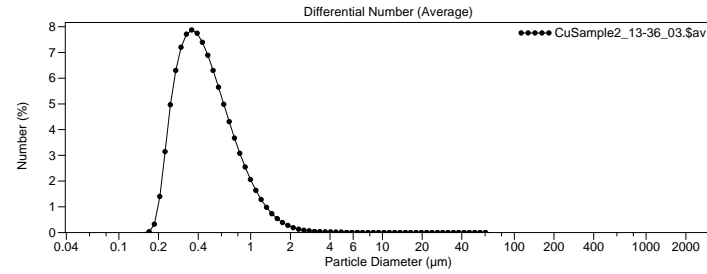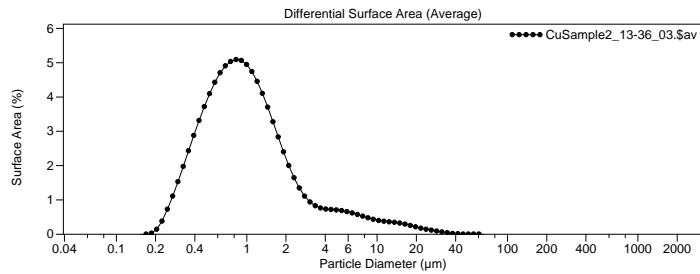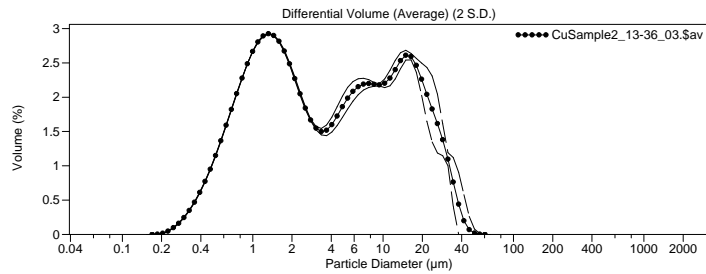
Differential Volume (Average) (2 S.D.)

Differential Number (Average)

Differential Surface Area (Average)

Volume Statistics (Arithmetic)   CuSample2_13-36_03.$av

Calculations from 0.0400 µm to 2000 µm

Volume:	100%		
Mean:	7.510 µm	S.D.:	8.468 µm
Median:	3.629 µm		
Mode:	1.321 µm		

<1 µm	<10 µm	<100 µm	<1000 µm
17.8%	71.6%	100%	100%

Surface Area Statistics (Arithmetic)   CuSample2_13-36_03.$av

Calculations from 0.0400 µm to 2000 µm

Surface Area:	100%		
Mean:	1.853 µm	S.D.:	3.238 µm
Median:	0.927 µm		
Mode:	0.829 µm		

<1 µm	<10 µm	<100 µm	<1000 µm
54.0%	96.9%	100%	100%

Number Statistics (Arithmetic)   CuSample2_13-36_03.$av

Calculations from 0.0400 µm to 2000 µm

Number:	100%		
Mean:	0.529 µm	S.D.:	0.368 µm
Median:	0.430 µm		
Mode:	0.358 µm		

<1 µm	<10 µm	<100 µm	<1000 µm
92.5%	99.99%	100%	100%

Figure B.2: Sample 2 Particle Size Data

File name: C:\LS32\Data\George\CuSample3_10-17_09.$av
File ID: CuSample3
Sample ID: CuOParticlesJonG
Optical model: Cu Particles.rfd   PIDS included
LS 230   Small Volume Module
Fluid: Water
 Average of 3 files:
 CuSample3_10-14_07.$ls
 CuSample3_10-15_08.$ls
 CuSample3_10-17_09.$ls
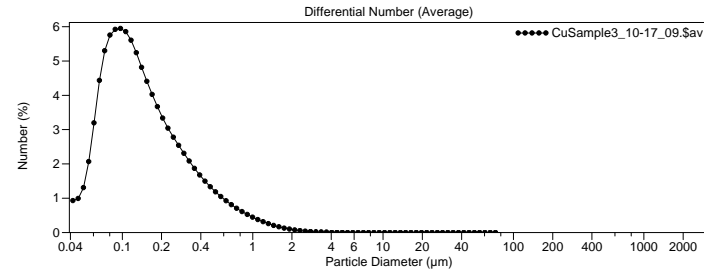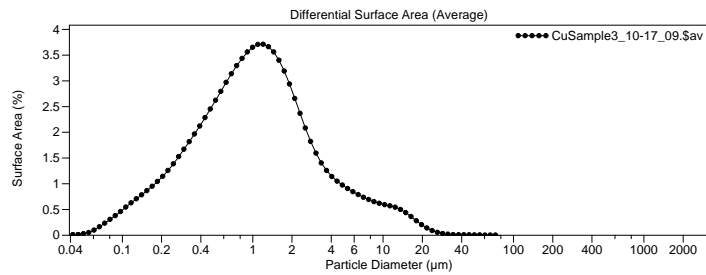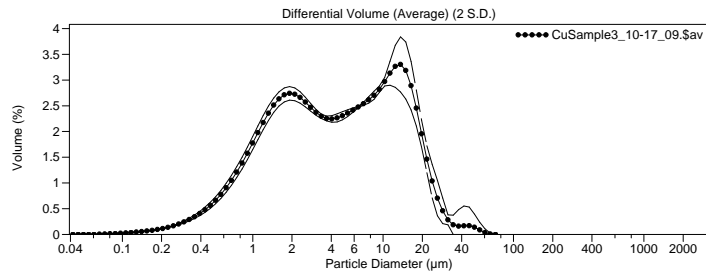
Differential Volume (Average) (2 S.D.)

●●●●● CuSample3_10-17_09.$av

Differential Surface Area (Average)

●●●●● CuSample3_10-17_09.$av

Differential Number (Average)

●●●●● CuSample3_10-17_09.$av

Volume Statistics (Arithmetic)   CuSample3_10-17_09.$av

Calculations from 0.0400 µm to 2000 µm

Volume:	100%		
Mean:	7.111 µm	S.D.:	7.345 µm
Median:	4.341 µm		
Mode:	13.61 µm		

<1 µm	<10 µm	<100 µm	<1000 µm
11.9%	72.5%	100%	100%

Surface Area Statistics (Arithmetic)   CuSample3_10-17_09.$av

Calculations from 0.0400 µm to 2000 µm

Surface Area:	100%		
Mean:	2.056 µm	S.D.:	3.224 µm
Median:	1.037 µm		
Mode:	1.204 µm		

<1 µm	<10 µm	<100 µm	<1000 µm
48.5%	96.2%	100%	100%

Number Statistics (Arithmetic)   CuSample3_10-17_09.$av

Calculations from 0.0400 µm to 2000 µm

Number:	100%		
Mean:	0.213 µm	S.D.:	0.277 µm
Median:	0.129 µm		
Mode:	0.0970 µm		

<1 µm	<10 µm	<100 µm	<1000 µm
98.0%	99.997%	100%	100%

106

Figure B.3: Sample 3 Particle Size Data

BECKMAN
COULTER™

File name: C:\LS32\Data\George\CuSample4_09-49_06.$av
File ID: CuSample4
Sample ID: CuOParticlesJonG
Optical model: Cu Particles.rfd   PIDS included
LS 230   Small Volume Module
Fluid: Water
 Average of 3 files:
 CuSample4_09-46_04.$ls
 CuSample4_09-47_05.$ls
 CuSample4_09-49_06.$ls
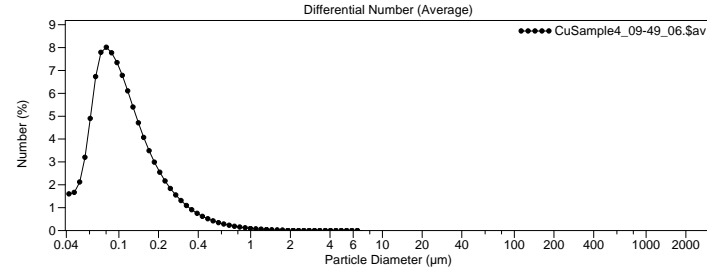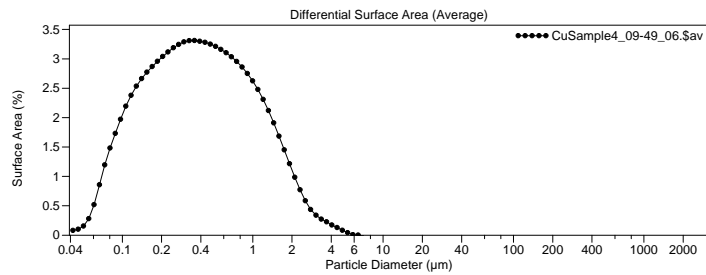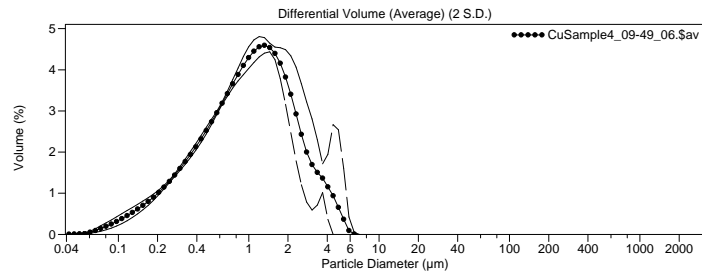
Differential Volume (Average) (2 S.D.)

●●●●● CuSample4_09-49_06.$av

Differential Surface Area (Average)

●●●●● CuSample4_09-49_06.$av

BECKMAN
COULTER™

Differential Number (Average)

●●●●● CuSample4_09-49_06.$av

Volume Statistics (Arithmetic)   CuSample4_09-49_06.$av

Calculations from 0.0400 µm to 2000 µm

Volume: 100%
Mean: 1.284 µm   S.D.:   1.013 µm
Median: 1.027 µm
Mode: 1.321 µm

<1 µm	<10 µm	<100 µm	<1000 µm
48.8%	100%	100%	100%

Surface Area Statistics (Arithmetic)   CuSample4_09-49_06.$av

Calculations from 0.0400 µm to 2000 µm

Surface Area: 100%
Mean: 0.610 µm   S.D.:   0.641 µm
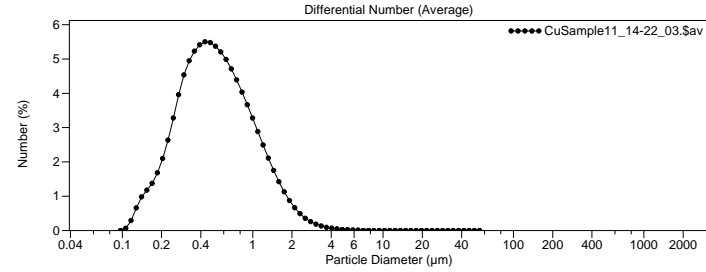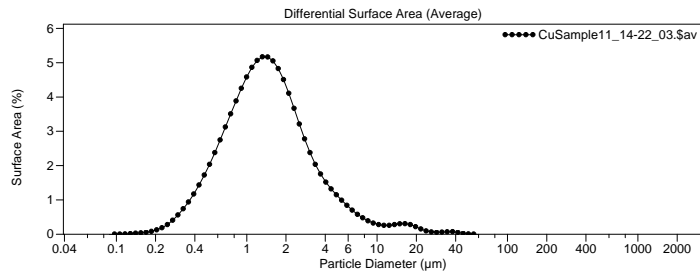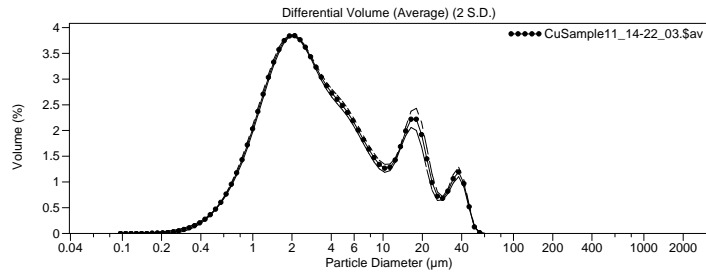Median: 0.384 µm
Mode: 0.358 µm

<1 µm	<10 µm	<100 µm	<1000 µm
81.5%	100%	100%	100%

Number Statistics (Arithmetic)   CuSample4_09-49_06.$av

Calculations from 0.0400 µm to 2000 µm

Number: 100%
Mean: 0.137 µm   S.D.:   0.128 µm
Median: 0.100 µm
Mode: 0.0805 µm

<1 µm	<10 µm	<100 µm	<1000 µm
99.7%	100%	100%	100%

Figure B.4: Sample 4 Particle Size Data

Figure B.5: Sample 5 Particle Size Data

LS Particle Size Analyzer

BECKMAN
COULTER™

9 Feb 2010 15:23

File name: C:\LS32\Data\George\CuSample6_15-23_03.$av
File ID: CuSample6
Sample ID: CuOParticlesJonG
Optical model: Cu Particles.rfd   PIDS included
LS 230   Small Volume Module
Fluid: Water
 Average of 3 files:
 CuSample6_15-19_01.$ls
 CuSample6_15-21_02.$ls
 CuSample6_15-23_03.$ls

Differential Volume (Average) (2 S.D.)

●●●●● CuSample6_15-23_03.$av
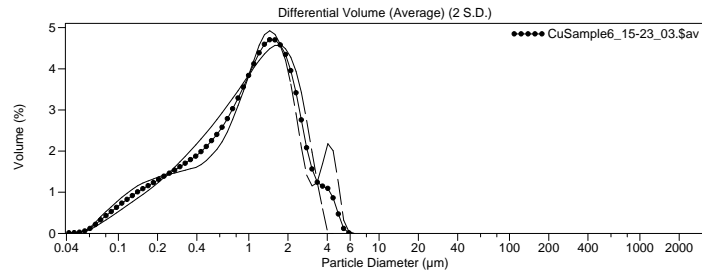
Volume Statistics (Arithmetic)   CuSample6_15-23_03.$av

Calculations from 0.0400 µm to 2000 µm

Volume: 100%
Mean: 1.250 µm   S.D.:   0.977 µm
Median: 1.050 µm
Mode: 1.451 µm

<1 µm	<10 µm	<100 µm	<1000 µm
47.9%	100%	100%	100%

Surface Area Statistics (Arithmetic)   CuSample6_15-23_03.$av

Calculations from 0.0400 µm to 2000 µm

Surface Area: 100%
Mean: 0.517 µm   S.D.:   0.616 µm
Median: 0.257 µm
Mode: 0.128 µm

<1 µm	<10 µm	<100 µm	<1000 µm
84.1%	100%	100%	100%

LS Particle Size Analyzer

BECKMAN
COULTER™

9 Feb 2010 15:23

Number Statistics (Arithmetic)   CuSample6_15-23_03.$av

Calculations from 0.0400 µm to 2000 µm

Number: 100%
Mean: 0.114 µm   S.D.:   0.096 µm
Median: 0.0899 µm
Mode: 0.0733 µm

<1 µm	<10 µm	<100 µm	<1000 µm
99.8%	100%	100%	100%

Figure B.6: Sample 6 Particle Size Data

LS Particle Size Analyzer

BECKMAN
COULTER ™

9 Feb 2010 15:39

LS Particle Size Analyzer

BECKMAN
COULTER ™

9 Feb 2010 15:39

File name: C:\LS32\Data\George\CuSample7_15-05_03.$av
File ID: CuSample7
Sample ID: CuOParticlesJonG
Optical model: Cu Particles.rfd   PIDS included
LS 230   Small Volume Module
Fluid: Water
 Average of 3 files:
 CuSample7_15-01_01.$ls
 CuSample7_15-03_02.$ls
 CuSample7_15-04_03.$ls
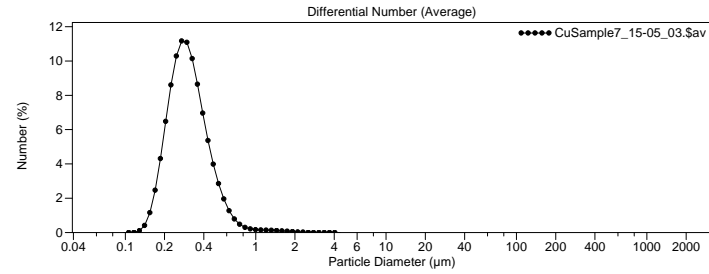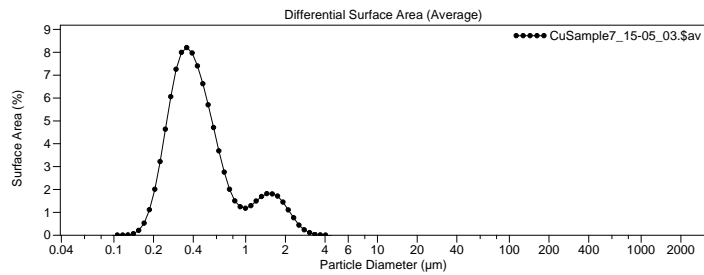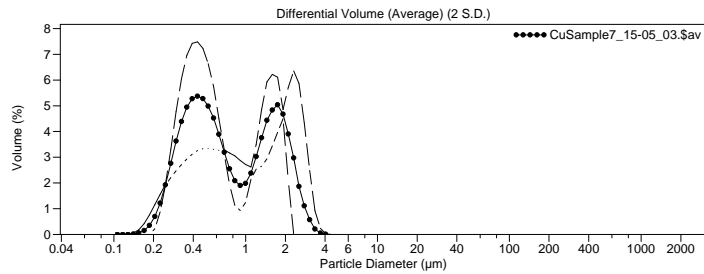
Differential Volume (Average) (2 S.D.)

●●●●● CuSample7_15-05_03.$av

Differential Surface Area (Average)

●●●●● CuSample7_15-05_03.$av

Differential Number (Average)

●●●●● CuSample7_15-05_03.$av

Volume Statistics (Arithmetic)   CuSample7_15-05_03.$av

Calculations from 0.0400 µm to 2000 µm

Volume: 100%
Mean: 0.988 µm   S.D.:   0.706 µm
Median: 0.667 µm
Mode: 0.431 µm

<1 µm   <10 µm   <100 µm   <1000 µm
60.2%   100%   100%   100%
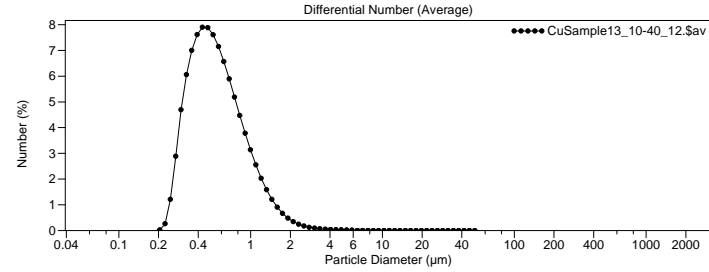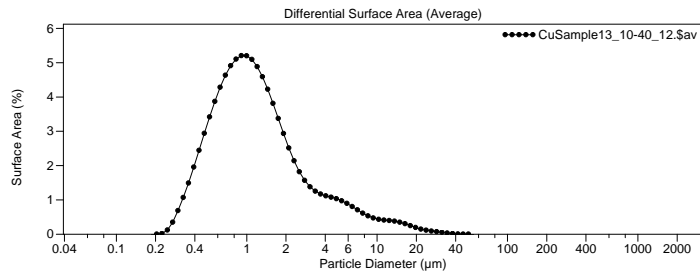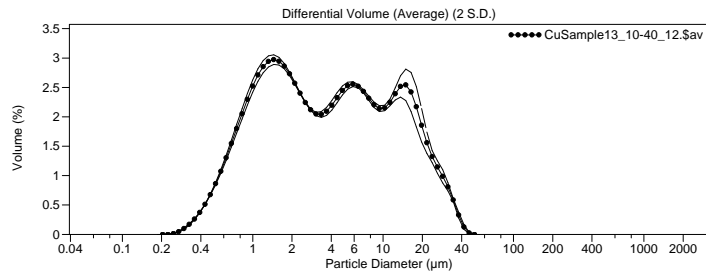
Surface Area Statistics (Arithmetic)   CuSample7_15-05_03.$av

Calculations from 0.0400 µm to 2000 µm

Surface Area: 100%
Mean: 0.594 µm   S.D.:   0.484 µm
Median: 0.416 µm
Mode: 0.358 µm

<1 µm   <10 µm   <100 µm   <1000 µm
85.5%   100%   100%   100%

Number Statistics (Arithmetic)   CuSample7_15-05_03.$av
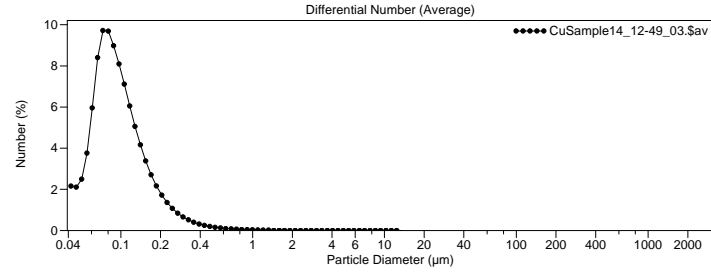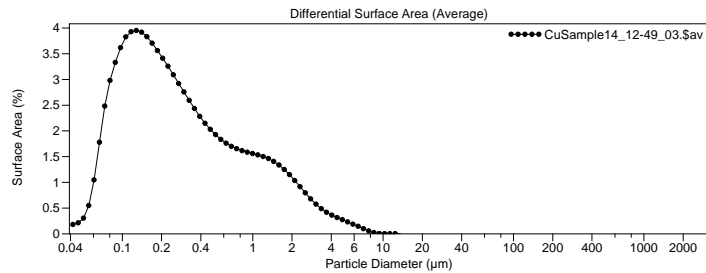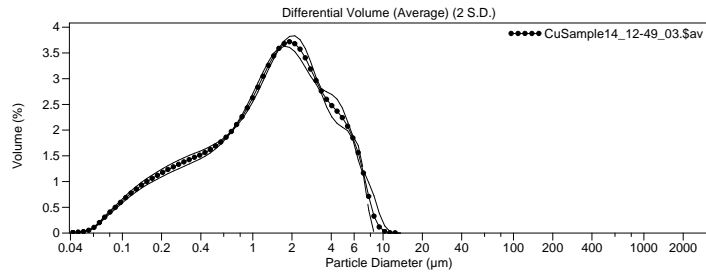
Calculations from 0.0400 µm to 2000 µm

Number: 100%
Mean: 0.330 µm   S.D.:   0.161 µm
Median: 0.296 µm
Mode: 0.271 µm

<1 µm   <10 µm   <100 µm   <1000 µm
99.1%   100%   100%   100%

110

Figure B.7: Sample 7 Particle Size Data

Figure B.8: Sample 8 Particle Size Data

Figure B.9: Sample 9 Particle Size Data

File name: C:\LS32\Data\George\CuSample10_14-04_06.$av
File ID: CuSample10
Sample ID: CuOParticlesJonG
Optical model: Cu Particles.rfd   PIDS included
LS 230   Small Volume Module
Fluid: Water
 Average of 3 files:
 CuSample10_14-01_04.$ls
 CuSample10_14-02_05.$ls
 CuSample10_14-04_06.$ls
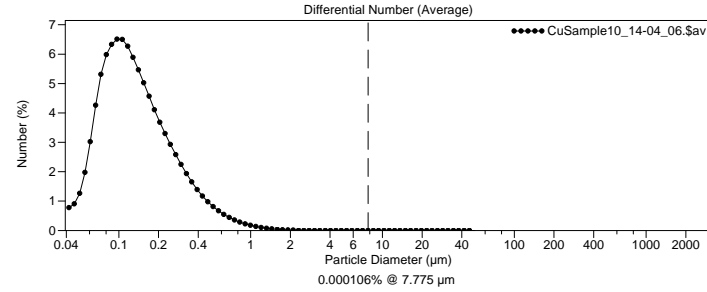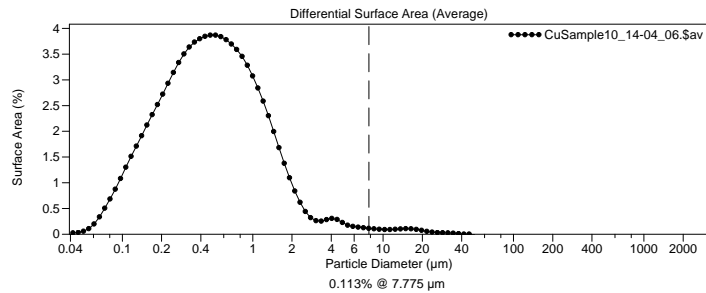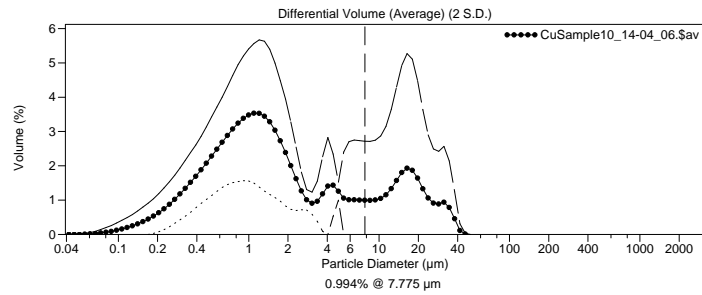
Differential Volume (Average) (2 S.D.)

0.994% @ 7.775 µm

Differential Surface Area (Average)

0.113% @ 7.775 µm

Differential Number (Average)

0.000106% @ 7.775 µm

Volume Statistics (Arithmetic)   CuSample10_14-04_06.$av

Calculations from 0.0400 µm to 2000 µm

Volume: 100%
Mean: 5.168 µm   S.D.:   7.855 µm
Median: 1.401 µm
Mode: 1.097 µm

<1 µm   <10 µm   <100 µm   <1000 µm
37.4%   81.4%   100%   100%

Surface Area Statistics (Arithmetic)   CuSample10_14-04_06.$av

Calculations from 0.0400 µm to 2000 µm

Surface Area: 100%
Mean: 0.883 µm   S.D.:   1.945 µm
Median: 0.475 µm
Mode: 0.520 µm

<1 µm   <10 µm   <100 µm   <1000 µm
78.9%   99.1%   100%   100%

Number Statistics (Arithmetic)   CuSample10_14-04_06.$av
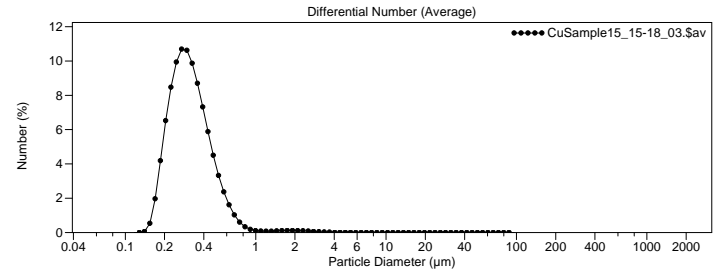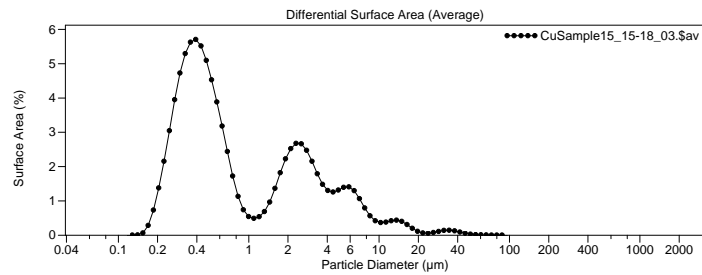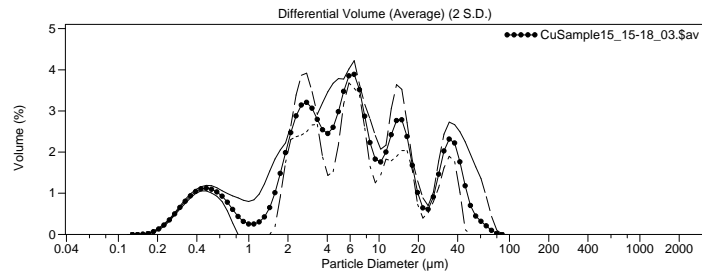
Calculations from 0.0400 µm to 2000 µm

Number: 100%
Mean: 0.174 µm   S.D.:   0.163 µm
Median: 0.124 µm
Mode: 0.0970 µm

<1 µm   <10 µm   <100 µm   <1000 µm
99.4%   100%   100%   100%

113

Figure B.10: Sample 10 Particle Size Data

LS Particle Size Analyzer

9 Feb 2010 15:40

File name: C:\LS32\Data\George\CuSample11_14-22_03.$av
File ID: CuSample11
Sample ID: CuOParticlesJonG
Optical model: Cu Particles.rfd   PIDS included
LS 230   Small Volume Module
Fluid: Water
 Average of 3 files:
 CuSample11_14-19_01.$ls
 CuSample11_14-20_02.$ls
 CuSample11_14-22_03.$ls

Differential Volume (Average) (2 S.D.)

●●●●● CuSample11_14-22_03.$av

Differential Surface Area (Average)

●●●●● CuSample11_14-22_03.$av

LS Particle Size Analyzer

9 Feb 2010 15:40

Differential Number (Average)

●●●●● CuSample11_14-22_03.$av

Volume Statistics (Arithmetic)   CuSample11_14-22_03.$av

Calculations from 0.0400 µm to 2000 µm

Volume: 100%
Mean: 7.167 µm   S.D.:   9.205 µm
Median: 3.124 µm
Mode: 2.107 µm

<1 µm   <10 µm   <100 µm   <1000 µm
9.42%   77.7%   100%   100%

Surface Area Statistics (Arithmetic)   CuSample11_14-22_03.$av

Calculations from 0.0400 µm to 2000 µm

Surface Area: 100%
Mean: 2.254 µm   S.D.:   3.328 µm
Median: 1.400 µm
Mode: 1.321 µm

<1 µm   <10 µm   <100 µm   <1000 µm
32.0%   97.2%   100%   100%

Number Statistics (Arithmetic)   CuSample11_14-22_03.$av

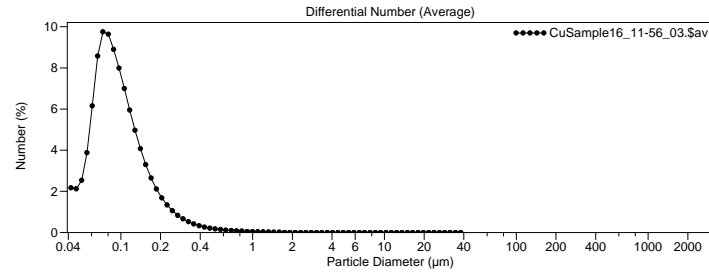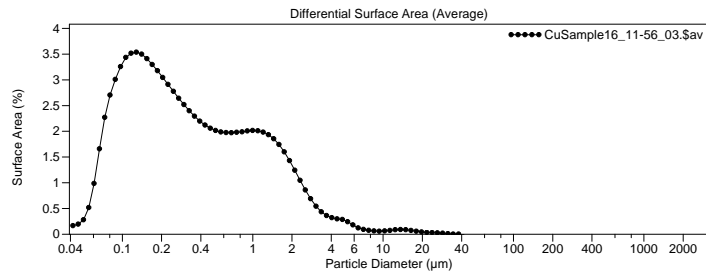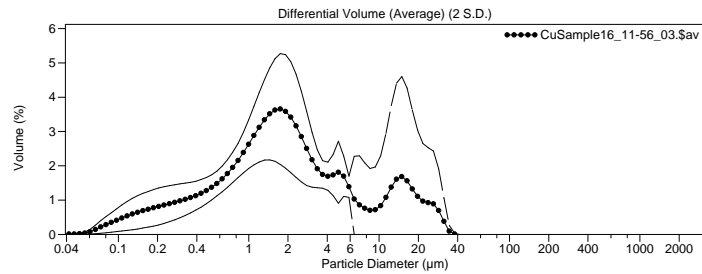Calculations from 0.0400 µm to 2000 µm

Number: 100%
Mean: 0.653 µm   S.D.:   0.535 µm
Median: 0.503 µm
Mode: 0.431 µm

<1 µm   <10 µm   <100 µm   <1000 µm
83.3%   99.99%   100%   100%

Figure B.11: Sample 11 Particle Size Data

Figure B.12: Sample 12 Particle Size Data

File name: C:\LS32\Data\George\CuSample13_10-40_12.$av
File ID: CuSample13
Sample ID: CuOParticlesJonG
Optical model: Cu Particles.rfd   PIDS included
LS 230   Small Volume Module
Fluid: Water
 Average of 3 files:
 CuSample13_10-37_10.$ls
 CuSample13_10-38_11.$ls
 CuSample13_10-40_12.$ls

Differential Volume (Average) (2 S.D.)

Differential Number (Average)

Differential Surface Area (Average)

Volume Statistics (Arithmetic)   CuSample13_10-40_12.$av

Calculations from 0.0400 µm to 2000 µm

Volume: 100%
Mean: 6.876 µm   S.D.:   7.610 µm
Median: 3.675 µm
Mode: 1.451 µm

<1 µm   <10 µm   <100 µm   <1000 µm
14.3%   75.2%   100%   100%

Surface Area Statistics (Arithmetic)   CuSample13_10-40_12.$av

Calculations from 0.0400 µm to 2000 µm

Surface Area: 100%
Mean: 2.062 µm   S.D.:   3.151 µm
Median: 1.092 µm
Mode: 0.910 µm

<1 µm   <10 µm   <100 µm   <1000 µm
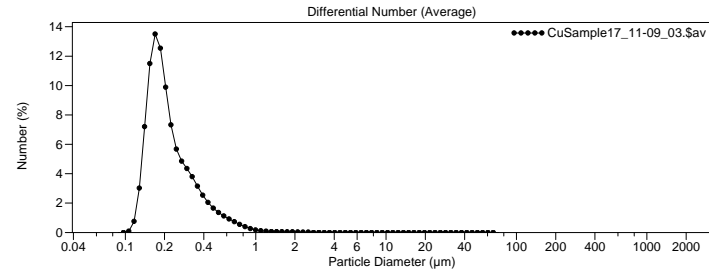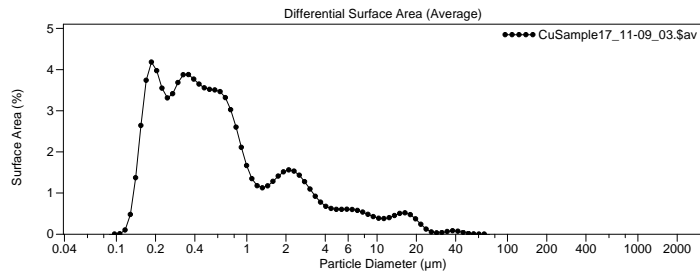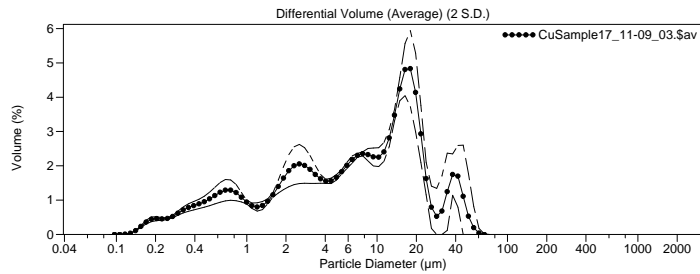45.1%   96.8%   100%   100%

Number Statistics (Arithmetic)   CuSample13_10-40_12.$av

Calculations from 0.0400 µm to 2000 µm

Number: 100%
Mean: 0.639 µm   S.D.:   0.439 µm
Median: 0.525 µm
Mode: 0.431 µm

<1 µm   <10 µm   <100 µm   <1000 µm
87.8%   99.99%   100%   100%

116

Figure B.13: Sample 13 Particle Size Data

File name: C:\LS32\Data\George\CuSample14_12-49_03.$av
File ID: CuSample14
Sample ID: CuOParticlesJonG
Operator: JonG
Optical model: Cu Particles.rfd   PIDS included
LS 230   Small Volume Module
Fluid: Water
 Average of 3 files:
 CuSample14_12-46_01.$ls
 CuSample14_12-48_02.$ls
 CuSample14_12-49_03.$ls

Differential Volume (Average) (2 S.D.)

Differential Surface Area (Average)

Differential Number (Average)

Volume Statistics (Arithmetic)   CuSample14_12-49_03.$av

Calculations from 0.0400 μm to 2000 μm

Volume: 100%
Mean: 1.968 μm   S.D.:   1.800 μm
Median: 1.444 μm
Mode: 1.919 μm

<1 μm   <10 μm   <100 μm   <1000 μm
38.0%   99.97%   100%   100%

Surface Area Statistics (Arithmetic)   CuSample14_12-49_03.$av

Calculations from 0.0400 μm to 2000 μm

Surface Area: 100%
Mean: 0.593 μm   S.D.:   0.903 μm
Median: 0.236 μm
Mode: 0.128 μm

<1 μm   <10 μm   <100 μm   <1000 μm
83.0%   99.998%   100%   100%
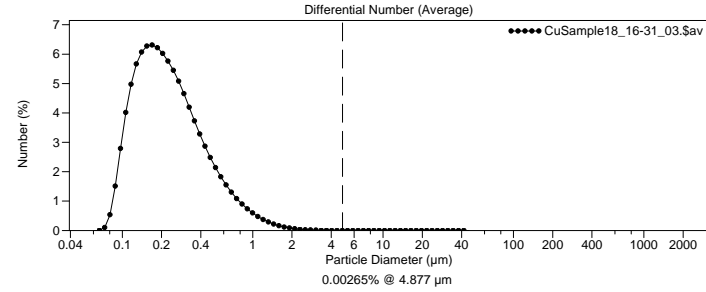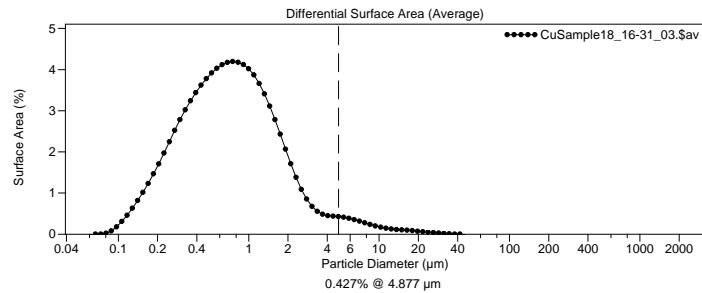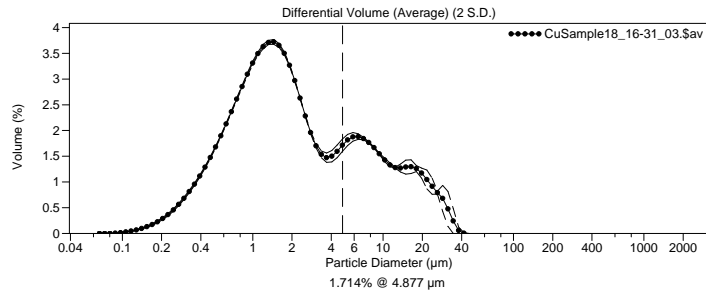
Number Statistics (Arithmetic)   CuSample14_12-49_03.$av

Calculations from 0.0400 μm to 2000 μm

Number: 100%
Mean: 0.112 μm   S.D.:   0.093 μm
Median: 0.0896 μm
Mode: 0.0733 μm

<1 μm   <10 μm   <100 μm   <1000 μm
99.9%   100%   100%   100%

Figure B.14: Sample 14 Particle Size Data

File name: C:\LS32\Data\George\CuSample15_15-18_03.$av
File ID: CuSample15
Sample ID: CuOParticlesJonG
Optical model: Cu Particles.rfd   PIDS included
LS 230   Small Volume Module
Fluid: Water
 Average of 3 files:
 CuSample15_15-15_01.$ls
 CuSample15_15-17_02.$ls
 CuSample15_15-18_03.$ls

Differential Number (Average)

Differential Volume (Average) (2 S.D.)

Volume Statistics (Arithmetic)   CuSample15_15-18_03.$av

Calculations from 0.0400 µm to 2000 µm

Volume: 100%
Mean: 10.50 µm   S.D.:   12.56 µm
Median: 5.595 µm
Mode: 6.452 µm

<1 µm   <10 µm   <100 µm   <1000 µm
12.3%   68.6%   100%   100%

Differential Surface Area (Average)

Surface Area Statistics (Arithmetic)   CuSample15_15-18_03.$av

Calculations from 0.0400 µm to 2000 µm

Surface Area: 100%
Mean: 2.151 µm   S.D.:   4.237 µm
Median: 0.570 µm
Mode: 0.393 µm
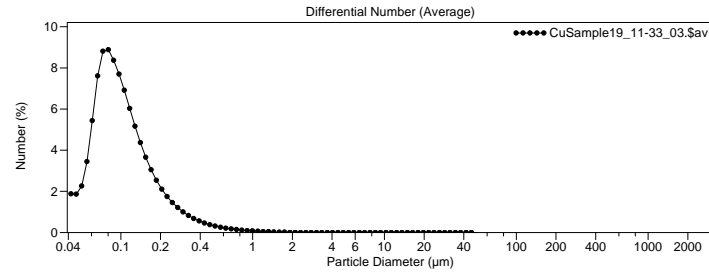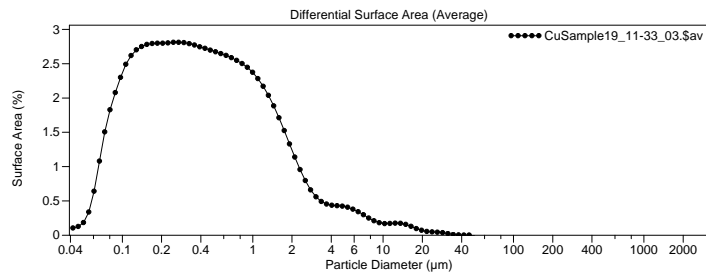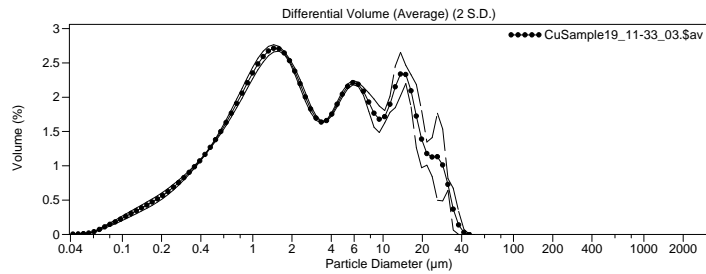
<1 µm   <10 µm   <100 µm   <1000 µm
61.5%   96.5%   100%   100%

Number Statistics (Arithmetic)   CuSample15_15-18_03.$av
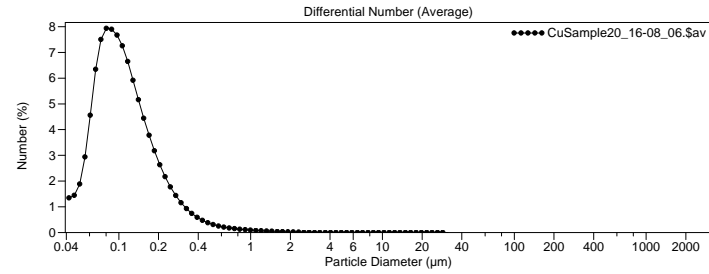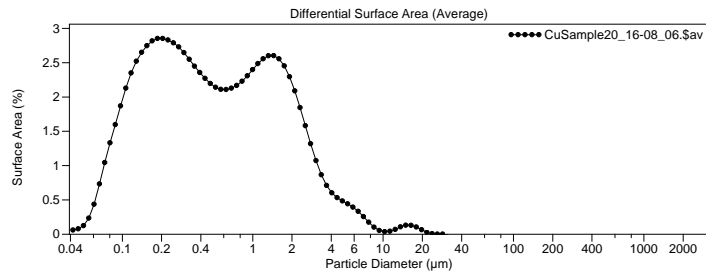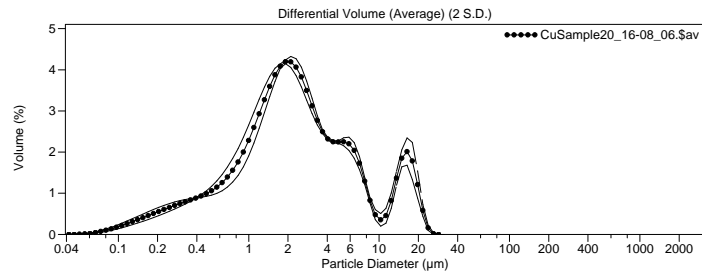
Calculations from 0.0400 µm to 2000 µm

Number: 100%
Mean: 0.352 µm   S.D.:   0.272 µm
Median: 0.303 µm
Mode: 0.271 µm

<1 µm   <10 µm   <100 µm   <1000 µm
98.7%   99.997%   100%   100%

118

Figure B.15: Sample 15 Particle Size Data

Figure B.16: Sample 16 Particle Size Data

119

File name: C:\LS32\Data\George\CuSample17_11-09_03.$av
File ID: CuSample17
Sample ID: CuOParticlesJonG
Optical model: Cu Particles.rfd   PIDS included
LS 230   Small Volume Module
Fluid: Water
 Average of 3 files:
 CuSample17_11-06_01.$ls
 CuSample17_11-07_02.$ls
 CuSample17_11-09_03.$ls

Differential Volume (Average) (2 S.D.)
●●●●● CuSample17_11-09_03.$av

Differential Surface Area (Average)
●●●●● CuSample17_11-09_03.$av

Differential Number (Average)
●●●●● CuSample17_11-09_03.$av

Volume Statistics (Arithmetic)   CuSample17_11-09_03.$av

Calculations from 0.0400 μm to 2000 μm

Volume: 100%
Mean: 10.64 μm   S.D.:   10.99 μm
Median: 7.139 μm
Mode: 18.00 μm

<1 μm	<10 μm	<100 μm	<1000 μm
16.6%	58.3%	100%	100%

Surface Area Statistics (Arithmetic)   CuSample17_11-09_03.$av

Calculations from 0.0400 μm to 2000 μm

Surface Area: 100%
Mean: 1.770 μm   S.D.:   3.963 μm
Median: 0.508 μm
Mode: 0.186 μm

<1 μm	<10 μm	<100 μm	<1000 μm
71.5%	95.8%	100%	100%

Number Statistics (Arithmetic)   CuSample17_11-09_03.$av

Calculations from 0.0400 μm to 2000 μm

Number: 100%
Mean: 0.253 μm   S.D.:   0.200 μm
Median: 0.198 μm
Mode: 0.170 μm

<1 μm	<10 μm	<100 μm	<1000 μm
99.3%	99.998%	100%	100%

Figure B.17: Sample 17 Particle Size Data

Figure B.18: Sample 18 Particle Size Data

Figure B.19: Sample 19 Particle Size Data

Figure B.20: Sample 20 Particle Size Data

REFERENCES

[1] Berkowitz, A. E., and Walter, J. L., 1987. "Spark erosion: A method for producing rapidly quenched fine powders." *Journa of Materials Research,* **2**, pp. 277–288. 1, 29, 30, 31, 32, 69

[2] Berkowitz, A. E., Hansen, M., Parker, F., K.S.Vecchio, Spada, F., Lavernia, E., and Rodriguez, R., 2003. "Amorphous soft magnetic particles produced byspark erosion." *Journal of Magnetism and Magnetic Materials,* **254-255**, pp. 1–6. 1, 32

[3] Kim, T.-Y., Hirano, T., Kitamoto, Y., and Yamazaki, Y., 2003. "Novel nanoparticle milling process for biyig dispersed transparent films." *IEEE Transaction On Magnetics,* **39**(4), July, pp. 2078–2080. 1

[4] Lewis, C. J., 2009. "Development of a methodology for numerical simulation of a dc arc discharge in a liquid dielectric media." PhD thesis, BYU. 2, 15

[5] Smith, D., 1965. Impulse breakdown of de-ionized water Tech. rep., Atomic Weapons Research Establishment, Nov. 3

[6] Descoeudres, A., 2006. "Characterization of electrical discharge machining plasmas." PhD thesis, Ecole Polytechnique Federale De Lausanne. 4, 23, 25

[7] Vasudevamurthy, G., and Knight, T. W., 2007. "Effect of system parameters on size distribution of 304 stainless steel particles produced by electrical discharge mechanism." *Materials Letters,* **61**(27), pp. 4872 – 4874. 16

[8] Guitrau, E. P., 1997. *The EDM Handbook.* hanser Gardner Publications. 21, 23

[9] Qackenbush, L. J., and Lawrence, W. N., 1971. *Electrical Discharge Machining for the 1970's.* Industrial Development Division , Institute of Science and Technology, The University of Michigan. 23, 26

[10] Mysinski, W., 2008. "Power supply unit for an electric discharge machine." In *2008 13th Internation Power Electronics and Motion Control Conference.* 25

[11] Odulio, C., Sison, L., and Escoto, M., 2005. "Energy-saving flyback converter for edm applications." In *TENCON 2005 2005 IEEE Region 10*, pp. 1–6. 25

[12] Boccadoro, M., and Dauw, D. F., 1995. "About the application of fuzzy controllers in high-performance die-sinking edm machines." *Annals of the CIRP,* **44**, pp. 147–150. 26

[13] Altpeter, F., Myszkorowski, P., Kocher, M., and Longchamp, R., 1997. "Friction Compensation: PID Synthesis and State Control." In *European Control Conference*, p. 1. 26, 27

[14] Chung, C., Chao, S.-Y., and Lu, M., 2009. "Modeling and control of die-sinking edm." *WSEAS Transactions on Systems,* **8**(6), June, pp. 713–722. 27

[15] Rogers, 2004. Voltage controlled arc spray, patent number 6683271. 28, 29

[16] Rotolico, A. J., 1972. Electric arc metal spray gun, patent number 3632952. 28

[17] larry Boyd Mark A. Boyd, 1999. Electric arc spray gun, patent number 6005215. 28

[18] Cabanillas, E., Lopez, M., Pasqualini, E., and Lombardo, D. C., 2004. "Production of uranium-molybdenum particles by spark-erosion." *Jounal of nuclear materials,* **324**, pp. 1–5. 32

[19] Cabanillas, E. D., 2007. "Tem observations of particles obtained by electro-erosion in kerosene." *Jornal of materials science,* **42**, March, pp. 3155–3160. 32

[20] Horvath, H., and Gangl, M., 2003. "A low-voltage spark generator for production of carbon particles." *Journal of Aerosol Science,* **34**, pp. 1581–1588. 32, 33, 34

[21] IEEE, 1991. Refinements of the Ziegler-Nichols Tuning formula, Vol. 138. 67

[22] NIST/SEMATECH, 2010. E-handbook of statistical methods, Internet, Feburary http://www.itl.nist.gov/div898/handbook/. 91

[23] Yan, M.-T., and Lai, Y.-P., 2007. "Surface quality improvement of wire-edm using a fine-finish power supply." *International Journal of Machine Tools and Manufacture,* **47**(11), pp. 1686 – 1694. 97